Thesis for the Master of Science

On the Dynamic Stability of Automotive Turbochargers: Case Studies with Various Bearing Configurations

Xiao Fang

Graduate School of Hanyang University

February 2018

Thesis for the Master of Science

On the Dynamic Stability of Automotive Turbochargers: Case Studies with Various Bearing Configurations

Thesis Supervisor: Keun Ryu

A thesis submitted to the graduate school of Hanyang University in partial fulfillment of the requirements for the degree of Master of Science

Xiao Fang

February 2018

Department of Mechanical Design Engineering

Graduate School of Hanyang University

This thesis, written by Xiao Fang, has been approved as a thesis for the degree of Master of Science.

February 2018

Committee Chairman: Wonchul Lee (Signature)

Committee member: Keun Ryu (Signature)

Committee member: Namwook Kim (Signature)

Graduate School of Hanyang University

Abstract

On the Dynamic Stability of Automotive Turbochargers:

Case Studies with various Bearing Configurations

(February 2018)

Xiao Fang, B.S., Hanyang University

Chair of Advisory Committee: Dr. Keun Ryu

The present study introduces a finite element structural rotor dynamic model to predict the stability of automotive turbochargers (TCs) supported on simple rigid geometry fluid film bearings (2-axial groove bearings or multi-lobe bearings or offset-half bearings). The turbocharger finite element (FE) structural model for linear analyses include lumped masses for compressor wheel, and turbine wheel. The free-free mode shapes and natural frequencies of a rotor are measured and compared with predictions. Stability of the TC rotor-bearing system is largely related to bearing dynamic coefficient (stiffness and damping coefficients). Rotordynamic predictions are conducted with a commercial TC rotor model from 10 krpm to 200 krpm. By comparing the bearing force coefficients of various configuration bearings, the results show the relationship between bearing configurations and rotor-bearing system stability. The higher offset provides higher direct stiffness and damping force coefficients of multi-lobe bearing when the bearings are preloaded. The higher pad angle provides higher direct stiffness and damping force coefficients of the multi-lobe bearings. The 3 lobe bearings provide higher direct dynamic coefficients than the 4 lobe bearings, offset-half bearings, and 2-axial groove bearings. Furthermore, the eigenvalue analysis show significantly different stability results among the 2-axial groove bearings, 3 lobe bearings, 4 lobe bearings, and offset half bearings.

Acknowledgments

First, I must thank my academic advisor, Dr. Keun Ryu; he helps me improve myself and teach me the way to study.

Second, I much appreciate the support and encouragement of my family and colleagues. When I feel confused, they helped me out of trouble.

Then, I want to thank Dr. Wonchul Lee and Dr. Namwook Kim. They provide guidance to improve this thesis.

Finally, I would like to thank the administrative personnel, for providing timely information support that I can meet all of my graduation requirements.

Nomenclature

C_b Bearing radial clearance [m]

C_p Pad radial clearance [m]

r_b Bearing radius at minimum clearance [m]

r_j Journal shaft radius [m]

W Static load on bearing [N]

R_p Pad radius [m]

R_b Bearing radius [m]

R_j Journal radius [m]

e Eccentricity [m]

m Preload [-]

α Offset [-]

θ_p Angle from the negative load vector (negative X-axis) to the line connecting the bearing center and the pad center of curvature [degree]

θ_l Angle from the negative load vector (negative X-axis) to leading edge of the first lobe [degree]

θ_t Angle from the negative load vector (negative X-axis) to trailing edge of the first lobe [degree]

δ Logarithmic decrement [-]

M Mass [kg]

C Damping coefficient [kN-s/m]

K Stiffness coefficient [MN/m]

Ω Rotor angular velocity [/s]

X Horizontal direction

Y Vertical direction

Table of Contents

List of Figures

List of Tables

Chapter 1. Introduction

Turbochargers (TCs) are turbomachinery that enhances the efficiency and the power output of internal combustion engines by forcing outside air into the combustion chamber. Researchers are focused on improving turbocharger designs for better performance at a lower cost as well as to improve reliability and increase operational life. The operating speed of turbocharger is very high, hence stability of entire system made a very high demand. Bearings are one of the important parts of TC rotor-bearing system.

The current study focuses on TC rotor systems supported on 2-axial groove bearings, offset-half bearings, and multi-lobe bearings. This study analysis and compare the stability effect of turbochargers using different bearing configurations. The most significant considerations for proper bearing selection are cost, manufacturability, easy for installation, interchangeability, static characteristics, and dynamic characteristics. The static characteristics and the dynamic characteristics of bearings are essential in a rotor-dynamic analysis. The results of bearing dynamic analysis and eigenvalue analysis are used to verify stability of rotor-bearing systems.

This study analyzes static characteristics, and dynamic characteristics of TCs supported on different types of bearings. After calculating stiffness and damping force coefficients of TC supported on each bearing, eigenvalue analysis can be used to compare the stability of each TC system. Compare TCs using different bearing configurations can find the source of the stability problem of TC.

Chapter 2. Literature review

Turbochargers are machines which enhance performances of internal combustion engines. Principal components of turbocharger include compressor wheel, turbine wheel, shaft and bearing. Turbochargers are high-performance rotation machines. Shaft speed of turbocharger can reach 100,000 rpm. Most of the researchers are focused on increasing efficiency of turbochargers, especially power output enhanced in a miniaturization turbocharger. Under these circumstances, turbochargers appear many problems like excessive levels of steady state synchronous rotor response, and sub- harmonic rotor instabilities. Previous researchers developed many kinds of bearings. These bearings show different stability effect on the turbocharger. To quantify rotor-bearing system stability, researchers introduced the concept of logarithmic decrements [5]. This concept needs to be further described later in this study. There are two ways to improve rotor-bearing system stability. One is to redesign all rotor-bearing system, and another one is to amend bearing configurations. Amend bearing configurations is more suitable when considering economy and manufacturability.

General bearings include following bearings: plain journal bearings, axial groove bearings, elliptical bearings, offset-half bearings, multi-lobe bearings, floating ring bearings, semi-floating ring bearings, and tilting pad bearings. This study compares performance difference of automotive turbochargers supported on some bearing types.

Multi-lobe bearings have better stability than plain cylindrical bearings. Zeidan et al. [1] describe many types of bearing configurations include preload. Preload is a parameter that is often used to change characteristics of the rotor-bearing system. Increased preload enhances fluid film stiffness. On the other hand, an increase in preload reduces damping in a rotor-bearing system.

Adams [2] introduces several bearings from Zeidan [1], along with a brief discussion of strengths and shortcomings of each: Floating axial groove bearings, four axial groove bearings, floating-ring bearings, and tilting pad bearings. By using rotor dynamics software (DyRoBeS), result shown tilting pad bearing design is most stable bearing design included in this research.

Similar to Michael, Alsaeed [3] introduce several bearings: floating ring bearings, six-oil-groove bearings (with different configurations as external damping), 6-pocket bearings, elliptical (lemon bore) bearings, and tilting-pad bearings. Though tilting-pad bearings provided stable turbocharger rotor-bearing system, they are still relatively expensive to produce. Other types of fluid-film journal bearings showed unaccepted instabilities in the linear running. However, a turbocharger supported on floating ring bearings has a least unstable whirling operation. Floating–ring design introduced an external damping by outer oil-film that re-stabilized whirling modes. Hence, an attempt was made to find an optimum external damping turbocharger supported on six-oil-groove bearings. Unfortunately, attempt to optimize whirling modes by adding damped supports to six-oil-groove bearings was not successful.

Mondschein [4] developed TC rotor-dynamic model using floating ring bearings, six axial groove bearings, eight axial groove bearings and ten axial groove bearings. Then they analyzed stability, and compare with experimental tests. Previous work suggests that modeling turbocharger load on compressor wheel rather than turbine wheel is more representative of actual operation characteristic [3]. Therefore, FR and 6AG cases were run applying 5, 10, 15, 20, and 25-pound loads force on the compressor. 6AG and 8AG bearings performed similarly with 15lbs of compressor loading. However, 8AG was unable to be loaded to 25lbs, and 6AG was unable to match the performance of floating ring bearings. Despite improved performance of 6AG bearings with compressor loading, linear analytical testing shows it fails to outperform stock FR bearings currently used in production turbochargers.

TC rotor dynamic performance defined by stiffness and damping coefficients of oil-lubricated bearings. Lund [6] discussed many bearings include elliptical bearings, 2-axial groove bearings, 3 lobe bearings, and offset cylindrical bearings. By calculating finite difference solutions of Reynolds equations, they calculate stiffness and damping coefficients.

On this basis, Ferron [7] considers heat transfer between film and bush and both shaft of a finite length journal bearing. They even considered cavitation and lubricant recirculation. They compare predicted results such as pressure and temperature distribution on bearing wall with experimental data. Their conclusion is bearing analysis should be considered thermal deformations. Along with differential thermal dilatation between journal and bearing also essential.

With the development of computer technology, more and more researchers use a computer to analyze thermal fluid dynamics. San Andrés [8] presents a thermo-hydrodynamic (THD) analysis and computer program to predict static and dynamic force response of hydrostatic journal bearings, annular seals, or damping bearings, and fixed arc-pad bearings. Especially six-recess hydrostatic bearings which are using Space Shuttle Main Engine high-pressure oxidizer turbopumps.

Based on finite element analysis for complete rotor dynamics analysis and comprehensive bearing performance calculations, Chen [9] developed computer software tool since 1991. This software is powerful, yet easy to learn and use, engineering design/analysis software tools. This study also uses this software to complete analysis of TC rotor-bearing system.

Most researchers discuss the performance of automotive TCs using floating ring bearings, tilting pad bearings, and plain cylindrical bearings. This study compares the stability of automotive TCs using 2-axial groove bearings, offset-half bearings, and multi-lobe bearings. Marine TCs are wildly using offset-half bearings and multi-lobe bearings. This study discusses the new area of these bearing types.

Chapter 3. Computational model of rotor-bearing system

This section describes a finite element model of an automotive TC rotating component using a commercial rotordynamic software.

The first section describes a finite element model of automotive TCs rotor. Validation of rotor-dynamics model requires a good correlation between measured and predicted rotor physical properties, as well as free-free natural frequencies and mode shapes. This step is essential for proving the accuracy of rotor structural model.

The second section describes models of each bearing using the computational bearing software. Each TC supported on two bearings which named a turbine side bearing and a compressor side bearing. This study discusses four types of bearings, every single TC using same bearing type. This study using a constant lubricant viscosity to the easier compare characteristics difference between each kind of bearings. Next chapter calculates characteristics of bearings such as stiffness and damping force coefficients.

3.1 Finite element (FE) rotor-bearing system model

Figure 1 shows TC rotor assembly. To validate computational FE model, first measured turbocharger dimension, polar moment of inertia and transverse moment of inertia, mass, the center of gravity, and free-free mode natural frequencies and mode shape of the turbocharger. The overall weight of the TC rotor is 1.51 N, and its center of gravity (C.G.) is located 76.901 mm from the compressor wheel end. The measured mass moment of inertia is 2.101×10-4 kg-m^2, and polar moment of inertia is 1.780×10-5 kg-m^2. Tables 1 through 4 list relevant dimensions of the TC rotor.

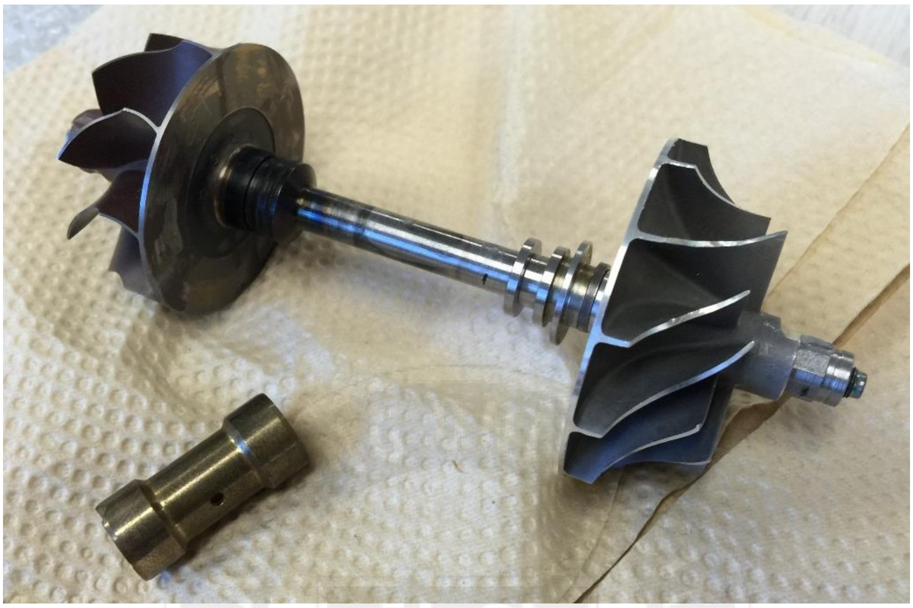

Fig. 1 Turbocharger rotor and bearing

Table 1 Length of TC rotor

	Shaft & Turbine	**Compressor**	**Thrust Collar**	**Thrust Washer**	**Compressor Nut**	**Assembled TC rotor**
Measurement [mm]	127.7	25.8	12	1.46	7	127.7
Prediction [mm]	127.7	25.8	12	1.46	7	127.7
Difference [%]	0%	0%	0%	0%	0%	0%

Table 2 Mass of TC rotor

	Shaft & Turbine	Compressor	Thrust Collar	Thrust Washer	Compressor Nut	Assembled TC rotor
Measurement [g]	109.3	32.8	6	1.1	1.9	151
Prediction [g]	109.280	32.800	6.044	1.098	1.900	151.12
Difference [%]	0%	0%	0%	0%	0%	0%

Table 3 Moment of inertia of TC rotor

	Shaft & Turbine	Compressor	Thrust Collar	Thrust Washer	Compressor Nut	Assembled TC rotor
Measurement [kg-m^2]	6.668×10^{-5}	4.177×10^{-6}	1.149×10^{-7}	8.216×10^{-10}	1.114×10^{-8}	2.101×10^{-4}
Prediction [kg-m^2]	6.668×10^{-5}	4.177×10^{-6}	1.129×10^{-7}	1.147×10^{-8}	1.114×10^{-8}	2.048×10^{-4}
Difference [%]	0%	0%	2%	93%	0%	3%

Table 4 Polar moment of inertia of TC rotor

	Shaft & Turbine	Compressor	Thrust Collar	Thrust Washer	Compressor Nut	Assembled TC rotor
Measurement [kg-m^2]	1.113×10^{-5}	6.215×10^{-6}	1.298×10^{-7}	2.529×10^{-8}	1.952×10^{-8}	1.750×10^{-5}
Prediction [kg-m^2]	1.113×10^{-5}	6.215×10^{-6}	1.256×10^{-7}	2.255×10^{-8}	1.952×10^{-8}	1.751×10^{-5}
Difference [%]	0%	0%	3%	12%	0%	0%

Figure 2 displays the TC rotor-dynamic structural model. The model includes lumped masses for the compressor wheel, the turbine wheel, and the thrust collar.

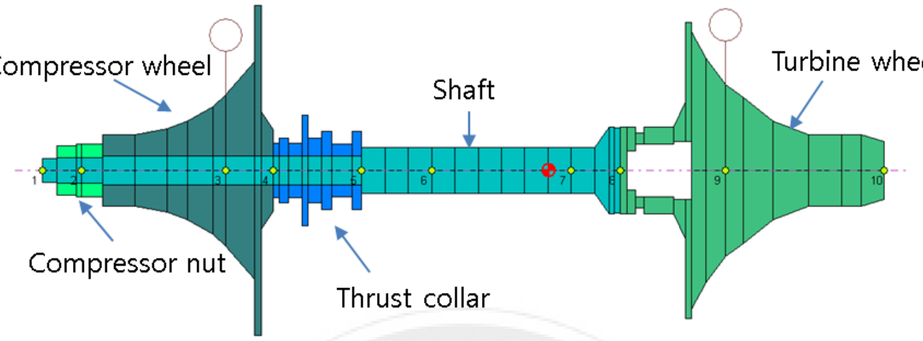

Fig. 2 Rotordynamic structural model of TC rotor

Free-free mode shapes and natural frequencies of TC rotor are measured, i.e., the rotor model does not include any support without rotation. The test rig consisted of FFT signal analyzer and a pair of acceleration sensors. Figure 3 displays the test rig of FFT signal analyzer and acceleration sensors.

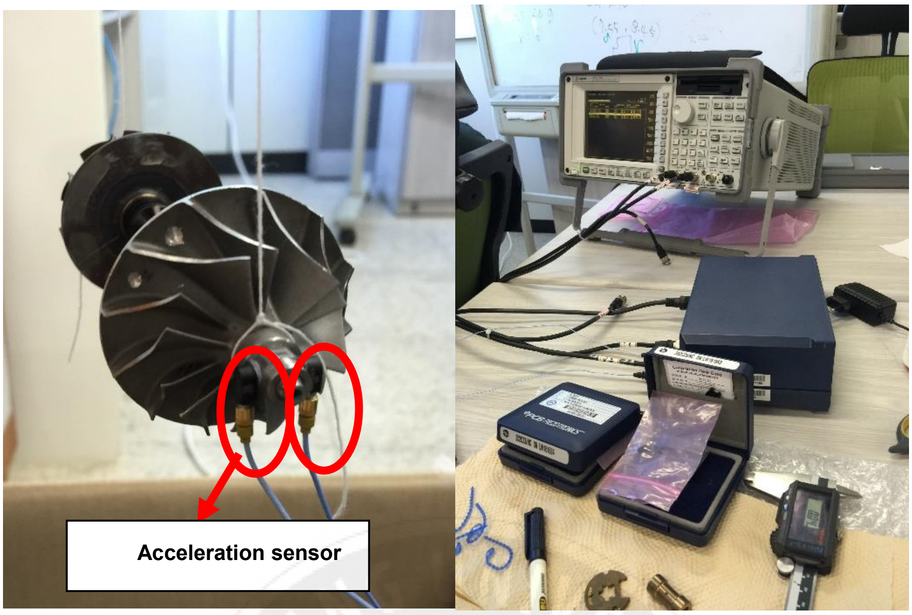

Fig. 3 Free-Free mode natural frequencies and mode shapes measurement using FFT signal analyzer and acceleration sensors

The measured values are similar to the predicted values. Figure 4 compares the measured and predicted results of first free-free mode shapes and natural frequencies of TC rotor. The measured and predicted first free-free natural frequency is 1,456 Hz and 1,339.6 Hz, respectively. Therefore, the difference between measurement and prediction is 8 %.

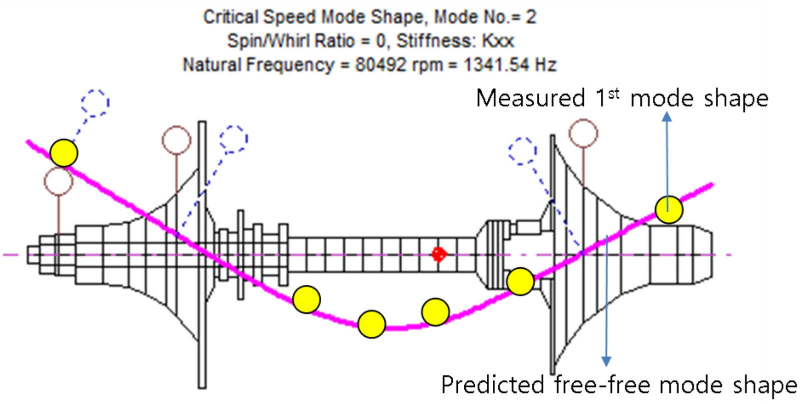

Fig. 4 Measured and predicted first free-free mode shapes of TC rotor

Figure 5 compares measurement and prediction of second free-free mode shapes and natural frequencies of TC rotor. The measured and predicted second free-free natural frequency is 4,282 Hz and 4,512.4 Hz, respectively. Therefore, the difference between measurement and prediction is 5.11%.

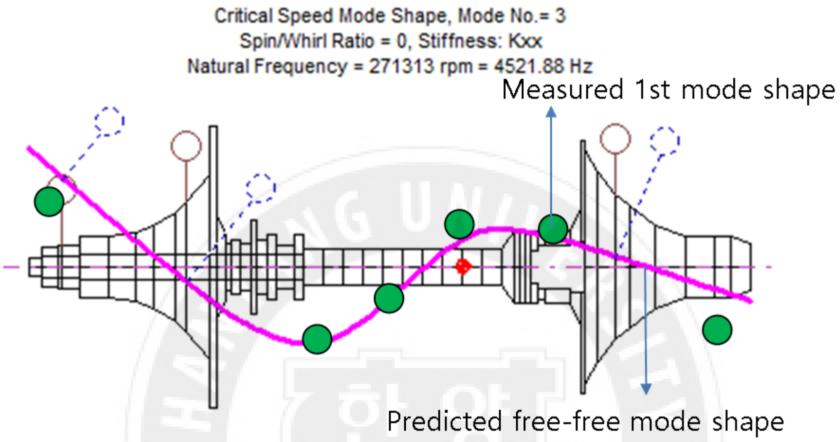

Fig. 5 Measured and predicted second free-free mode shapes of TC rotor

Figure 6 displays TC rotor dynamic structural model supported on fluid film bearings. This model includes 49 finite elements (12 stations), two bearings and four imbalance masses. Each spring connections represent one fluid film bearing.

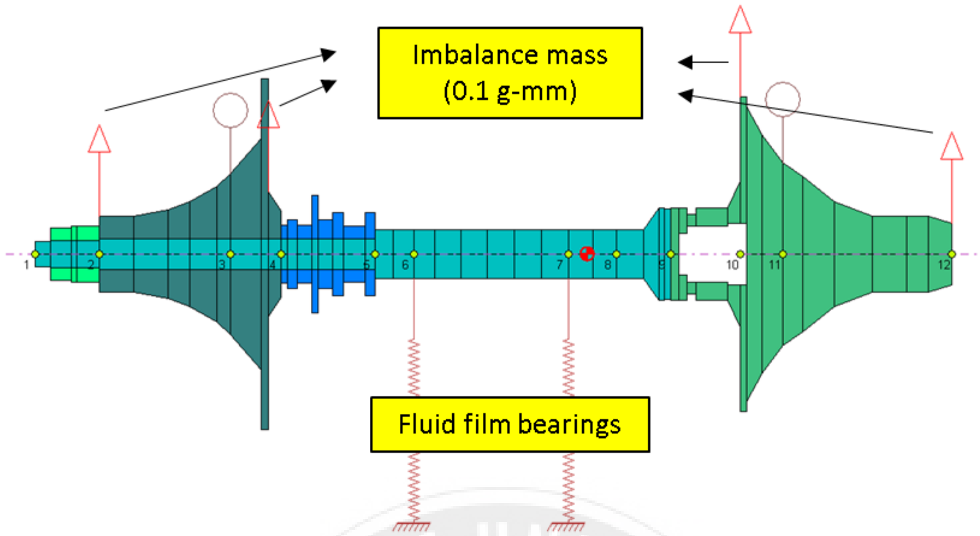

Fig. 6 Rotordynamic model for TC rotor-bearing system.

3.2 Bearing modeling

As shown in figure 7, static loads of compressor side bearing are -0.1821N, and turbine side bearing are 1.673N, respectively.

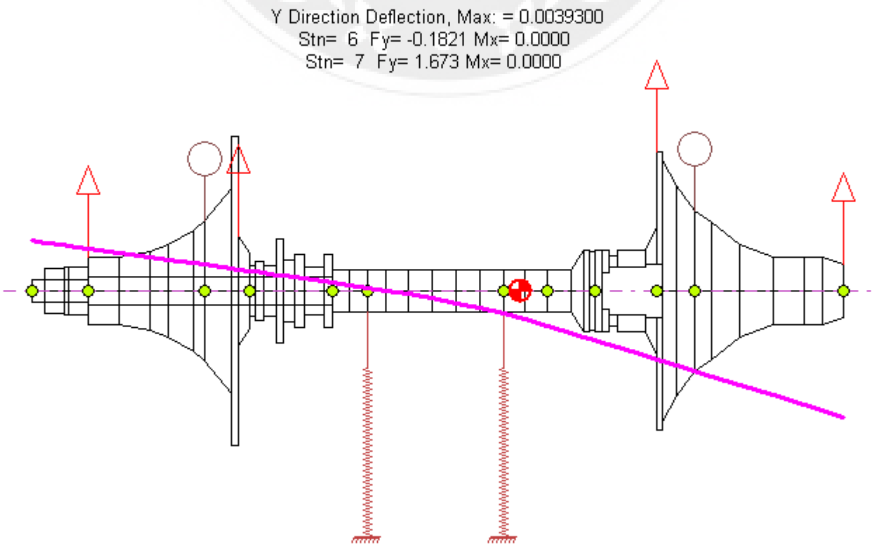

Fig. 7 Static load of TC rotor

The commercial bearing program calculates static and dynamic characteristic based on bearing operating in equilibrium position for a designated shaft speed range. Rotor speed ranges from 10,000 rpm to 200,000 rpm. The value of lubricant (SAE 0W30) viscosity is 6493(Pa-s), and the density value is 0.7785(grams/CC).There are four types of bearings discussion in this study. Offset-half bearings have 160 degrees of each pad, 3 lobe bearings have 100 degrees of each pad, and 4 lobe bearings have 70 degrees of each pad. On the purpose of this study, all bearings using similar physical properties. Tables 5 and 6 display input properties of bearing analysis. Figure 9 describes the schematic view of 2-axial groove bearing, offset-half bearings, 3 lobe bearings and 4 lobe bearings. Appendix A includes the detail inputs of each bearing (Figure A.16 through A.23).

Table 5 Bearing dimensions and support loads

	Axial Length (mm)	Rotor Diameter, D (mm)	Bearing Diameter, D_b (mm)	Radial Clearance, C_b (mm)	Bearing Load (N)
Turbine side bearing	6	6.934	6.993	0.030	1.673
Compressor side bearing	6	6.934	6.993	0.030	-0.1821

Table 6 Lubricant performances and other bearing configurations

	Lubricant Dynamic viscosity (cP)	Lubricant density (g/CC)	Preload	Offset
Two axial groove bearing (160 degree pad)	6.493	0.7785	0	0
offset half bearing （160 degree pad）	6.493	0.7785	0.5	0.8
3 lobe bearing (100 degree pad)	6.493	0.7785	0.5	0.8
4 lobe bearing (70 degree pad)	6.493	0.7785	0.5	0.8

Bearing preload and offset determine dynamic coefficients (stiffness and damping). Preload bearings mean bearing pads have a larger radius than a journal. Preloading let pad center of curvature move closer to journal, to create a higher pressure. Variable L often define preload value of a bearing by which defined as equation (1):

$$m = (C_p\text{-}C_b)/C_p = 1\text{-}C_b/C_p \tag{1}$$

$$C_b = r_b\text{-}r_j \text{ and } C_p = r_p\text{-}r_j$$

where C_b is the bearing minimum assembled radial clearance; C_p is the pad machined radial clearance; r_b is the bearing assembled radial at minimum clearance, and r_j is the journal shaft radial.

When preload value is zero means no preload, then the center of the rotor and the center of the bearing are coinciding. In this configuration, this bearing is a cylindrical journal bearing. When preload value equal to 1, the shaft contact the bearing.

When preload exists on bearing and shaft always rotated in one direction, pads can be offset, which is another important configuration of bearings. In mathematical significance, the offset value is a fraction of converging pad surface to full arc length. When offset value is equal to 0.5 means, there is no offset of the pad. If offset value less than 0.5, that means pad surface becomes diverging. Otherwise, offset value larger than 0.5 provides convergent pad surface. Offset value defined by equation (2):

$$\alpha = (\theta_p-\theta_l)/ (\theta_t-\theta_l) \tag{2}$$

where θ_p is the angle from negative load vector (y-axis) to a line connects bearing center and pad center of curvature. θ_l is the angle from negative load vector (y-axis) to leading edge of the first lobe. θ_t is the angle from negative load vector (y-axis) to trailing edge of the first lobe. To better understand preload and offset, Figure 8 describes an illustration of a 3 lobe bearing.

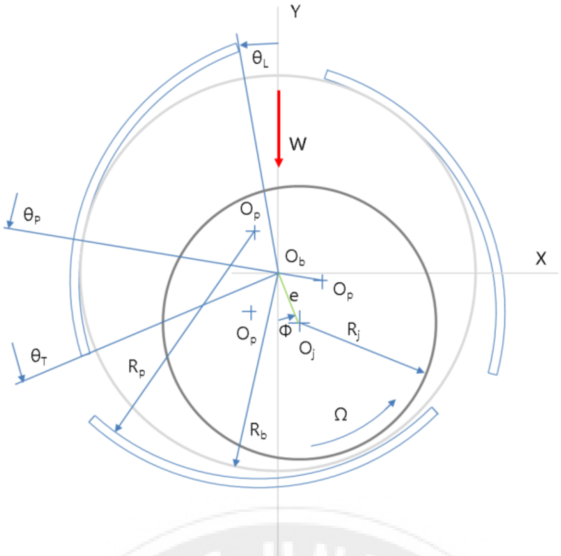

Fig. 8 Preload and offset of a 3 lobe bearing

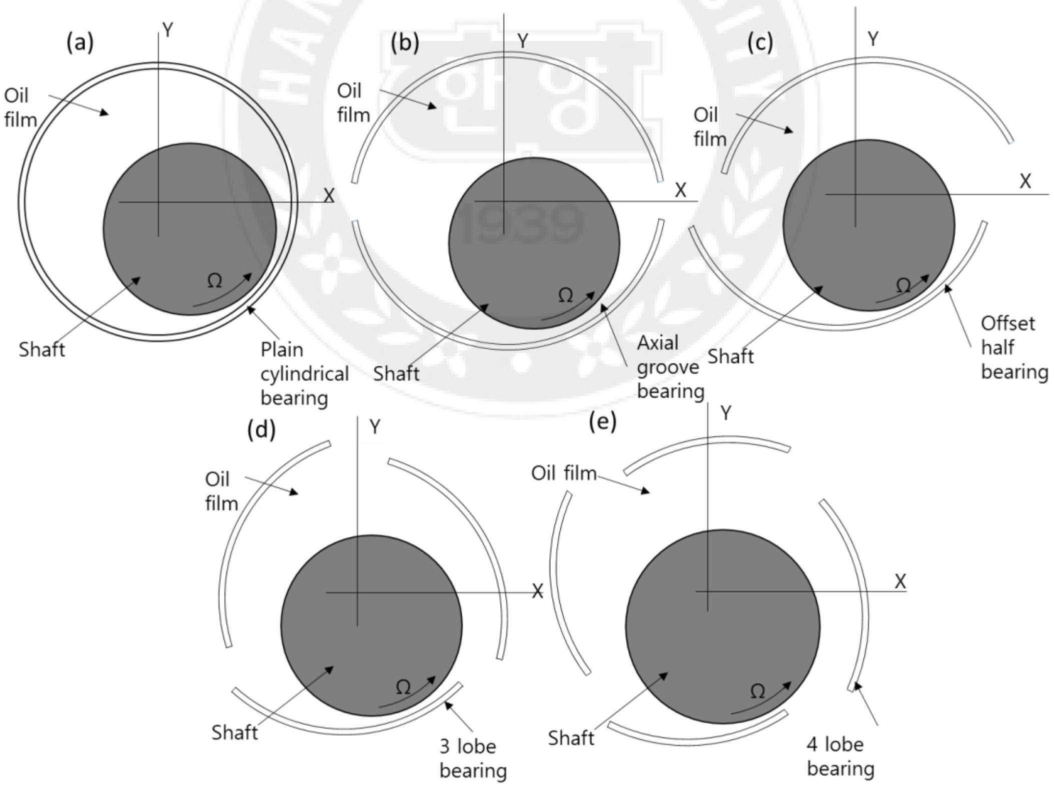

Fig. 9 Schematic view of (a) plain cylindrical bearing, (b) axial groove bearing, (c) offset half bearing, (d) 3 lobe bearing, and (e) 4 lobe bearing

Chapter 4. Predicted results

The first section of this chapter presents the static characteristic of fluid-film bearing analysis, including predicted eccentricity ratio, attitude angle, minimum film thickness and maximum film pressure and frictional power loss of lubricant films versus rotor speed. These analyses are to investigate the effect of bearing configurations on bearing performance. Static characteristics can calculate dynamic characteristics (stiffness and damping coefficients).

Next, analytical procedure results of estimating stability on turbocharger rotor are given by eigenvalue analysis. Moreover, compare the effect of different configurations of bearings on rotor-bearing system stability.

4.1 Predicted bearing performance

This section presents the static and the dynamic characteristic of bearing analysis. To more intuitive comparison of the bearing configuration on performance impact, export the calculation result to make a table. Because of the same reason, this study tries to use same axis dimensions in one kind of particular result. These bearing analysis inputs show in Appendix A.

Bearing reaction force from oil film bearing varies with different rotor speeds, which means that the equilibrium position is becoming different with different rotor speed. Confirm the rotor center locus with rotor speed variation, eccentricity ratio, and attitude angle are using to achieve this goal. Figure 10 and 11 describe eccentricity ratios versus rotor speed of each bearing. All figures show that when rotor speed increases, eccentricity ratio becomes lower. The result showed that center of rotor and journal become closer when rotor speed increases. At low speed, turbine side bearings have much higher eccentricity ratio than compressor side bearings; this may because turbine side bearings forced on higher static load from the rotor. On the other hand, these figures show the center of 2-axial groove bearings has the lowest eccentricity in operation rotor speed.

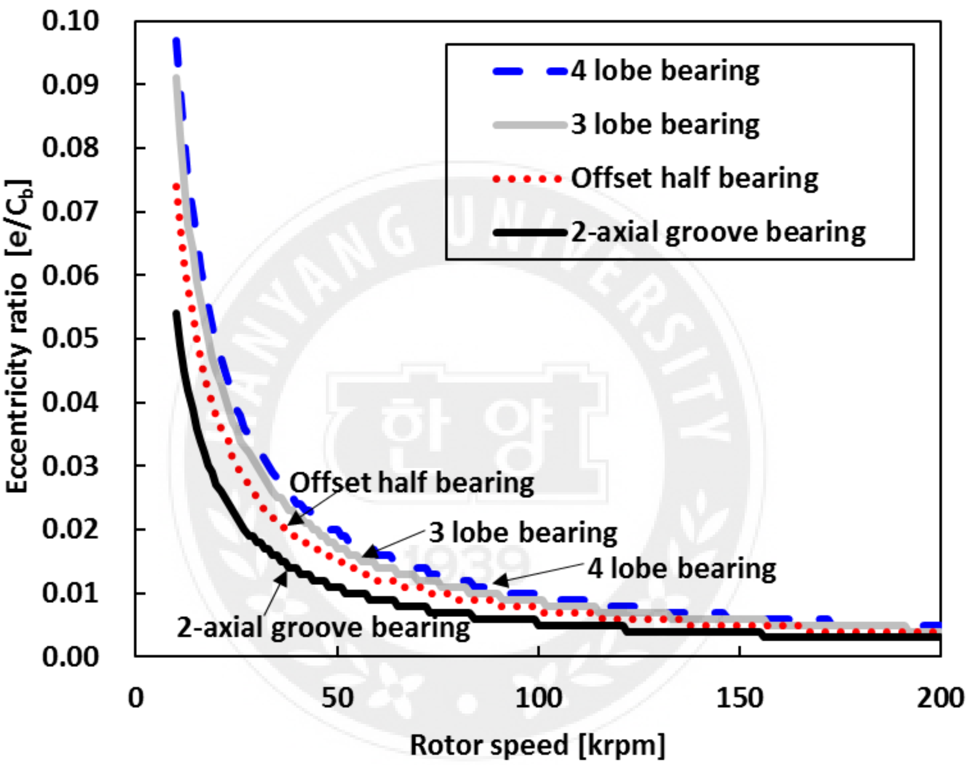

Fig. 10 Eccentricity ratio of compressor side bearing

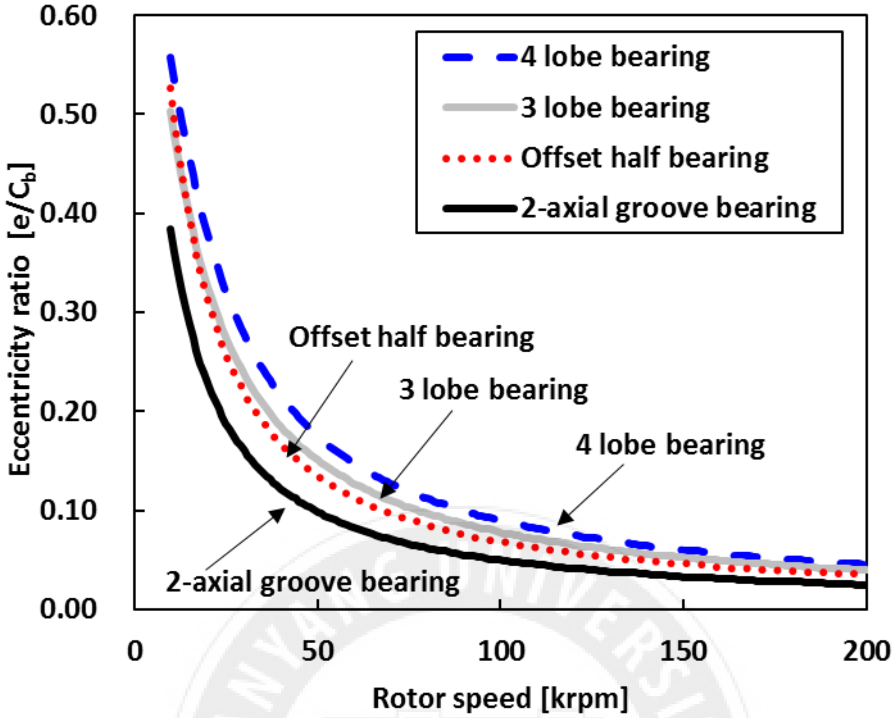

Fig. 11 Eccentricity ratio of turbine side bearing

Figures 12 and 13 describe attitude angles [degree] of each bearing. Attitude angles of each bearing tend to increase when shaft speed became higher. Attitude angles increased amplitude in compressor side bearings are very small, close to constant. On the other hand, attitude angles in compressor side bearings are more significant than turbine side bearings. Reason for these phenomena may be the static load on compressor side is negative. Note that offset-half bearings have lower attitude angles than other bearings.

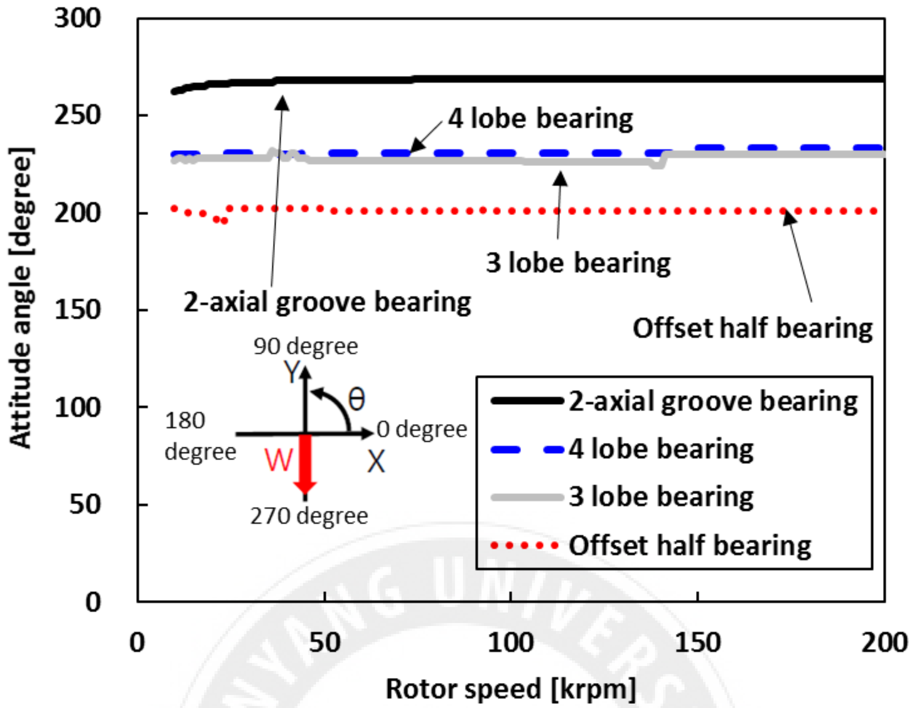

Fig. 12 Attitude angle of compressor side bearing.

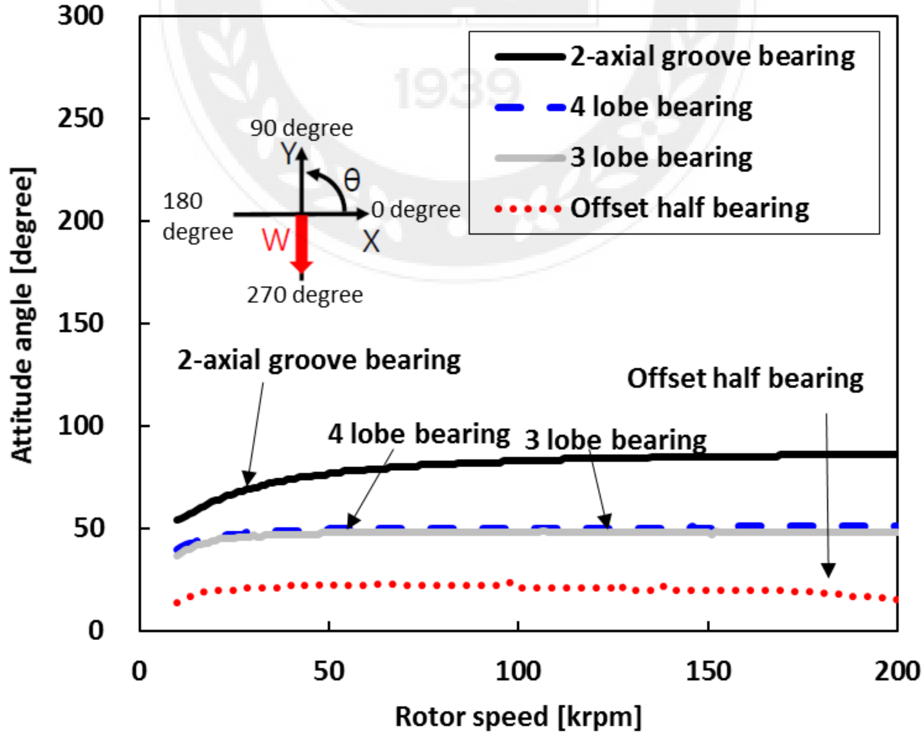

Fig. 13 Attitude angle of turbine side bearing.

Figures 14 and 15 describe ratios between film thickness and bearing clearance of each bearing. As the name suggests, bearing contacts journal wall if the minimum film thickness is 0. During Reynold's equation, the position of minimum film thickness presents highest flow rate of highest pressure. Minimum film thickness decreases mean shaft center close to journal center. Minimum film thickness becomes higher when shaft speed increases.

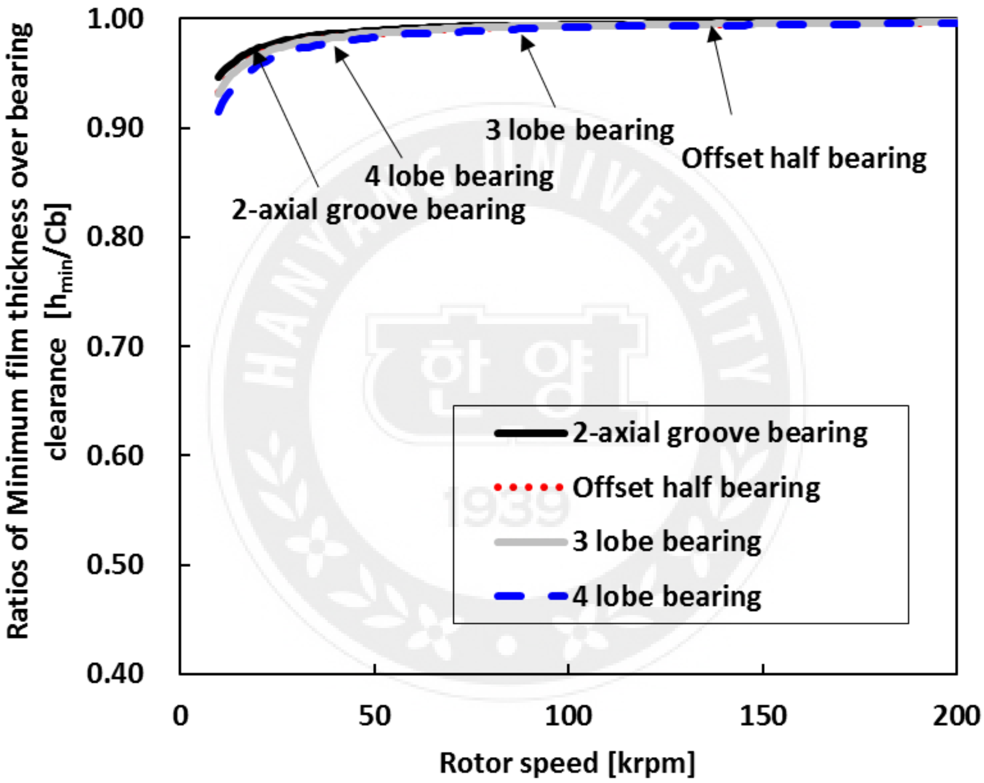

Fig. 14 Ratios of minimum film thickness over bearing clearance of compressor side bearing.

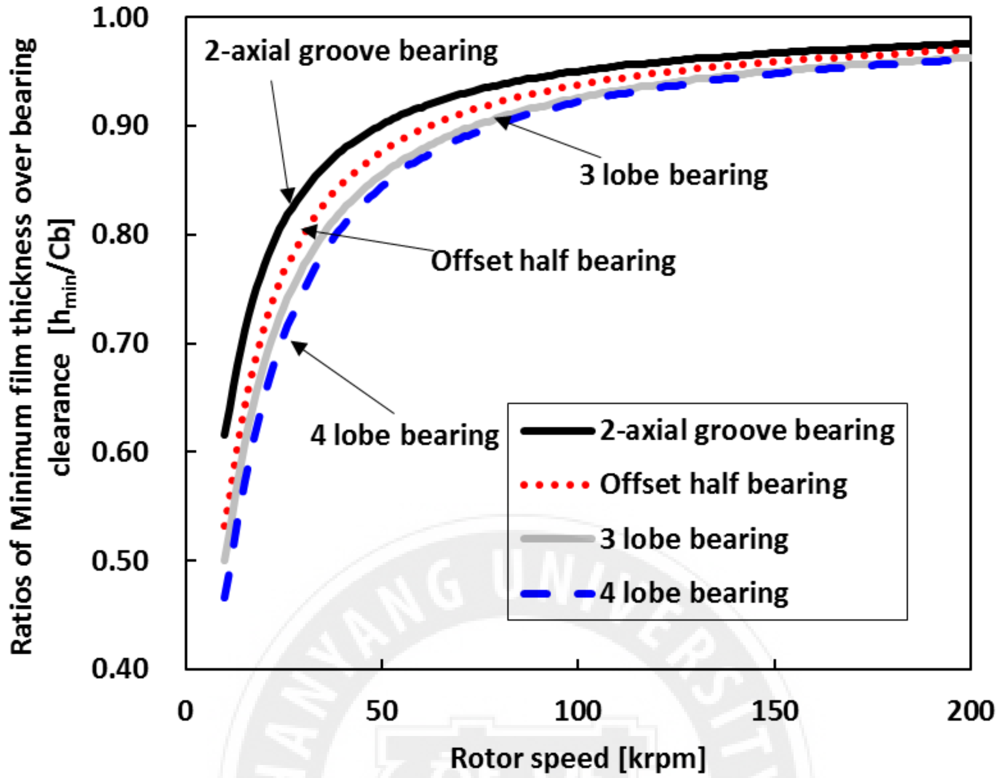

Fig. 15 Ratios of minimum film thickness over bearing clearance of turbine side bearing.

Figures 16 and 17 present maximum film pressures of each bearing. Apparently, offset bearings have a significant impact on maximum film pressure. In 2-axial groove bearings, maximum film pressures almost constant when increasing shaft speed. The pressure in turbine side bearings was larger than compressor side at low shaft speed, which because of the difference of static loads from the rotor. Maximum film pressures are approximately linearly increasing with shaft speed to offset bearings. 3 lobe bearings have secondary maximum film pressures on both sides. 4 lobe bearings have less maximum film pressures than three lobe bearings. 2-axial groove bearings have lowest maximum film pressures.

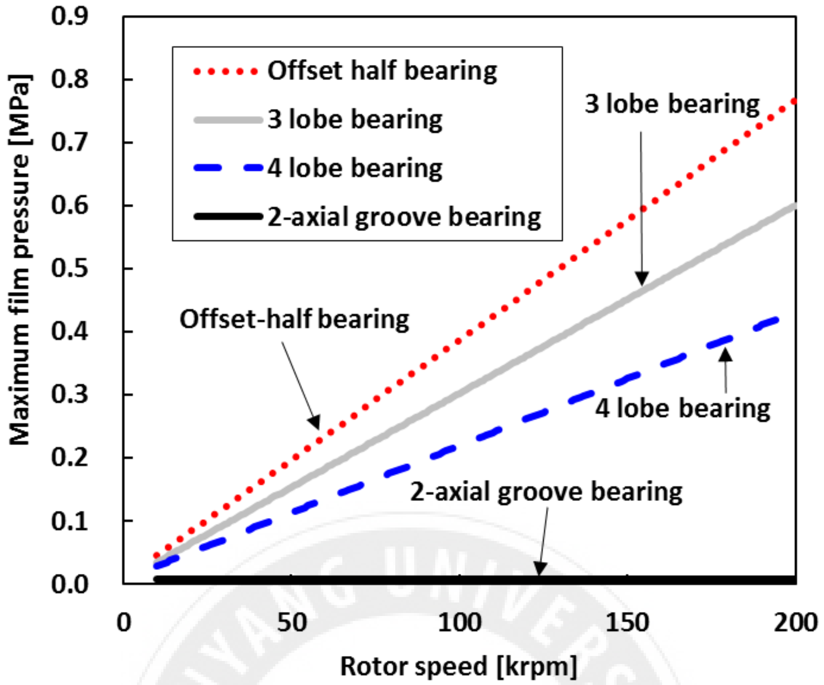

Fig. 16 Maximum film pressure of compressor side bearing.

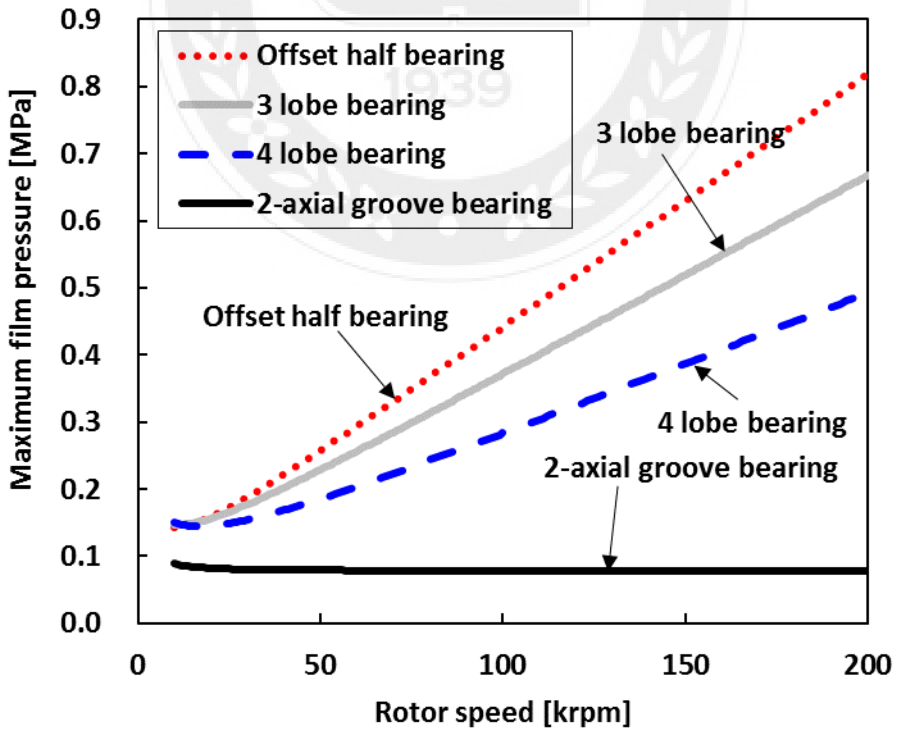

Fig. 17 Maximum film pressure of turbine side bearing

Stiffness coefficients are proportional to rotational speed and fluid viscosity. It means there is no fluid film bearing stiffness without rotation. Figure 18 and Figure 19 present stiffness coefficients K_{xx} of each bearing. Naturally, offset-half bearings and multi-lobe bearings present higher stiffness coefficients K_{xx} than 2-axial groove bearings. Similar to the result of maximum film pressure, higher shaft speed increases higher stiffness coefficients K_{xx} absolute value than other bearings, and this process is approximately linear. In both side bearings, 3 lobe bearing stiffness coefficients K_{xx} are highest, 4 lobe bearing stiffness coefficients K_{xx} are higher than offset half bearing stiffness coefficients K_{xx} and lowest stiffness coefficients K_{xx} are coming from 2-axial groove bearings. Note that on turbine side, this situation becomes precisely opposite when rotor speed at low speed (<25,000 rpm).

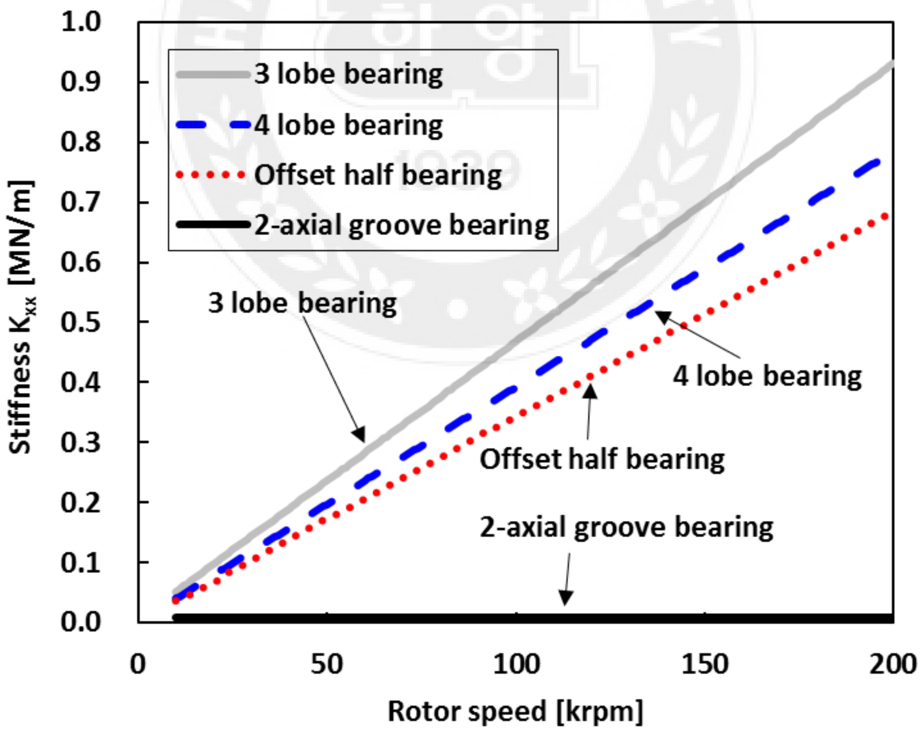

Fig. 18 Stiffness coefficients K_{xx} of compressor side bearing

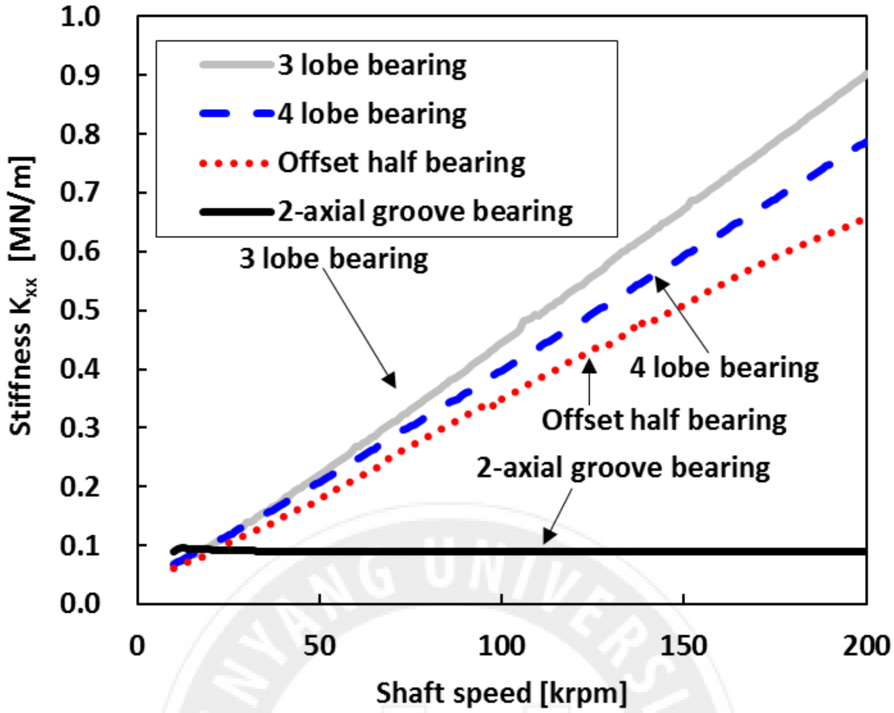

Fig. 19 Stiffness coefficients K_{xx} of turbine side bearing

Figures 20 through 23 present cross-coupled stiffness coefficients of each bearing. Similar to stiffness coefficients K_{xx}, higher shaft speed increases higher cross-coupled stiffness absolute value than other bearings. Moreover, this process is also approximately linear. In both side bearings, cross-coupled stiffness coefficients K_{xy} in 3 lobe bearings are larger than other bearings. 4 lobe bearings have larger cross-coupled stiffness coefficients K_{xy} than the 2-axial groove bearing. Offset half bearings have lowest cross-coupled stiffness coefficients K_{xy}.

All cross-coupled stiffness coefficients K_{yx} are negative values. In both side bearings, cross-coupled stiffness coefficients K_{yx} in 4 lobe bearings are larger than other bearings. 3 lobe bearings have larger cross-coupled stiffness coefficients K_{yx} than offset half bearing. 2-axial groove bearings have lowest cross-coupled stiffness coefficients K_{yx}.

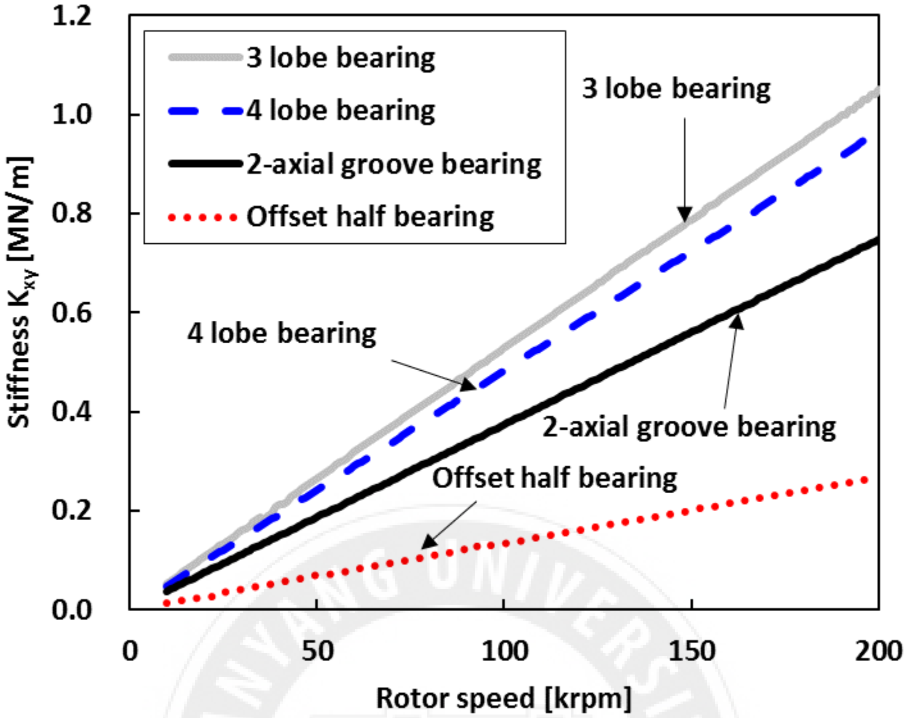

Fig. 20 Stiffness coefficients K_{xy} of compressor side bearing.

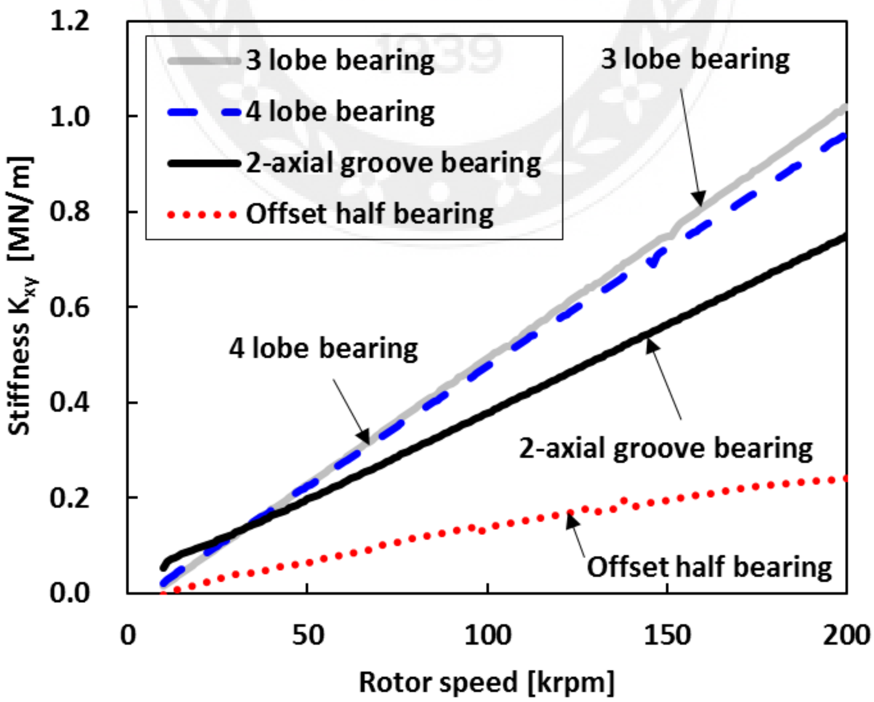

Fig. 21 Stiffness coefficients K_{xy} of turbine side bearing.

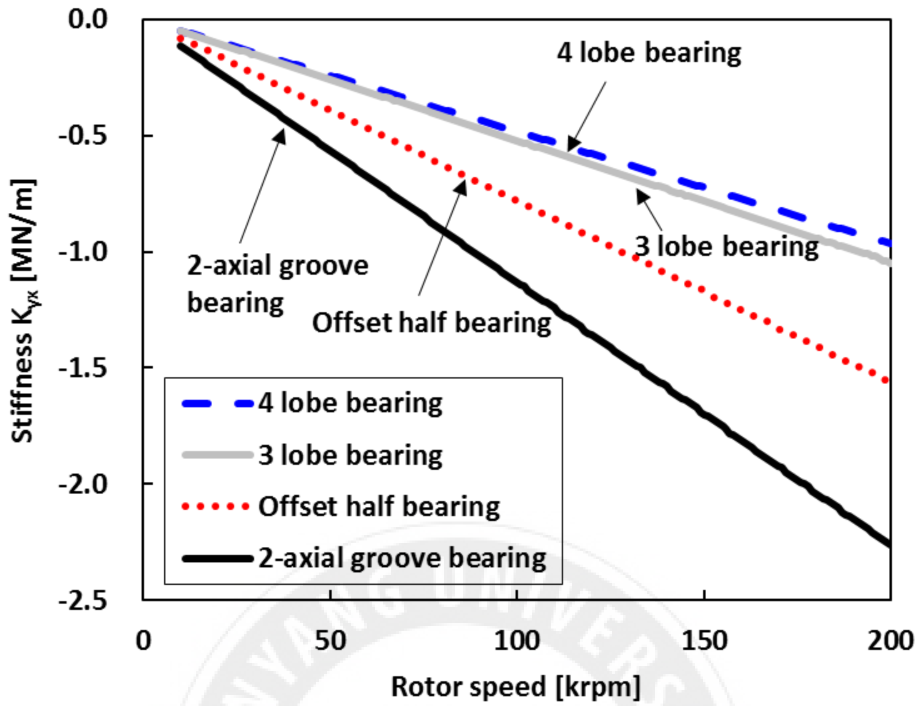

Fig. 22 Stiffness coefficients K_{yx} of compressor side bearing.

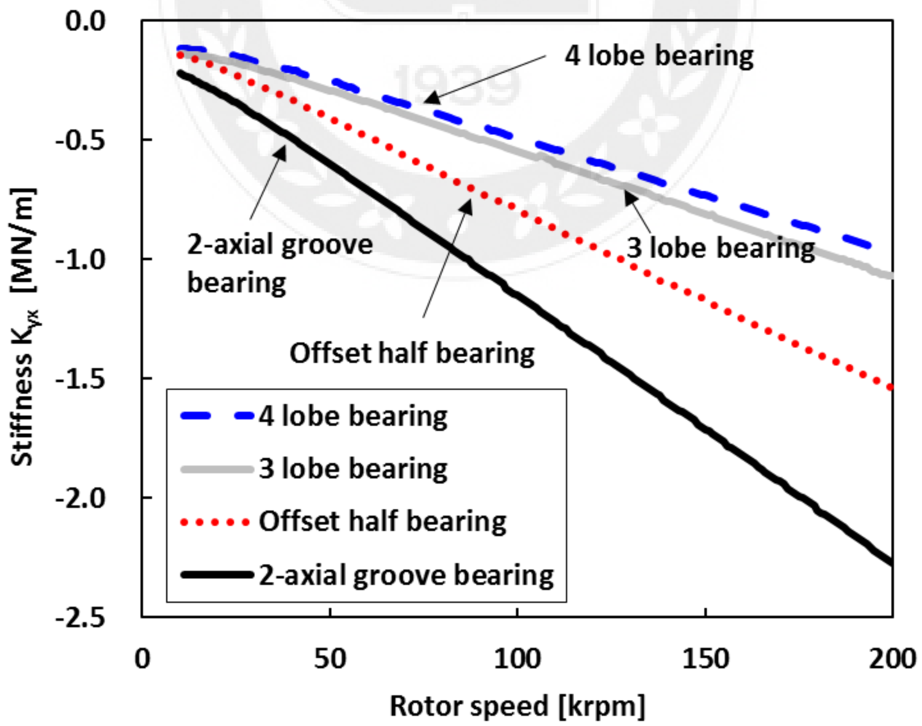

Fig. 23 Stiffness coefficients K_{yx} of turbine side bearing.

Figures 24 and 25 show analysis results of stiffness coefficients in the y-direction, offset-half bearings present higher stiffness coefficients K_{yy} than other bearings. Similar to stiffness coefficients K_{xx}, higher shaft speed of bearings have higher stiffness coefficients than other bearings. Moreover, this process is approximately linear. In both side bearings, offset half bearing stiffness coefficients K_{yy} are highest, 3 lobe bearing stiffness coefficients K_{yy} are higher than 4 lobe bearing stiffness coefficients K_{yy}, and lowest bearings stiffness coefficients K_{yy} are coming from 2-axial groove bearings.

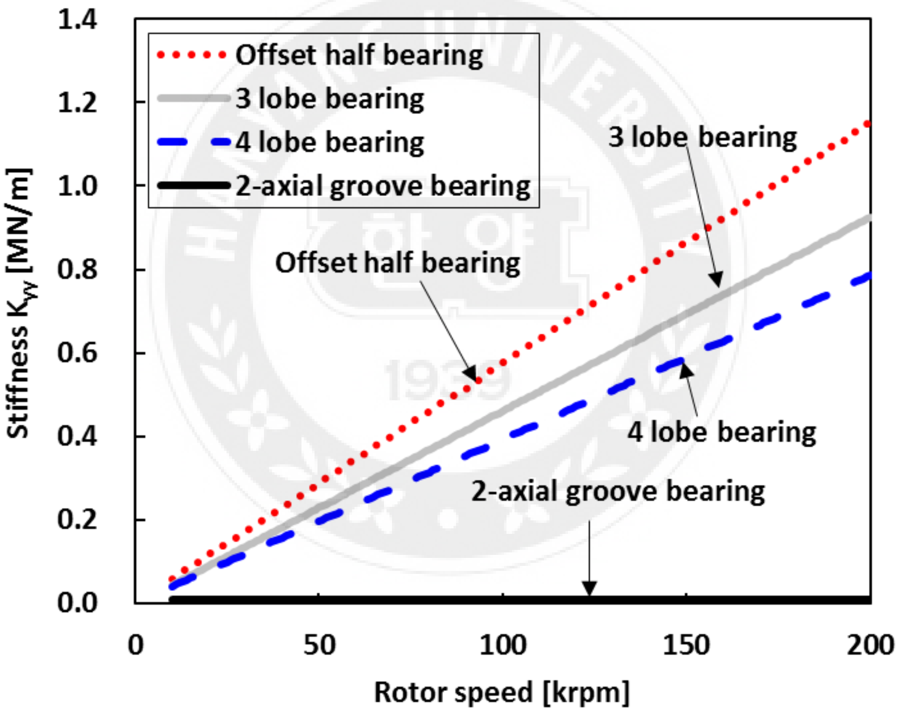

Fig. 24 Stiffness coefficients K_{yy} of compressor side bearing.

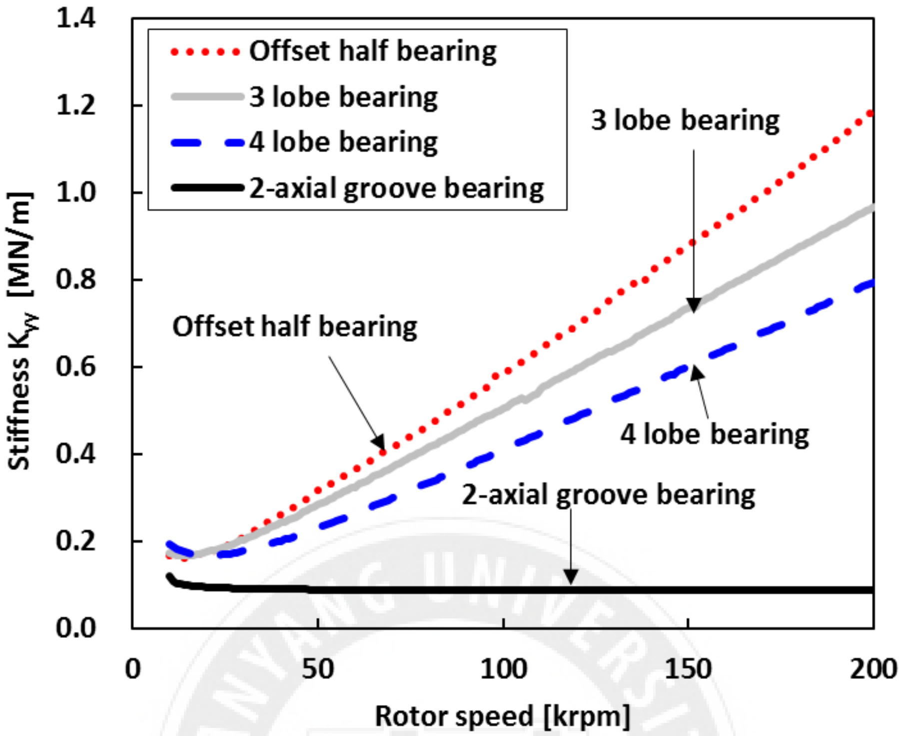

Fig. 25 Stiffness coefficients K_{yy} of turbine side bearing.

Damping coefficients depend on fluid viscosity and journal equilibrium position. When the viscosity is a constant value, damping coefficient only depends on equilibrium position. Figures 26 and 27 present damping coefficients of each bearing. Damping coefficients C_{xx} of compressor side bearings are almost constant. 3 lobe bearings show highest damping coefficients on the compressor side. 4 lobe bearing damping coefficients C_{xx} are higher than 2-axial groove bearings, and lowest damping coefficients C_{xx} are coming from offset half bearings. On turbine side, these damping coefficients C_{xx} are similar in high shaft speed (> 25,000 rpm).

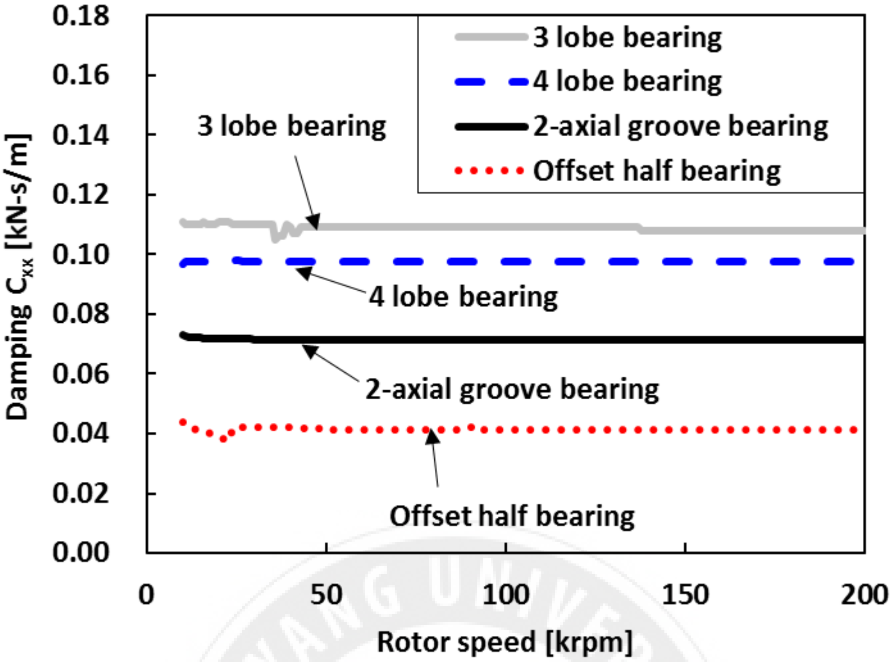

Fig. 26 Damping coefficients C_{xx} of compressor side bearing.

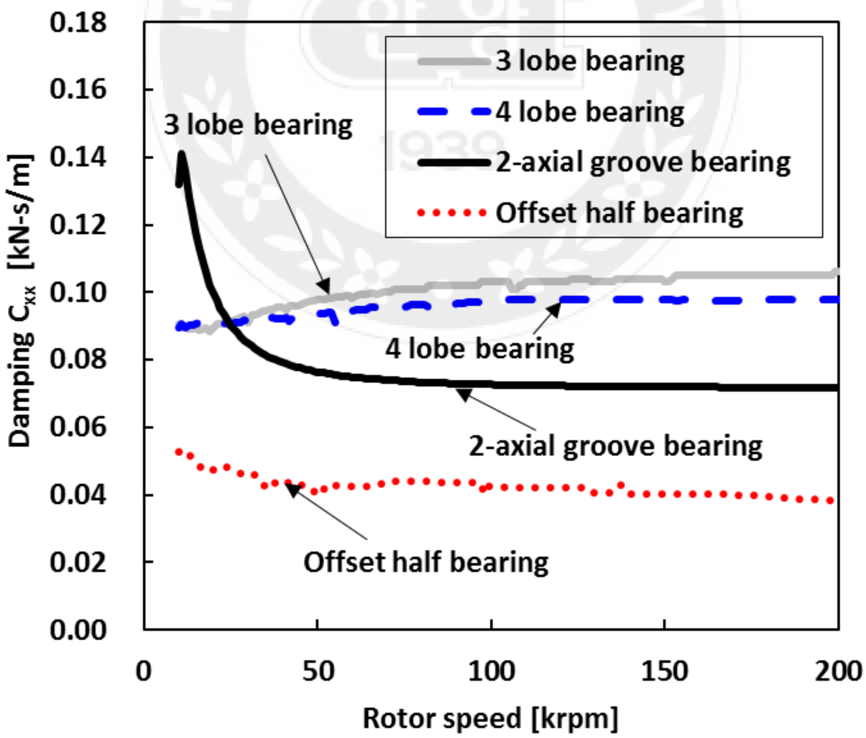

Fig. 27 Damping coefficients C_{xx} of turbine side bearing.

Figures 28 and 29 present negative value of cross-coupled damping coefficients C_{xy} of each bearing. When rotation speed is increasing, all bearings cross-coupled damping coefficients C_{xy} increase slowly. 0045ven in compressor side offset-half bearings, cross-coupled damping coefficients are almost constant value in whole operation speed range. Turbine side bearing has relatively significant changes in damping coefficients C_{xy}. It means equilibrium position also has a relatively significant change. Compare lobe number, offset half bearings had smallest damping coefficients C_{xy} in turbine side bearing. By the way, Figures 30 and 31 show figures of damping coefficients C_{yx} are similar to damping coefficients C_{xy}.

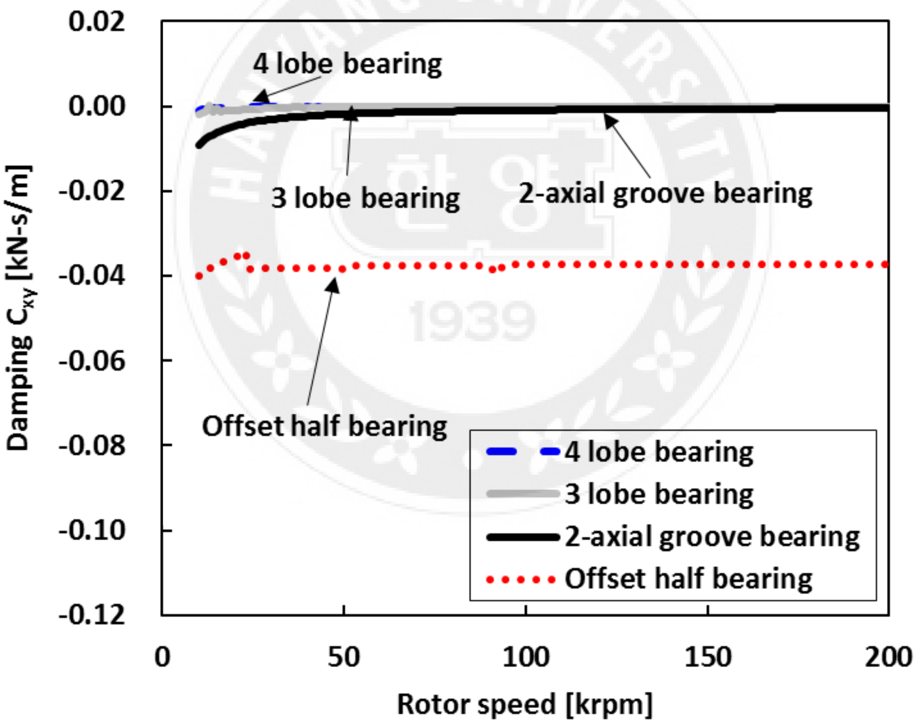

Fig. 28 Damping coefficients C_{xy} of compressor side bearing.

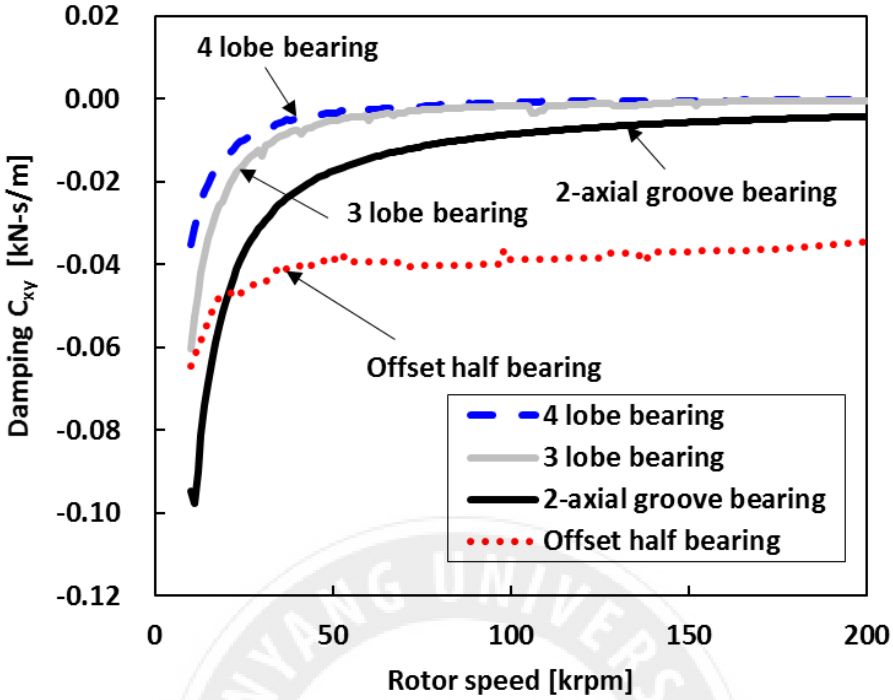

Fig. 29 Damping coefficients C_{xy} of turbine side bearing.

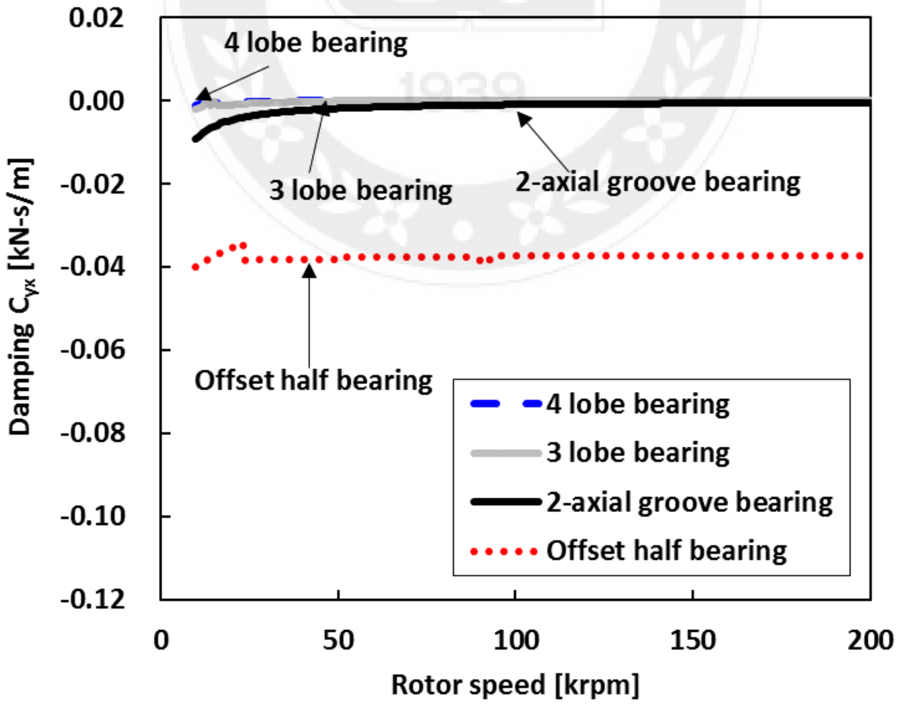

Fig. 30 Damping coefficients C_{yx} of compressor side bearing.

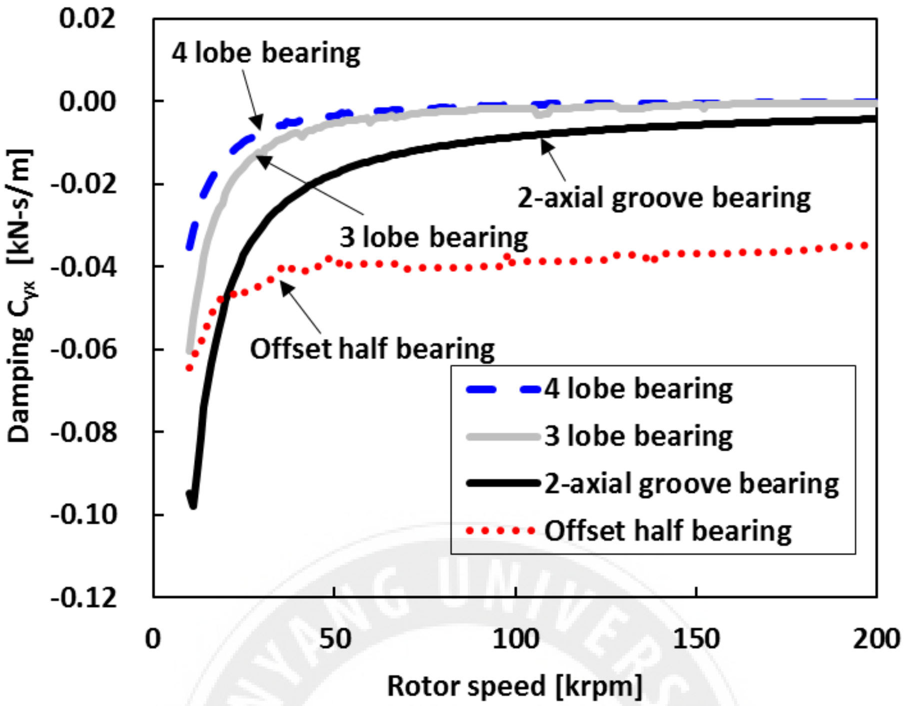

Fig. 31 Damping coefficients C_{yx} of turbine side bearing.

Below two damping coefficient figures shown damping coefficients C_{yy}. Apparently, 2-axial groove bearings have highest damping coefficient $C_{yy;}$ other bearings have damping coefficients C_{yy} almost equal to 0. Figures 32 and 33 present damping coefficients C_{yy} of TC supported on each bearing.

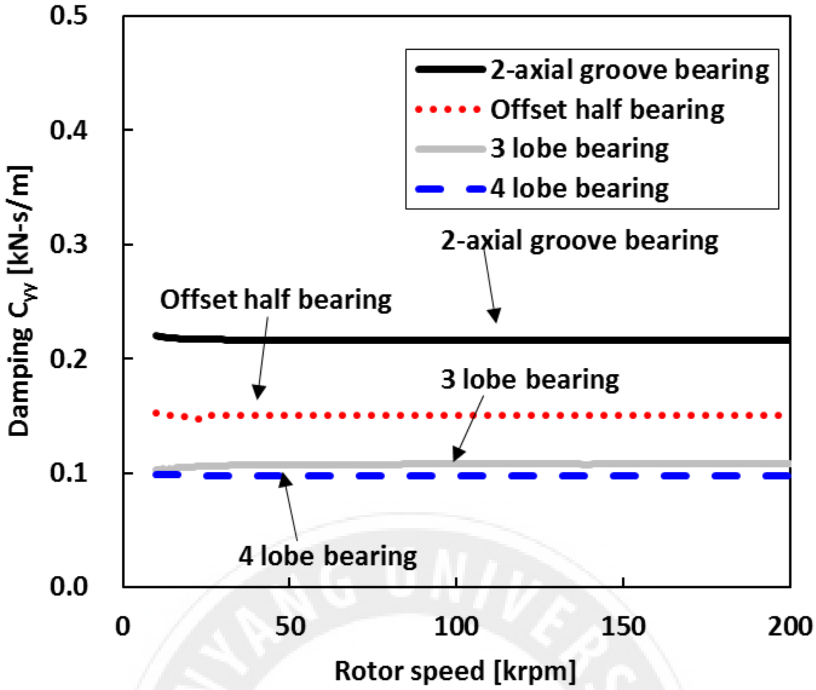

Fig. 32 Damping coefficients C_{yy} of compressor side bearing.

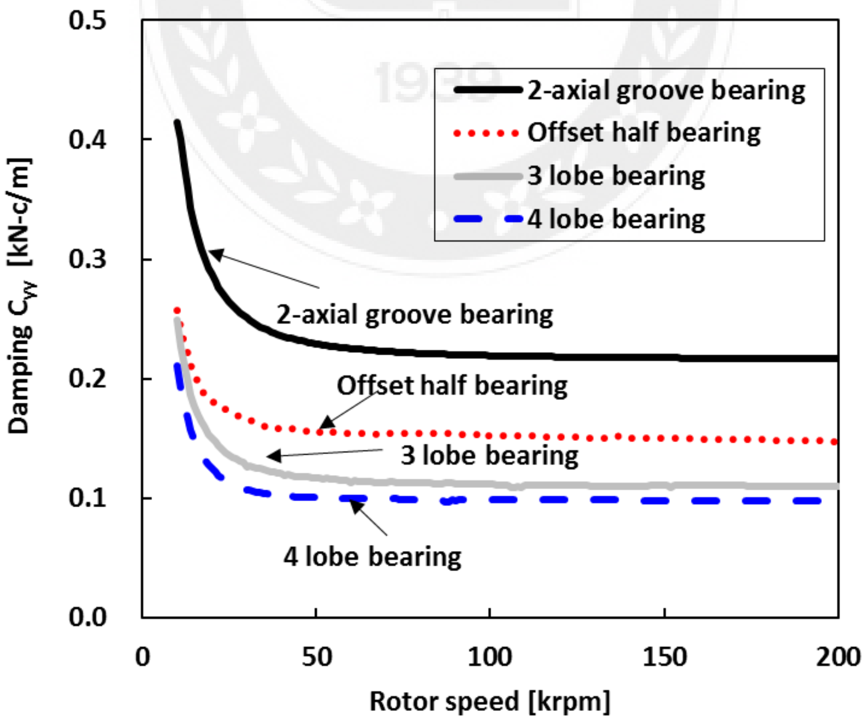

Fig. 33 Damping coefficients C_{yy} of turbine side bearing.

Preload *m* and offset *α* are the significant configurations of multi-lobe bearing analysis. For a more intuitive analysis of these configurations effect of the multi-lobe bearing. The next research compares the dynamic force coefficients (stiffness and damping) of 3 lobe bearing using different preload and offset. When preload is equal to 0, the offset does not make sense in this condition.

Figures 34 through 37 show direct stiffness force coefficients K_{xx} and K_{yy} of 3 lobe bearing using different preload and offset. When preload=0, the direct stiffness force coefficients change negligible (or even decreases) as rotor speed increases. When preload is not equal to 0, the direct stiffness force coefficients increases as rotor speed increases. In this case, higher offset provides higher stiffness force coefficients. On the other hand, higher preload provides higher stiffness force coefficients in the same offset condition. Appendix A include the input data of these bearings (Figures A. 1 through A. 12).

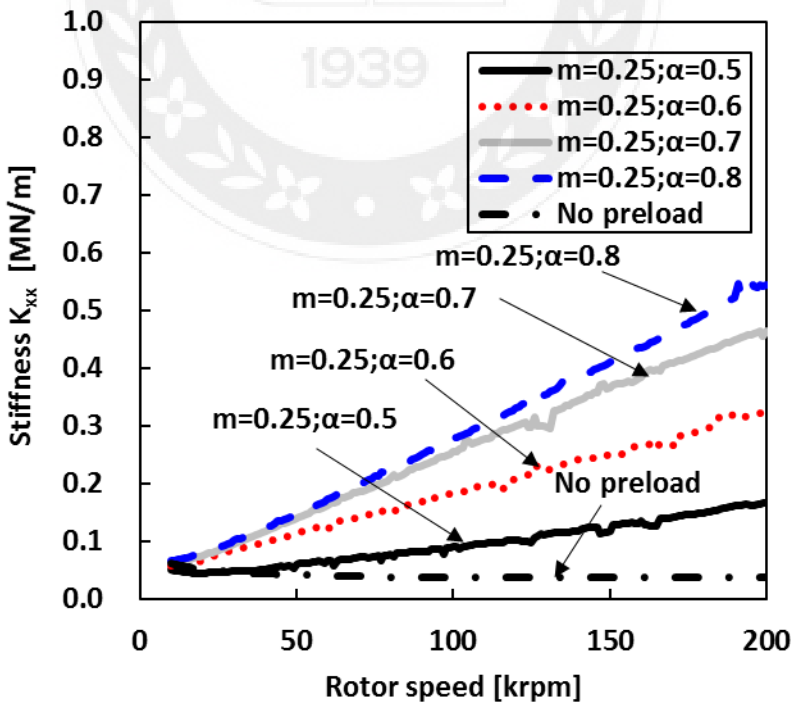

Fig. 34 Stiffness coefficients K_{xx} of 3 lobe bearing (preload=0.25; no preload)

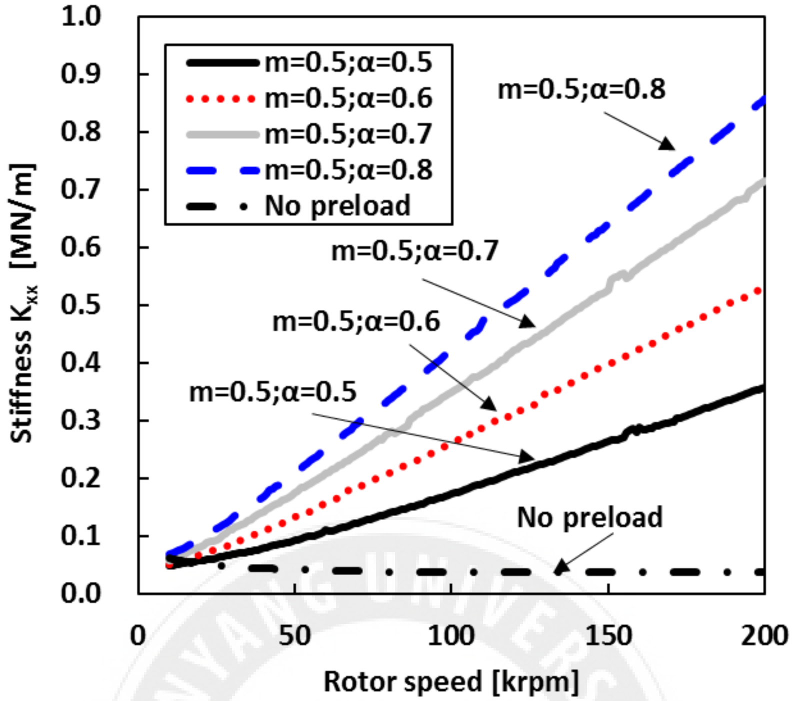

Fig. 35 Stiffness coefficients K_{xx} of 3 lobe bearing (preload=0.5; no preload)

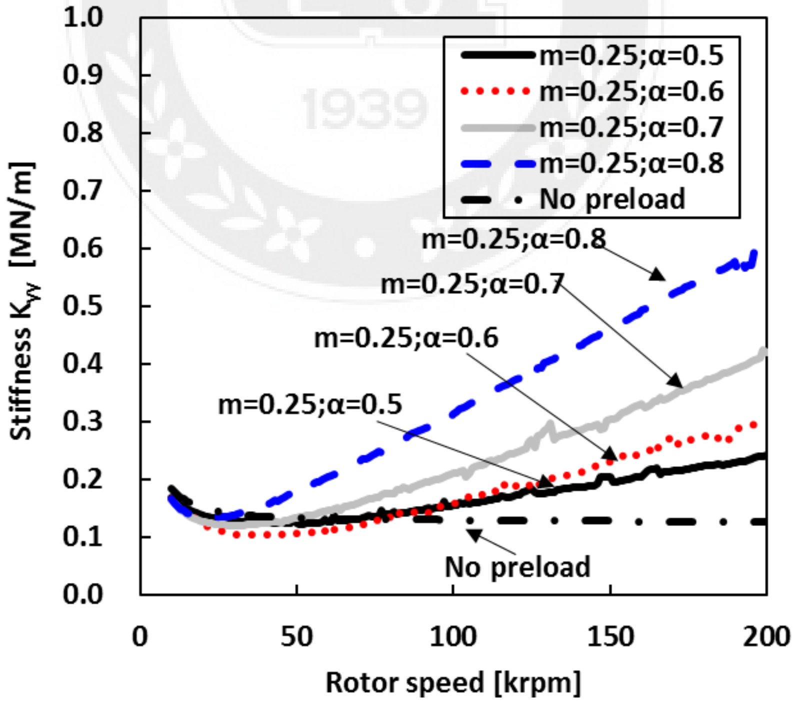

Fig. 36 Stiffness coefficients K_{yy} of 3 lobe bearing (preload=0.25; no preload)

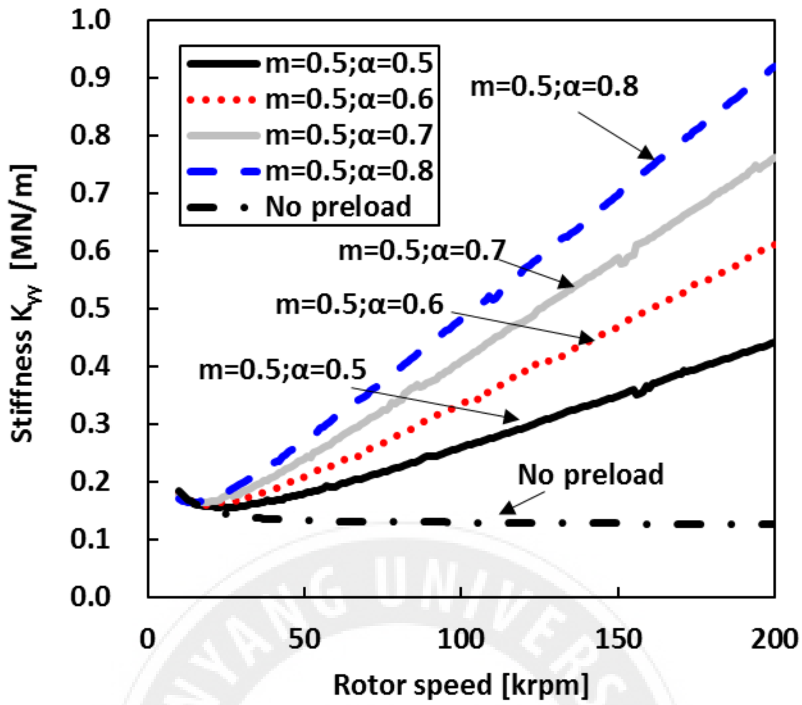

Fig. 37 Stiffness coefficients K_{yy} of 3 lobe bearing (preload=0.5; no preload)

Figures 38 through 41 show cross-coupled stiffness force coefficients K_{xy} and K_{yx} of 3 lobe bearing using different preload and offset. When preload is not equal to 0, the direct stiffness force coefficients increases as rotor speed increases. In this case, higher offset provides higher stiffness force coefficients. On the other hand, higher preload provides lower stiffness force coefficients in the same offset condition.

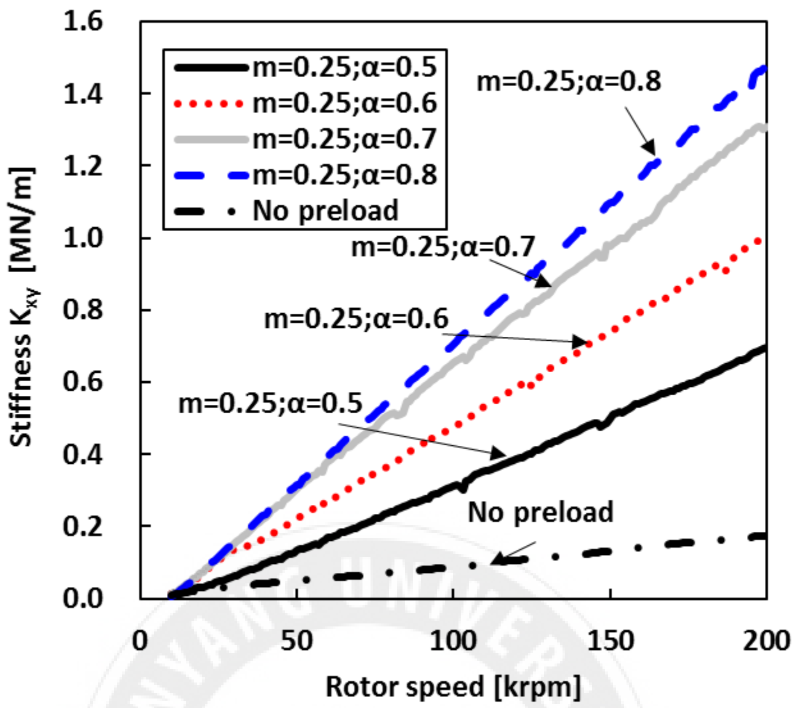

Fig. 38 Stiffness coefficients K_{xy} of 3 lobe bearing (preload=0.25; no preload)

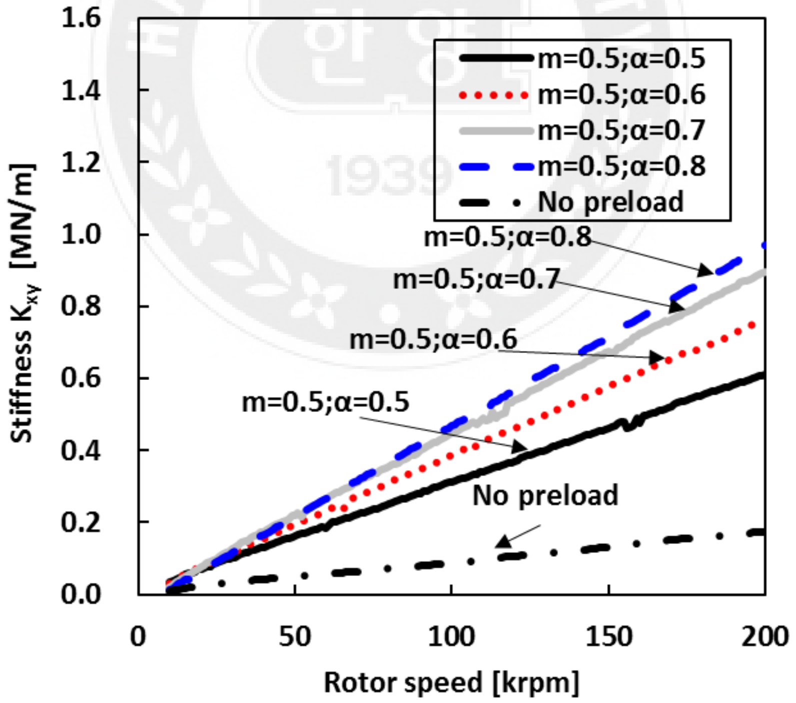

Fig. 39 Stiffness coefficients K_{xy} of 3 lobe bearing (preload=0.5; no preload)

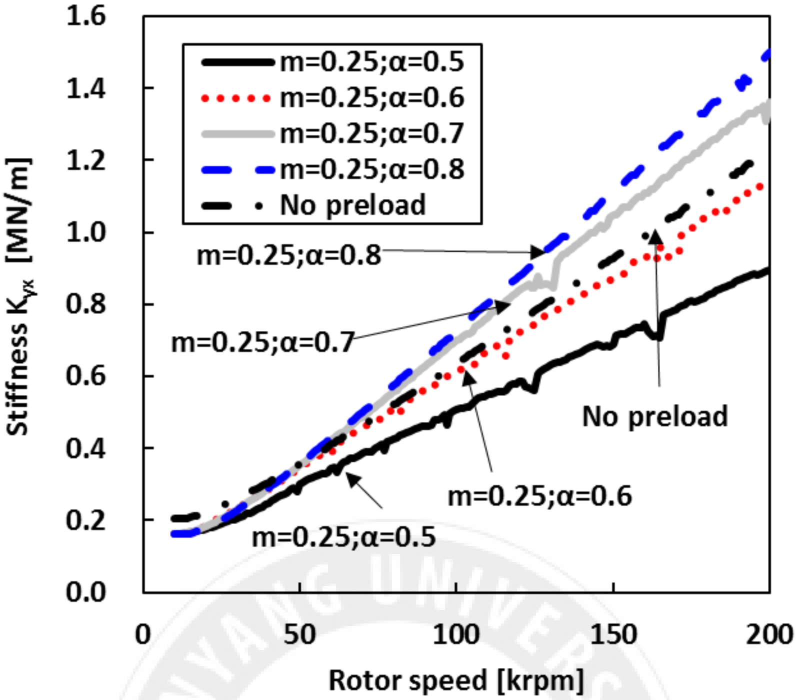

Fig. 40 Stiffness coefficients -K_{yx} of 3 lobe bearing (preload=0.25; no preload)

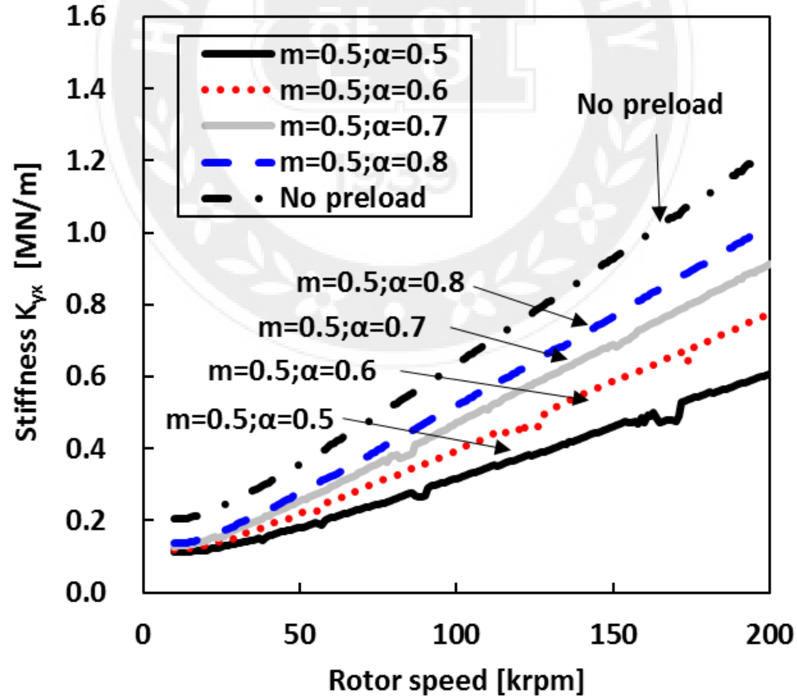

Fig. 41 Stiffness coefficients -K_{yx} of 3 lobe bearing (preload=0.5; no preload)

Figures 42 through 45 show direct damping force coefficients C_{xx} and C_{yy} of 3 lobe bearing using different preload and offset. When preload=0, the direct damping force coefficients change negligible (or even decreases) as rotor speed increases. When preload is not equal to 0, the direct damping force coefficients C_{xx} are lowest. In this case, higher offset provides higher damping force coefficients. On the other hand, higher preload provides lower damping force coefficients in the same offset condition.

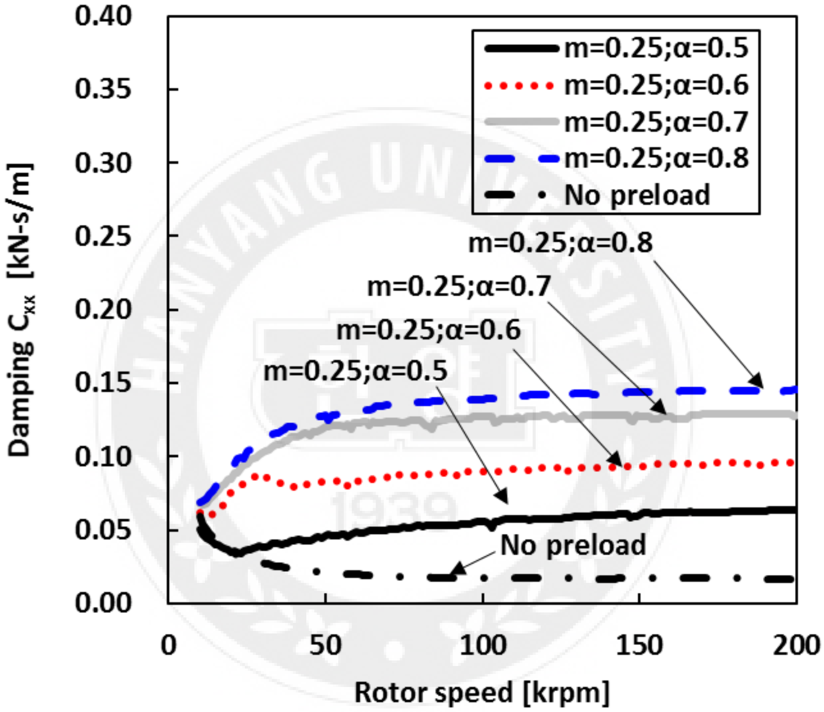

Fig. 42 Damping coefficients C_{xx} of 3 lobe bearing (preload=0.25; no preload)

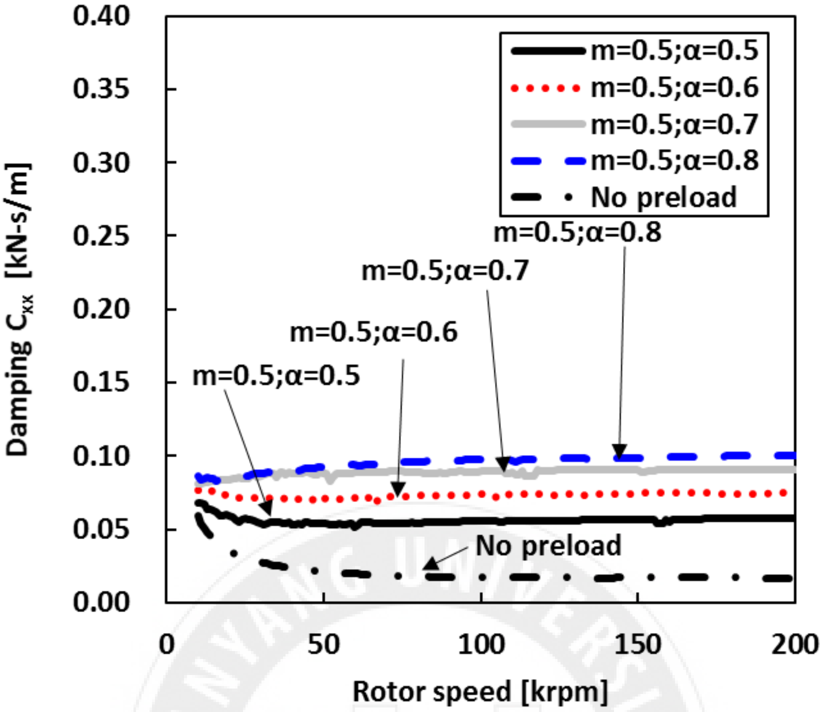

Fig. 43 Damping coefficients C_{xx} of 3 lobe bearing (preload=0.5; no preload)

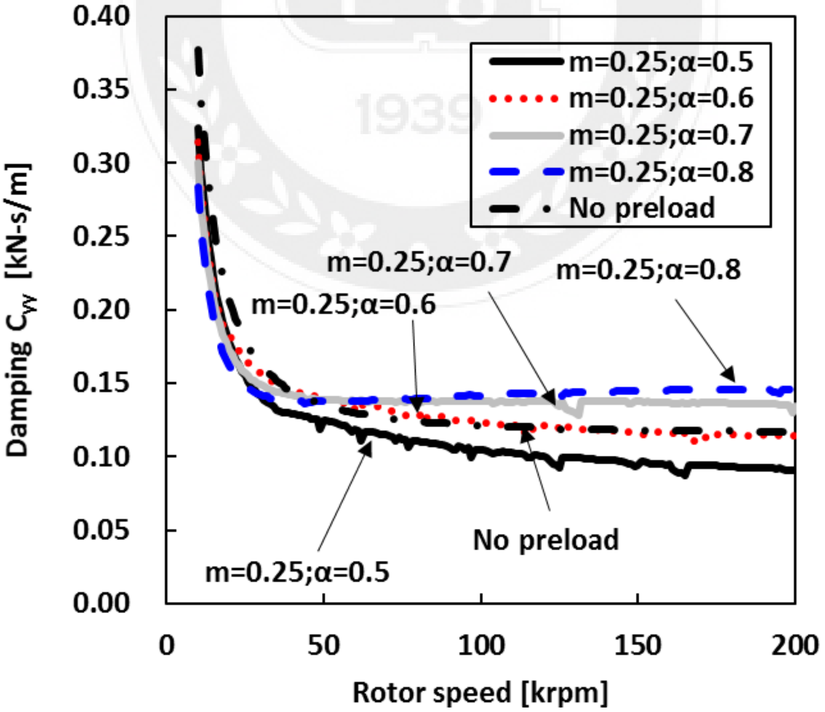

Fig. 44 Damping coefficients C_{yy} of 3 lobe bearing (preload=0.25; no preload)

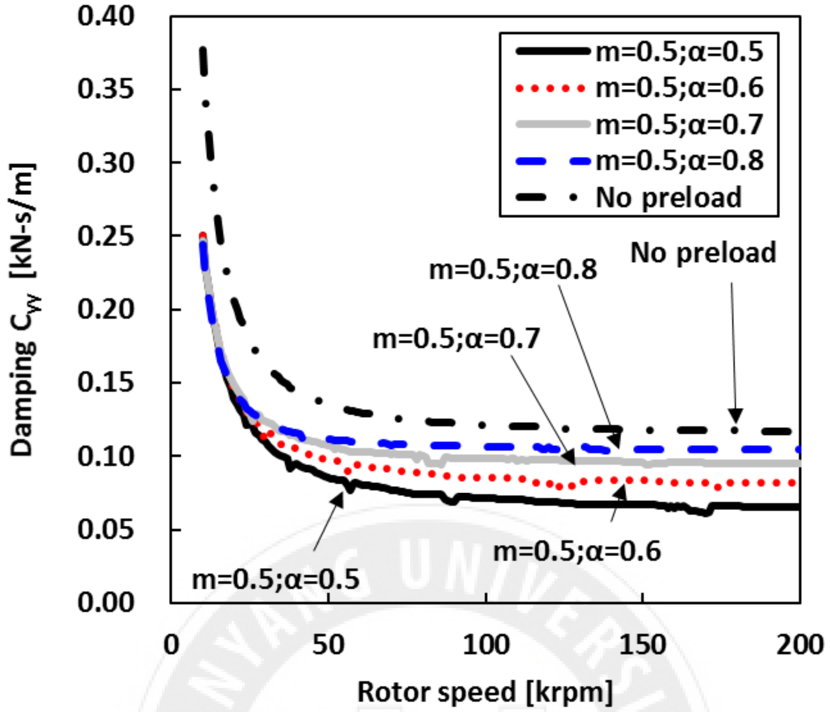

Fig. 45 Damping coefficients C_{xx} of 3 lobe bearing (preload=0.5; no preload)

Figures 46 through 49 show cross-coupled damping force coefficients C_{xy} and C_{yx} of 3 lobe bearing using different preload and offset. All the cross-coupled damping force coefficients C_{xy} and C_{yx} become 0 when rotor speed increase.

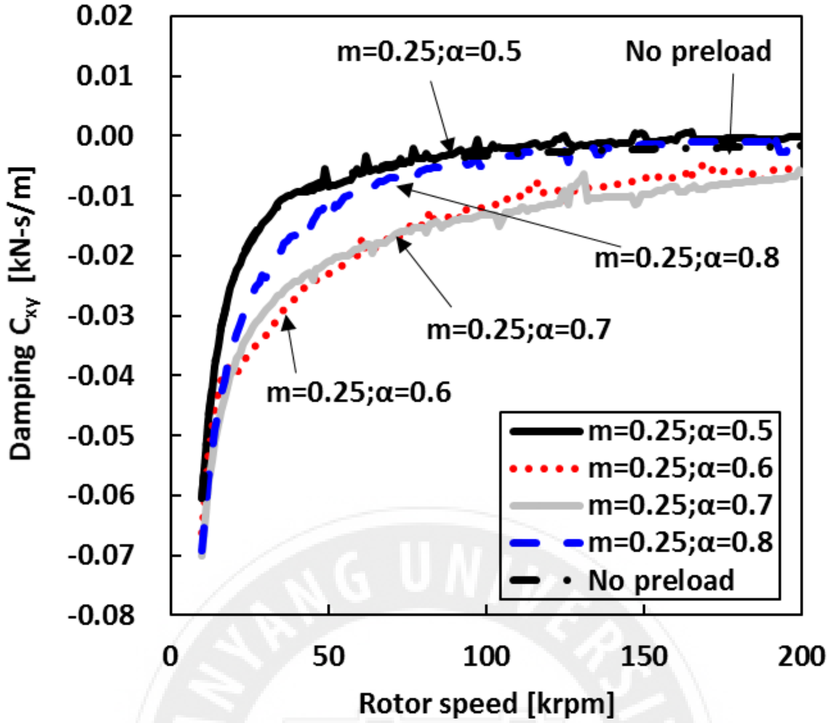

Fig. 46 Damping coefficients C_{xy} of 3 lobe bearing (preload=0.25; no preload)

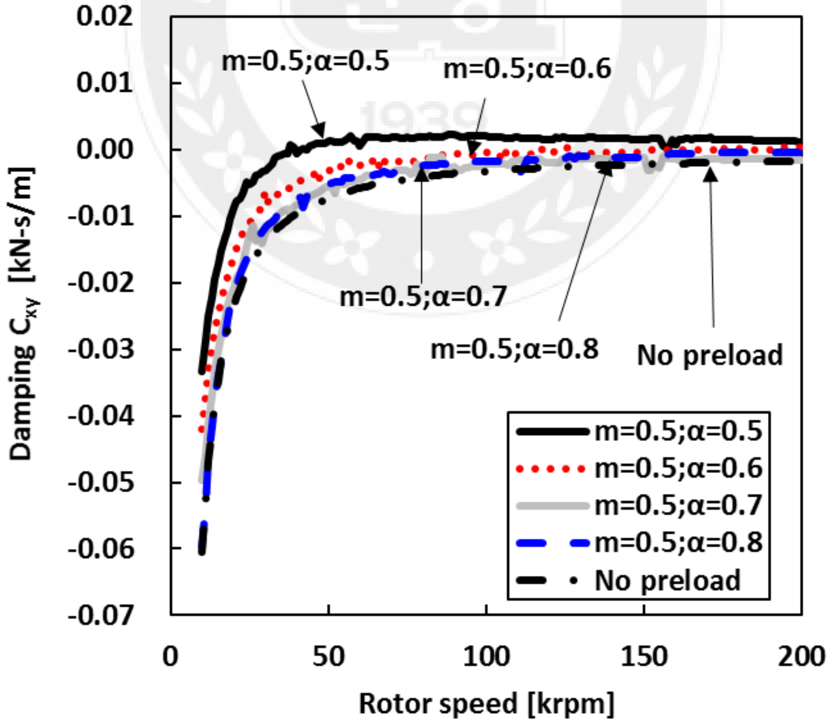

Fig. 47 Damping coefficients C_{xy} of 3 lobe bearing (preload=0.5; no preload)

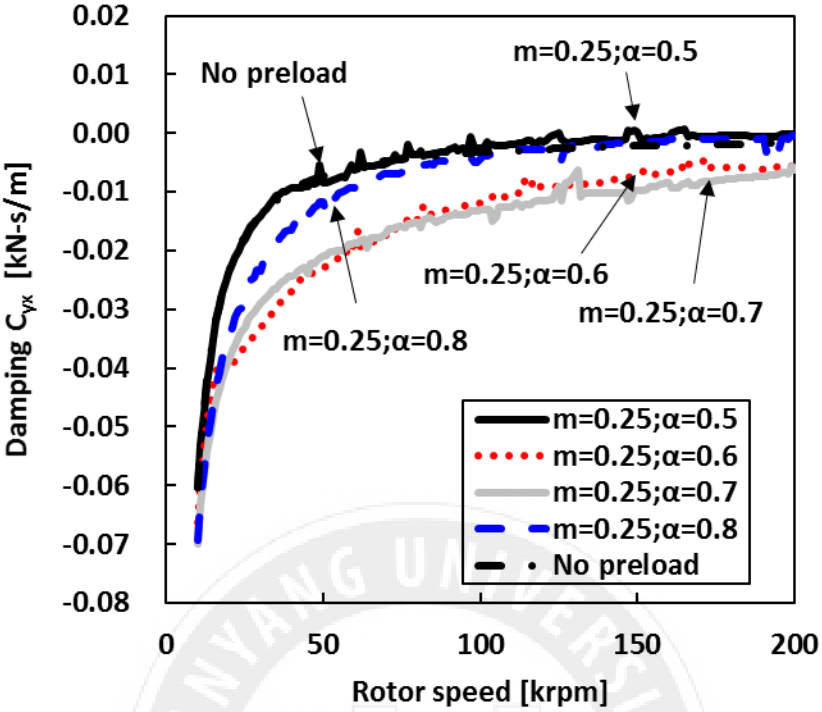

Fig. 48 Damping coefficients C_{yx} of 3 lobe bearing (preload=0.25; no preload)

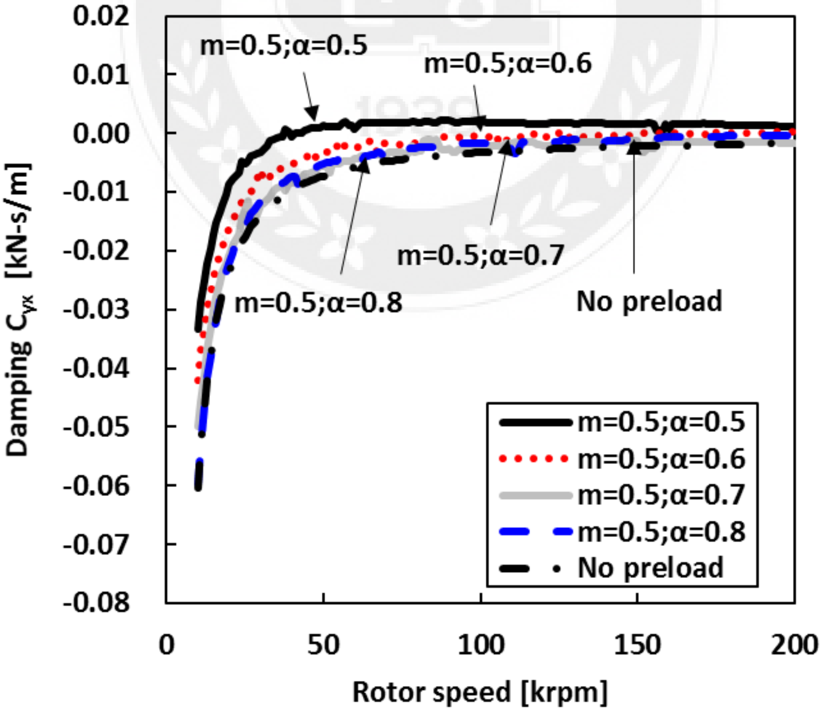

Fig. 49 Damping coefficients C_{yx} of 3 lobe bearing (preload=0.5; no preload)

In the multi-lobe bearing, the pad length of bearing lobe is an important configuration. For a more intuitive analysis of this configuration effect of the multi-lobe bearing. The next research compares the dynamic force coefficients (stiffness and damping) of a 3 lobe bearing using different pad angle. The bearing preload=0.5 and offset=0.5 in this comparison.

Figures 50 and 51 show direct stiffness force coefficients K_{xx} and K_{yy} of 3 lobe bearing using different pad angle. Obviously, higher pad angle provides higher direct stiffness force coefficients of the 3 lobe bearing.

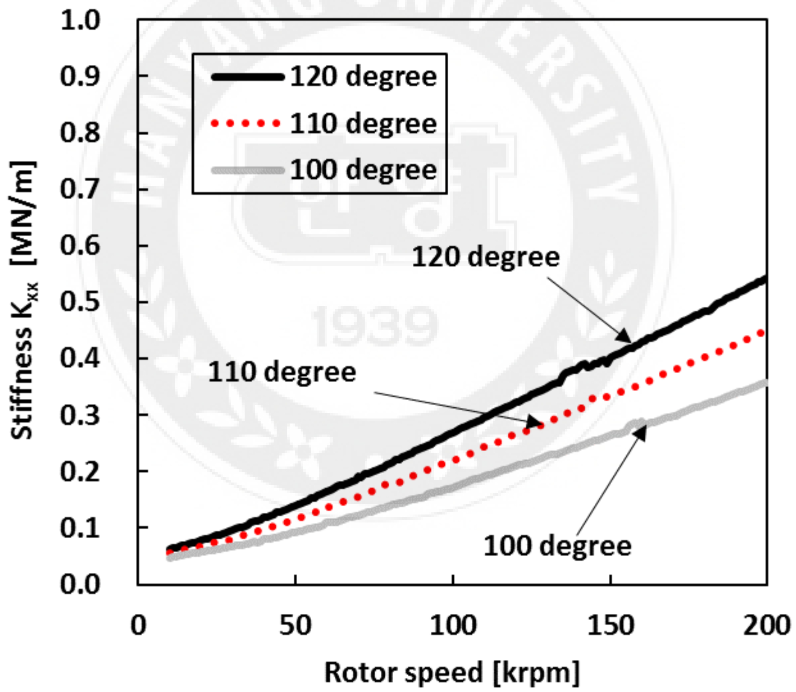

Fig. 50 Stiffness coefficients K_{xx} of 3 lobe bearing. Pad length of 120, 110, and 100 degrees

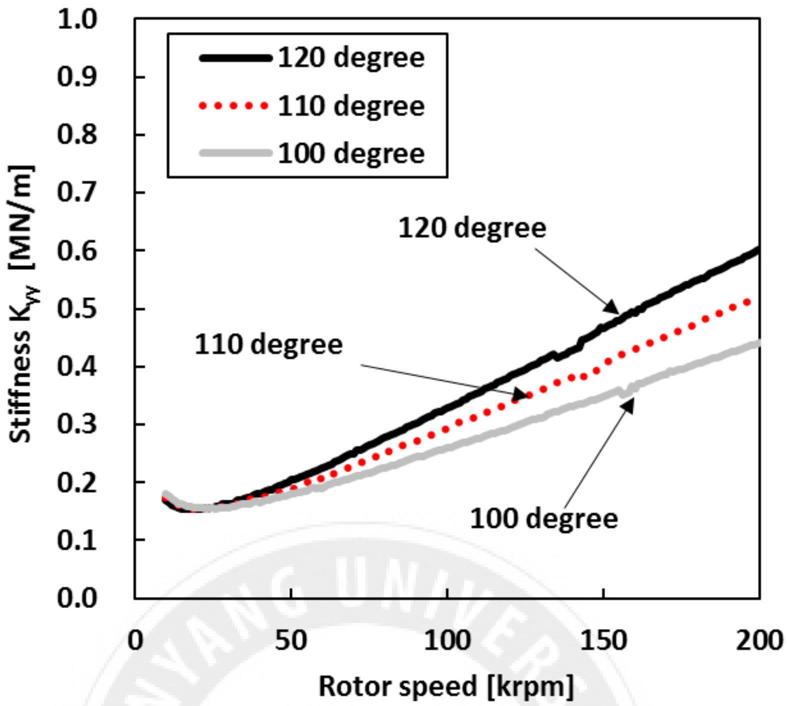

Fig. 51 Stiffness coefficients K_{yy} of 3 lobe bearing. Pad length of 120, 110, and 100 degrees

Figures 52 and 53 show cross-coupled stiffness force coefficients K_{xy} and K_{yx} of 3 lobe bearing using different pad angle. Obviously, higher pad angle provides higher cross-coupled stiffness force coefficients of the 3 lobe bearing.

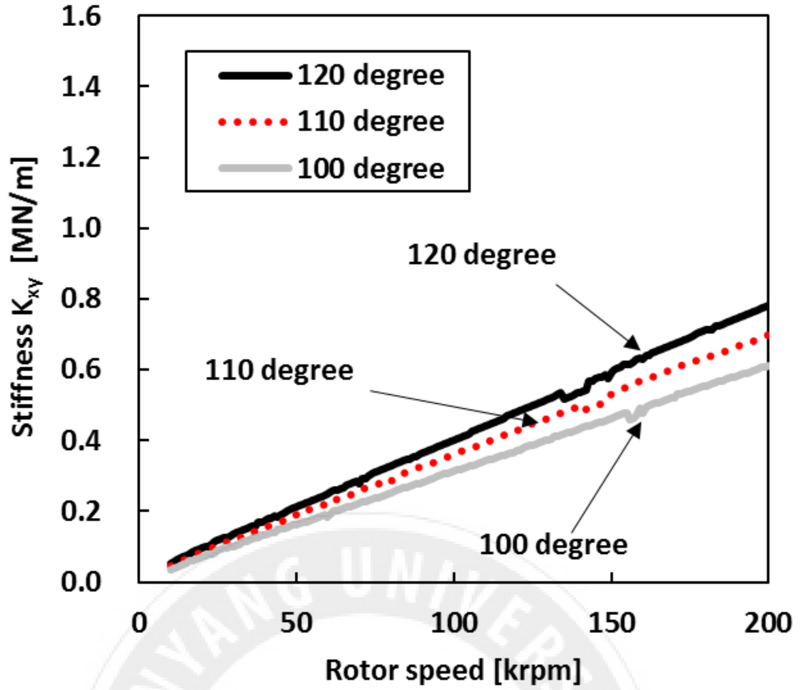

Fig. 52 Stiffness coefficients K_{xy} of 3 lobe bearing. Pad length of 120, 110, and 100 degrees

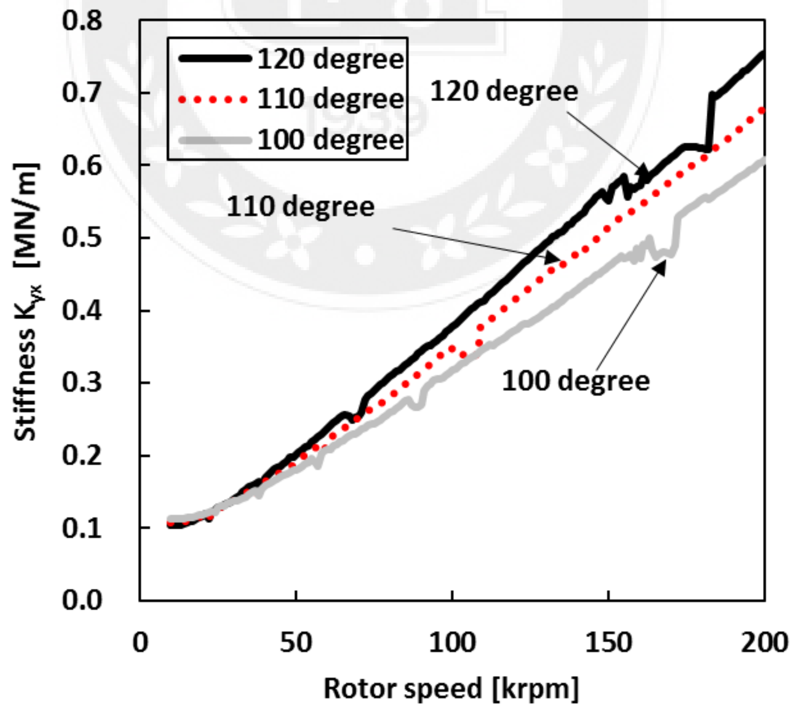

Fig. 53 Stiffness coefficients K_{yx} of 3 lobe bearing. Pad length of 120, 110, and 100 degrees

Figures 54 and 55 show direct damping force coefficients C_{xx} and C_{yy} of 3 lobe bearing using different pad angle. Obviously, higher pad angle provides higher direct damping force coefficients of the 3 lobe bearing.

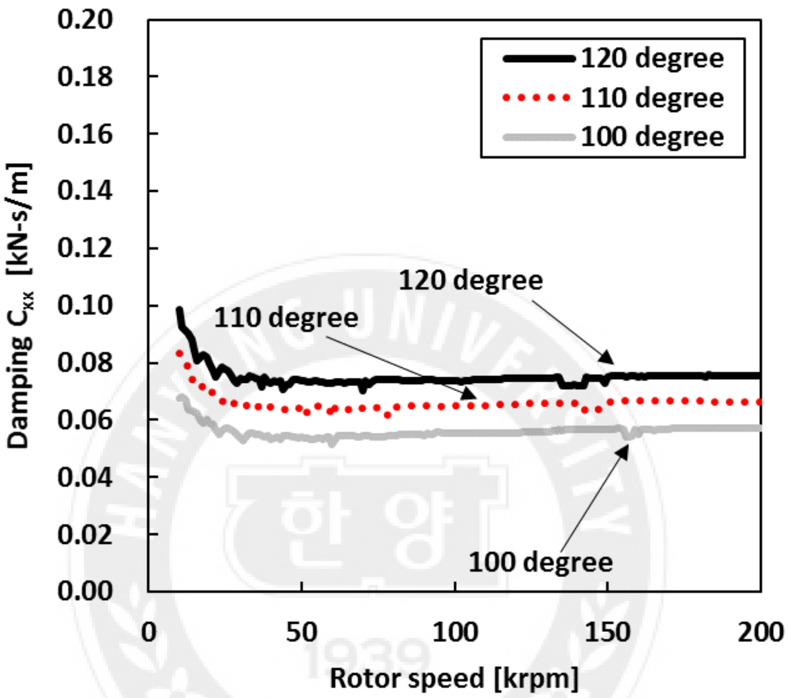

Fig. 54 Damping coefficients C_{xx} of 3 lobe bearing. Pad length of 120, 110, and 100 degrees

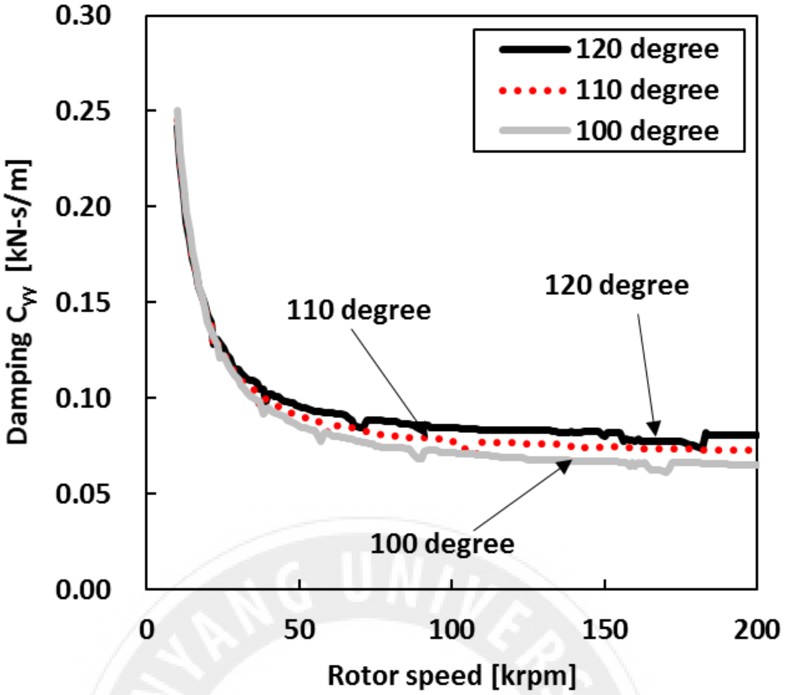

Fig. 55 Damping coefficients C_{yy} of 3 lobe bearing. Pad length of 120, 110, and 100 degrees

Figures 54 and 55 show cross-coupled damping force coefficients C_{xx} and C_{yx} of 3 lobe bearing using different pad angles. These figures show similar cross-coupled damping force coefficients of 3 lobe bearing using different pad angles.

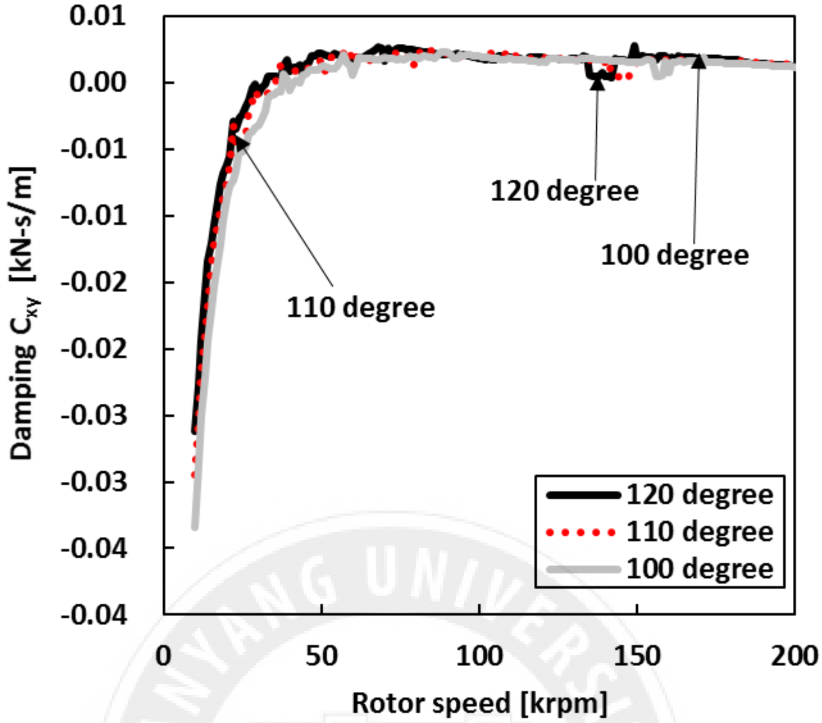

Fig. 56 Damping coefficients C_{xy} of 3 lobe bearing. Pad length of 120, 110, and 100 degrees

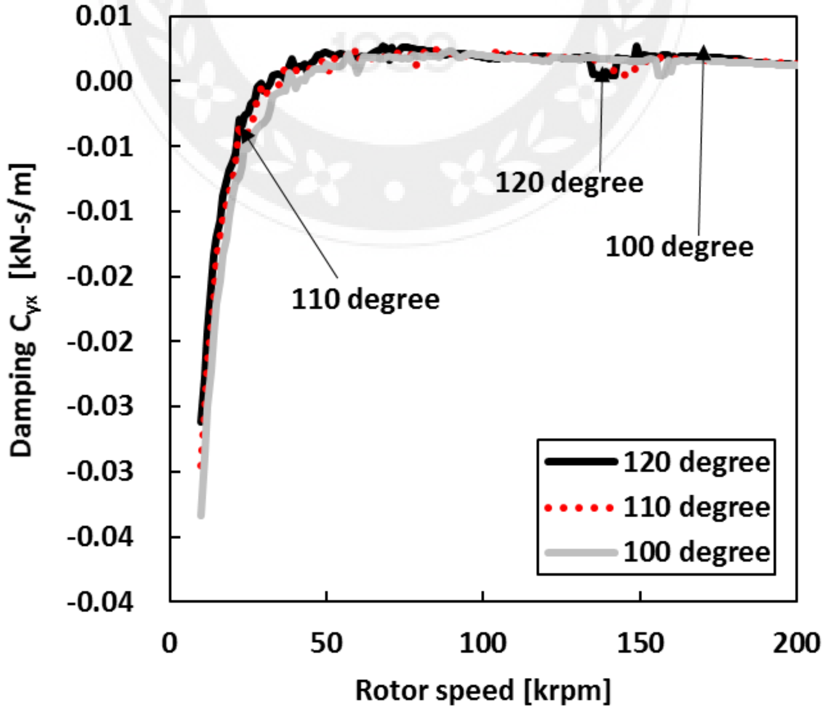

Fig. 57 Damping coefficients C_{yx} of 3 lobe bearing. Pad length of 120, 110, and 100 degrees

After analysis of bearings, this study export dynamic force coefficients (stiffness and damping) into rotor-bearing system dynamic analysis.

4.2 Predicted rotordynamic performance

Input characteristic of this analysis is shaft rotational speeds and number of modes. The number of modes is used to specify the number of processional modes that calculate mode shapes (eigenvectors). Only lowest 4 to 6 processional modes are essential. More modes need for large systems.

A complex eigenvalue λ (lambda) is given by:

$$\lambda_i = \sigma_i + j\omega_{di} \tag{3}$$

Subscript *i* is mode number. If the damped natural frequency is non-zero, this is a processional mode. Here oscillating frequency and damped natural frequency are same. If the damped natural frequency is zero, this is a real mode (pure rigid body) or non-oscillating mode. Here is the equation of logarithmic decrements:

$$\delta = ln\left(\frac{x_i}{x_{i+1}}\right) \tag{4}$$

where δ (Delta) logarithmic decrement

x_i amplitude of vibration at cycle *i*

x_{i+1} amplitude of vibration at cycle *i+1*

Logarithmic decrement reduced from vibrations equation of motion:

$$\delta = \frac{2\pi\zeta}{\sqrt{1-\zeta^2}} \tag{5}$$

where: $\zeta = \frac{C}{C_c}; \;\; C_c = 2Mw_n = 2\sqrt{KM}$

And where M mass

C damping

K stiffness

δ Log. Dec.

$\delta > 0$ stable or damped system

$\delta = 0$ threshold of instability

$\delta < 0$ unstable system

ζ damping ratio or damping factor

Linear eigenvalue analysis relies on the specification of stiffness and damping force coefficients for lubricant oil films at turbine and compressor side bearings. Linearized stiffness and damping force coefficients are calculated using commercial fluid film bearing program previously.

Existing configuration of turbocharger consists of the main rotor supported by four kinds of bearings. Turbocharger operational speed ranges between 2,000 to 200,000 rpm. This analysis input shows in Appendix B.

Figures 34 through 37 depict TC rotor mode shape plots at these three critical speeds supported on each bearing. This study chooses mode shapes on same rotor speed (120 krpm) to compare mode shapes easier. Mark "C" means compressor side and mark "T" means turbine side. In all operational range, this research assumes rotor speed from 2 krpm to 200 krpm, 1st critical speed is related to the conical mode of the rotor. In the conical mode, the frequency is from 43.26 Hz to 301.21 Hz. 2nd critical speed is related to rotor cylindrical-bending mode, showing greater motions at compressor side bearing than at turbine side bearing of the rotor-bearing system. Linear eigenvalue analysis shows frequency is from 66.77 Hz to 537.52 Hz in rotor speed from 2 krpm to 200 krpm. Last critical speed is related to first bending mode of the rotor. In first bending mode, the frequency is from 1278.1 Hz to 2520.5 Hz.

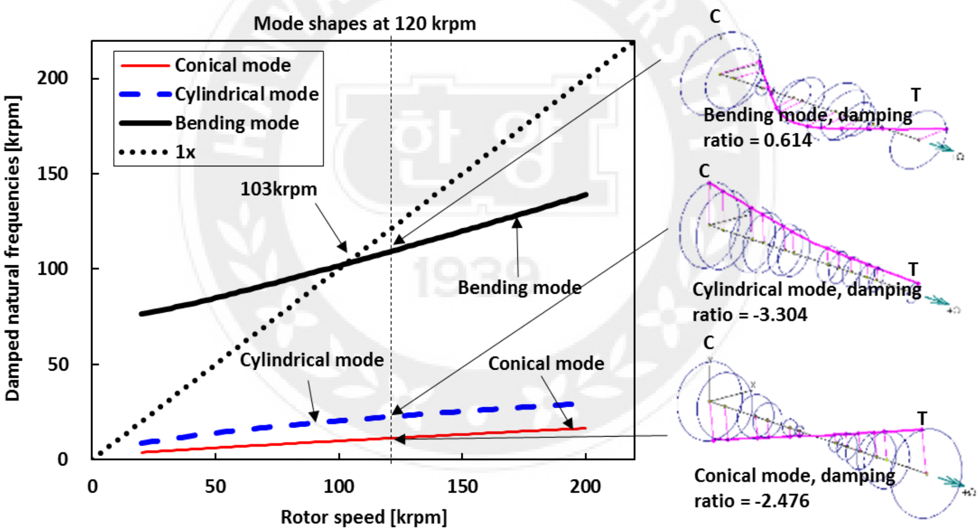

Fig. 58 TC rotor natural frequencies versus shaft speed. Rotor supported on 2-axial groove bearings.

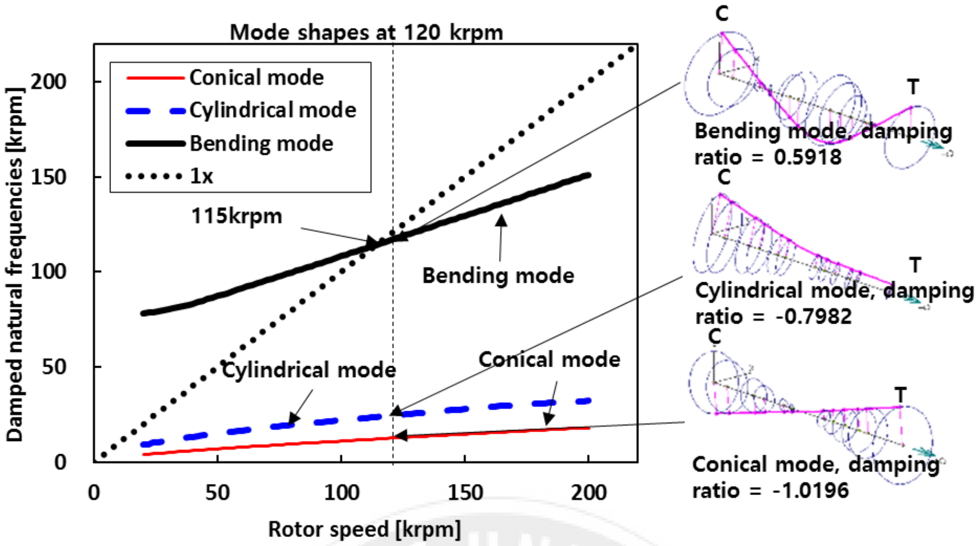

Fig. 59 TC rotor natural frequencies versus shaft speed. Rotor supported on offset-half bearings.

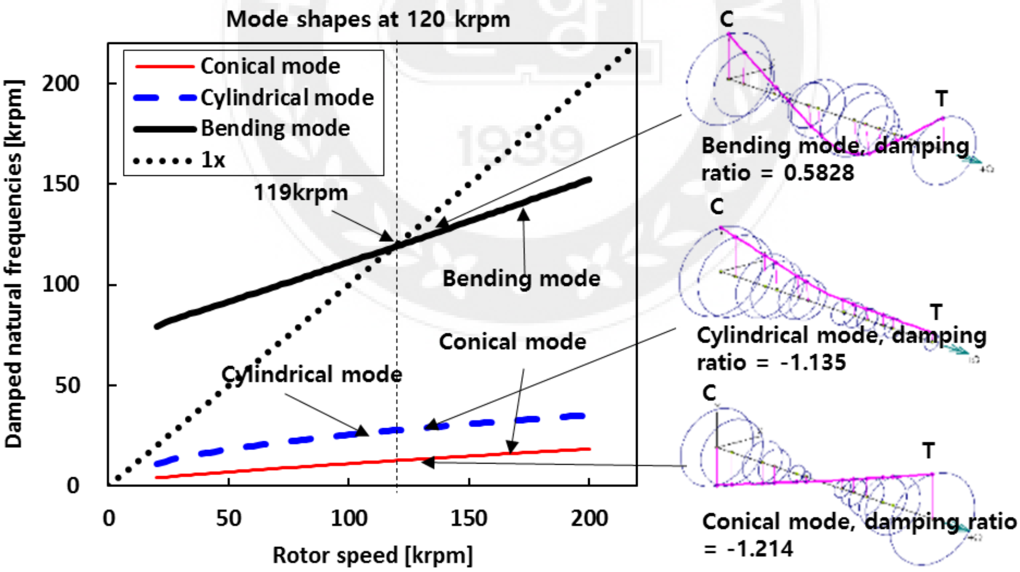

Fig. 60 TC rotor natural frequencies versus shaft speed. Rotor supported on 3 lobe bearings.

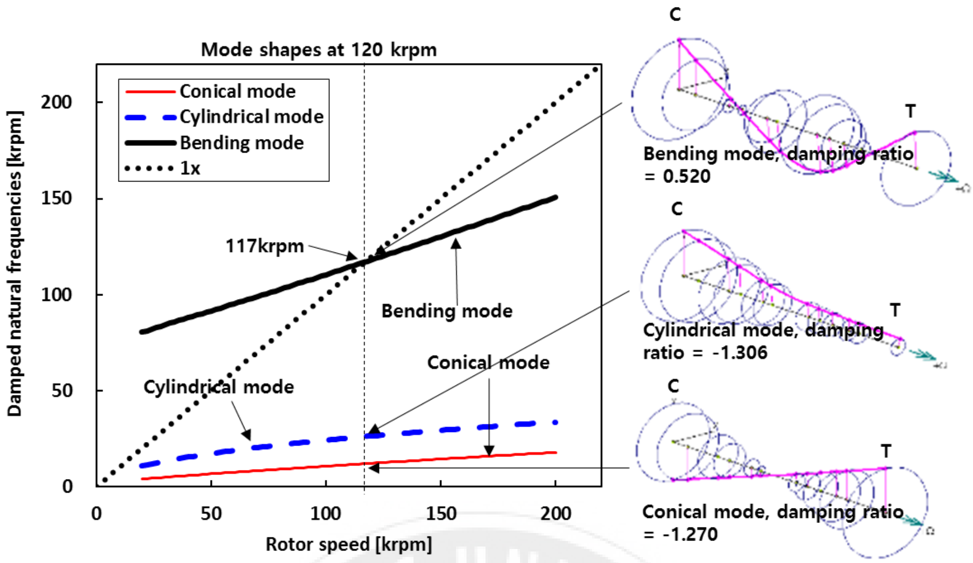

Fig. 61 TC rotor natural frequencies versus shaft speed. Rotor supported on 4 lobe bearings.

Figures 38 through 41 depict TC damping ratios supported on each bearing. A stable system has a damping ratio >0, and an unstable system has a negative damping ratio. Results show all rotor-bearing systems are unstable. After analyzing each mode shapes, conical modes are unstable of all bearings, and bending modes are stable of all bearings. The difference comes from the cylindrical mode, 2-axial groove bearings and offset-half bearings have an unstable cylindrical mode in operational range. 3 lobe bearing cylindrical mode become stable to unstable from rotor speed increased from 30 to 32 krpm and 4 lobe bearing cylindrical mode become stable to unstable from rotor speed increased from 26 to 28 krpm.

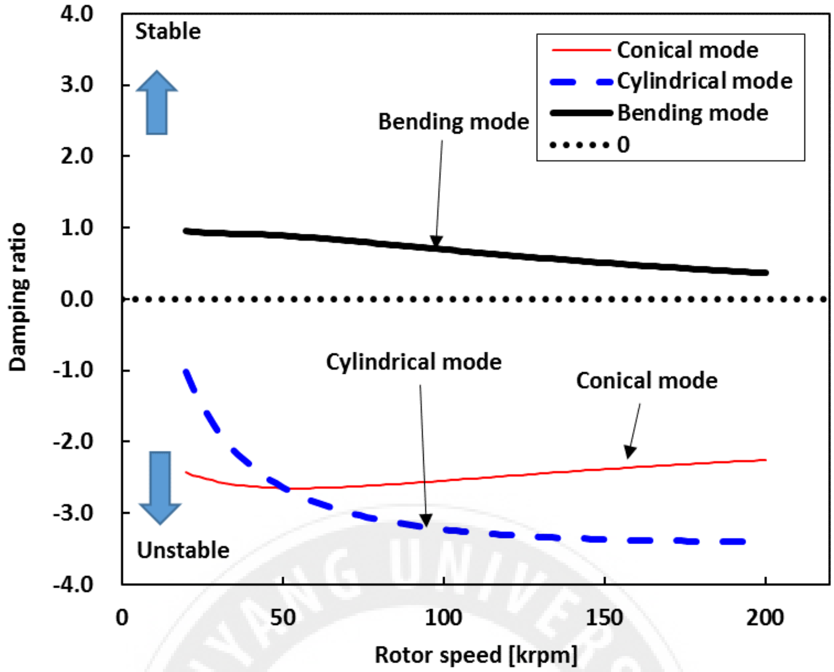

Fig. 62 Damped eigenvalues (damping ratios). Rotor supported on 2-axial groove bearings.

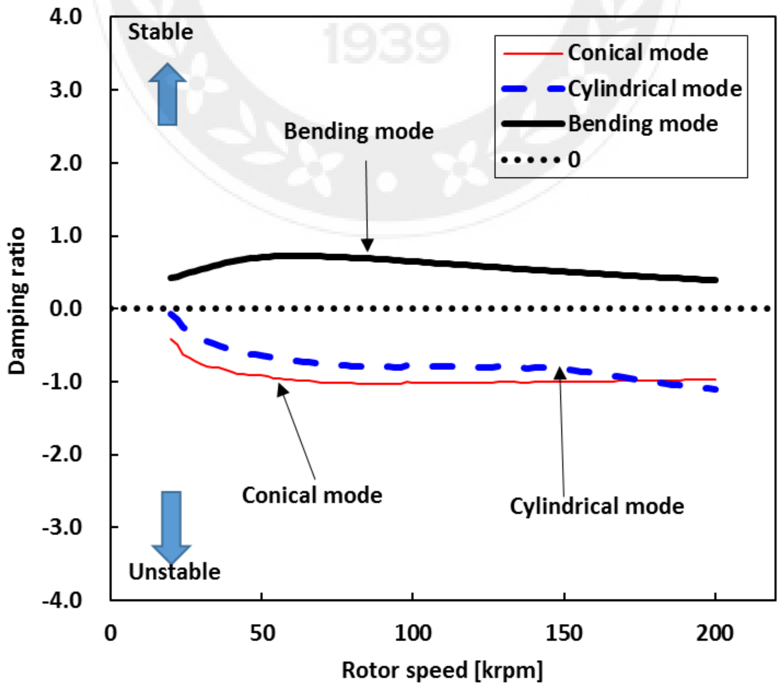

Fig. 63 Damped eigenvalues (damping ratios). Rotor supported on offset-half bearings.

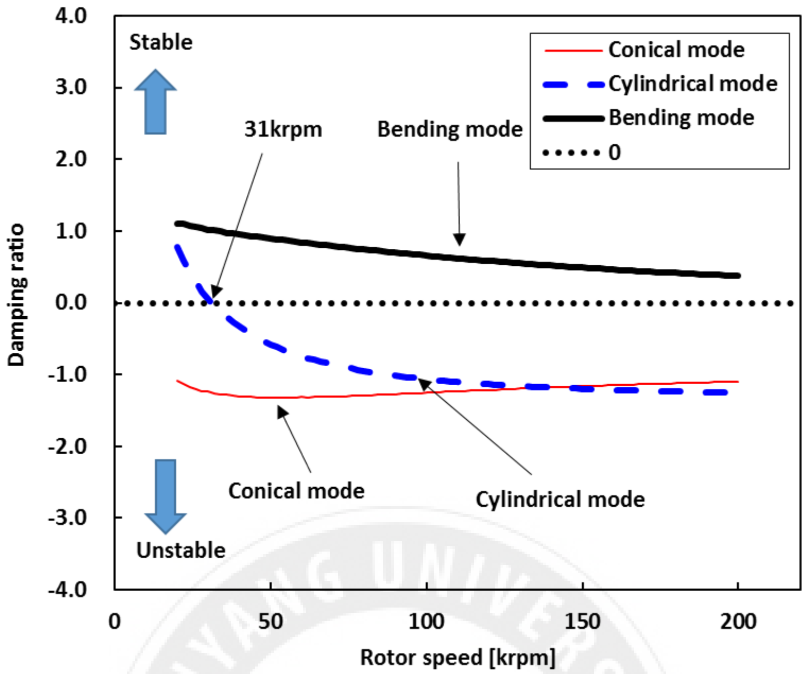

Fig. 64 Damped eigenvalues (damping ratios). Rotor supported on three lobe bearings.

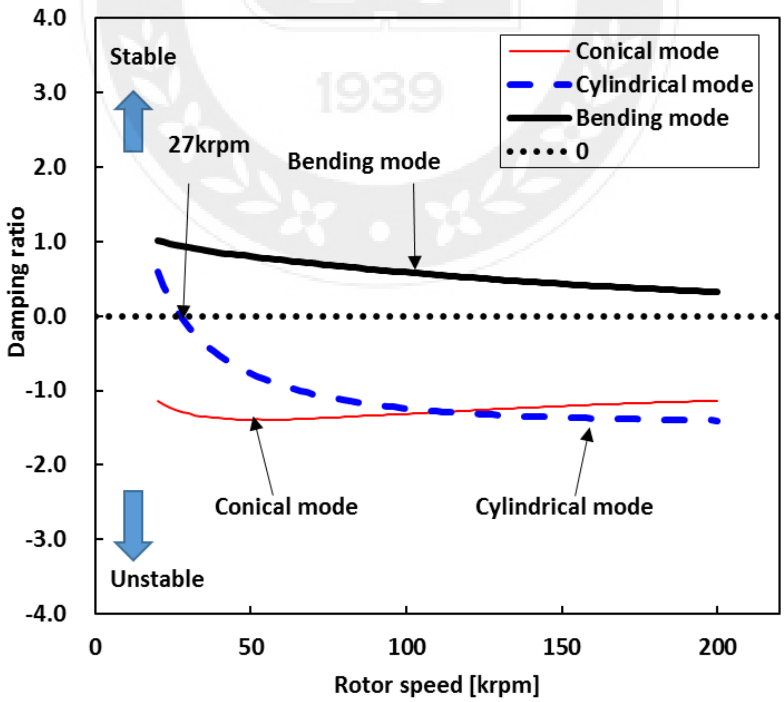

Fig. 65 Damped eigenvalues (damping ratios). Rotor supported on four lobe bearings.

The imbalance response needs to analysis shaft motion response. Figure 42 describes shaft motion response versus shaft speed. Choose a position on compressor side because generally, the maximum amplitude is happening at compressor end. Unit of amplitude is mm (peak-peak). For each bearing, 4 lobe bearing has the most significant amplitude of 0.0658 mm when rotor speed reaches 122 krpm.

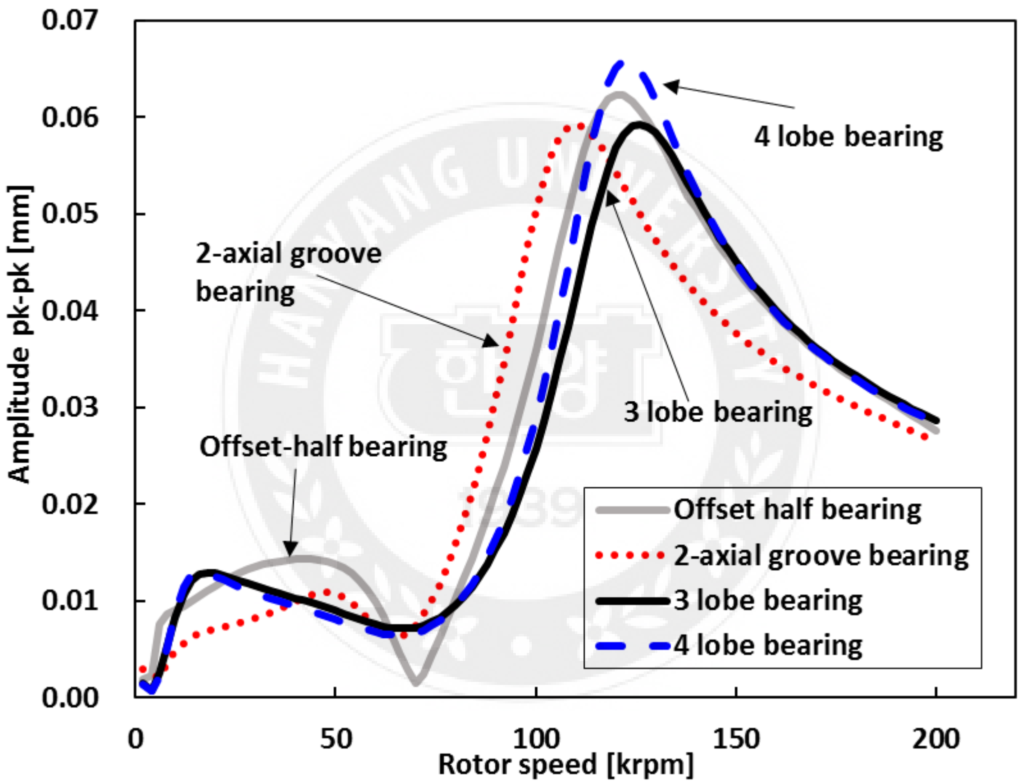

Fig. 66 Shaft motion amplitude versus shaft speed on compressor side.

Other significant results are transmitted bearing forces. Figures 43 and 44 describe transmitted bearing forces versus shaft speed by using each kind of bearings. On both sides, offset-half bearing support maximum transmitted force. Transmitted bearing force becomes maximum during shaft speed from 100 krpm to 130 krpm of each bearing.

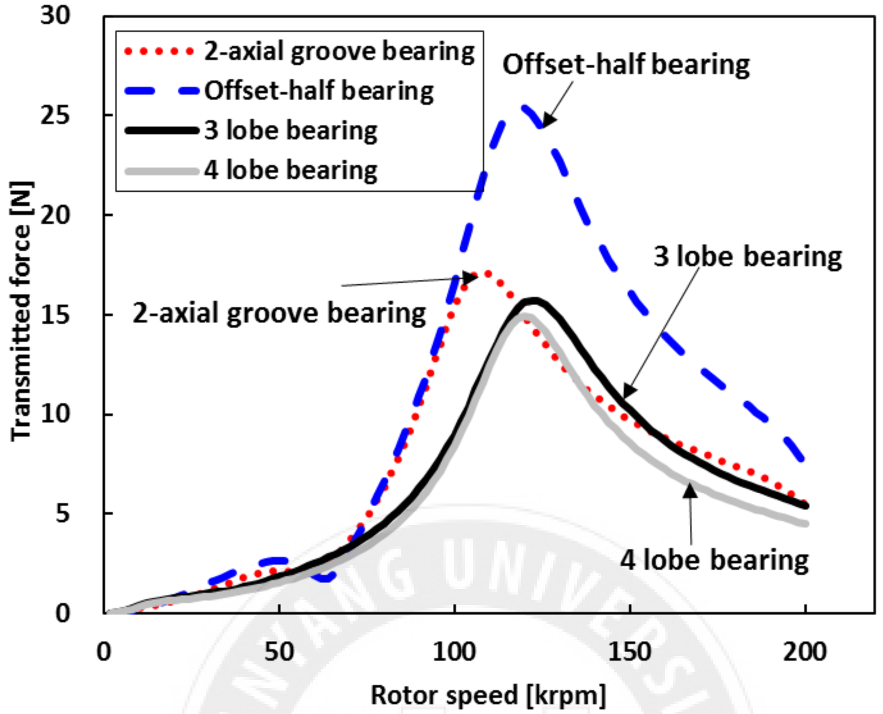

Fig. 67 Transmitted bearing force versus shaft speed on compressor side bearings

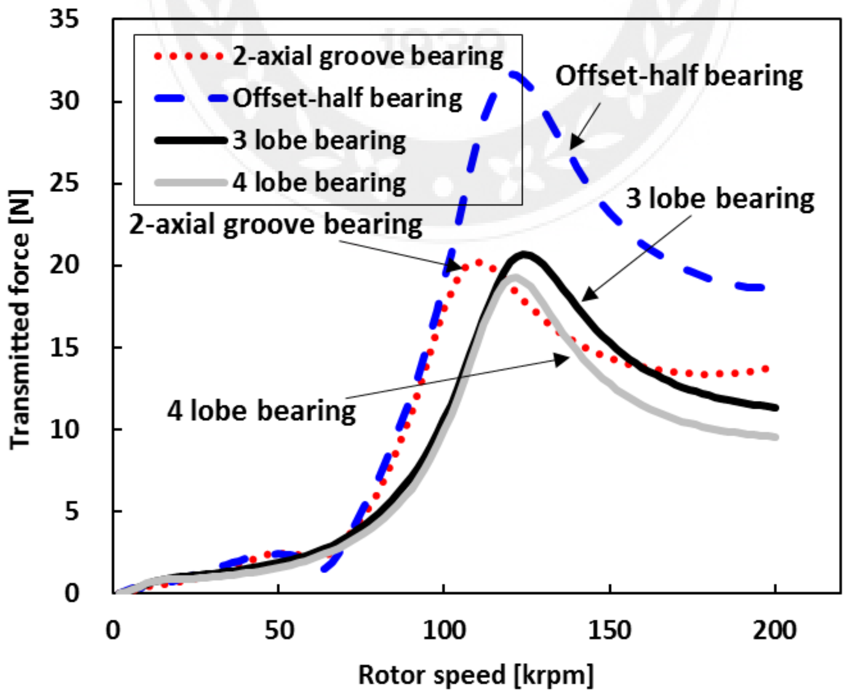

Fig. 68 Transmitted bearing force versus shaft speed on turbine side bearings.

Chapter 5. Conclusions

The current study presents progress on the automotive turbocharger rotor-bearing system performance prediction using rotordynamics models. The predicted results show that the TC rotor dynamic performance strongly relies on the bearing configurations. More importantly, this study demonstrates the importance of using accurate rotor dynamic models for accurate predictions of turbocharger dynamic stability. Most significant conclusions of this research follow.

The bearing configurations preload and offset have a significant impact on bearing dynamic performance. The higher offset provides higher direct stiffness and damping force coefficients of multi-lobe bearing (if bearing preloaded). If bearing preload equal to 0, the offset does not make sense of bearing performance. The preload does have the effect of bearing dynamic force coefficients (stiffness and damping), but the relationship needs further research.

The bearing pad angles have a significant impact on bearing dynamic performance. The higher pad angle provides higher direct stiffness and damping force coefficients of the multi-lobe bearing. The higher pad angle even provides higher cross-coupled stiffness force coefficients of the multi-lobe bearing.

All predicted results show unstable conical modes, and stable bending modes. The TC supported on 2-axial groove bearings, and offset-half bearings have unstable cylindrical modes in the operational range. The TC supported on 3 lobe bearing cylindrical mode becomes unstable when the rotor speed reaches 32 krpm. The TC supported on 4 lobe bearing cylindrical mode become unstable when the rotor speed reaches 28 krpm.

4 lobe bearings have most significant imbalance response at the compressor end. When the TC rotor supported on offset-half bearings, the transmitted bearing force is more significant than other types of bearings.

References

[1] Zeidan, F. Y., and Herbage, B. S., 1991, "Fluid Film Bearing Fundamentals and Failure Analysis," Proc. Proceedings of the Twentieth Turbomachinery Symposium, Texas A&M University, pp. 161-186.

[2] Alsaeed, A. A., 2005, "Dynamic Stability Evaluation of an Automotive Turbocharger Rotor-Bearing System," M.S. thesis, Blacksburg, VA.

[3] Mondscehin, B. D., 2010, "Evaluation of Alternate Bearing Designs in a High Speed Automotive Turbocharger," M.S. thesis, Blacksburg, VA.

[4] Michael S. A., 2012, "Stability Analysis of a Turbocharger for Marine Diesel Engine Service," M.S., Blacksburg, VA.

[5] Inman, Daniel J., 2008. "Engineering Vibration," Upper Saddle, NJ: Pearson Education, Inc. pp. 43–48. ISBN 0-13-228173-2.

[6] Lund, J. W. and Thomsen, K. K., 1978, "A Calculation Method and Data for the Dynamic Coefficients of Oil-Lubricated Journal Bearing," Topics in Fluid Film Bearing and Rotor Bearing System Design and Optimization, ASME.

[7] Ferron, J., Frene, J., and Boncompain, R., 1983, "A Study of the Thermohydrodynamic Performance of a Plain Journal Bearing Comparison between Theory and Experiments," J. of Lubrication Tech, 105(3), pp. 422-428.

[8] San Andrés, 1995, "Thermohydrodynamic Analysis of Fluid Film Bearings for Cryogenic Applications," Journal of Propulsion and Power 11(5), pp. 964-972.

[9] Chen. W. J., Edgar J. G., 2007, Dynamics of Rotor-Bearing Systems, Trafford Publishing, ISBN 1426990502, 9781426990502, pp 108-120

Appendix A

Figure A.1 through A.12 depict the input data of preload and offset effects of 3 lobe bearing analysis. The pad angle of 3 lobe bearings is 100 degree for each analysis condition.

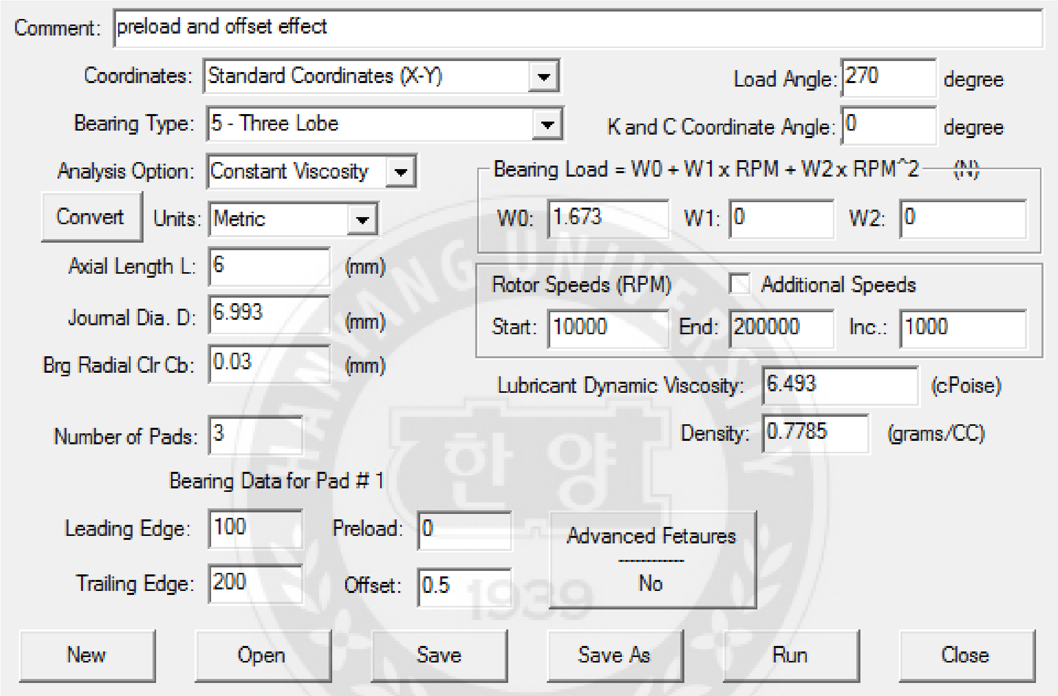

Fig. A. 1 Input data of preload and offset effect (3 lobe bearing turbine side; preload=0; offset=0.5)

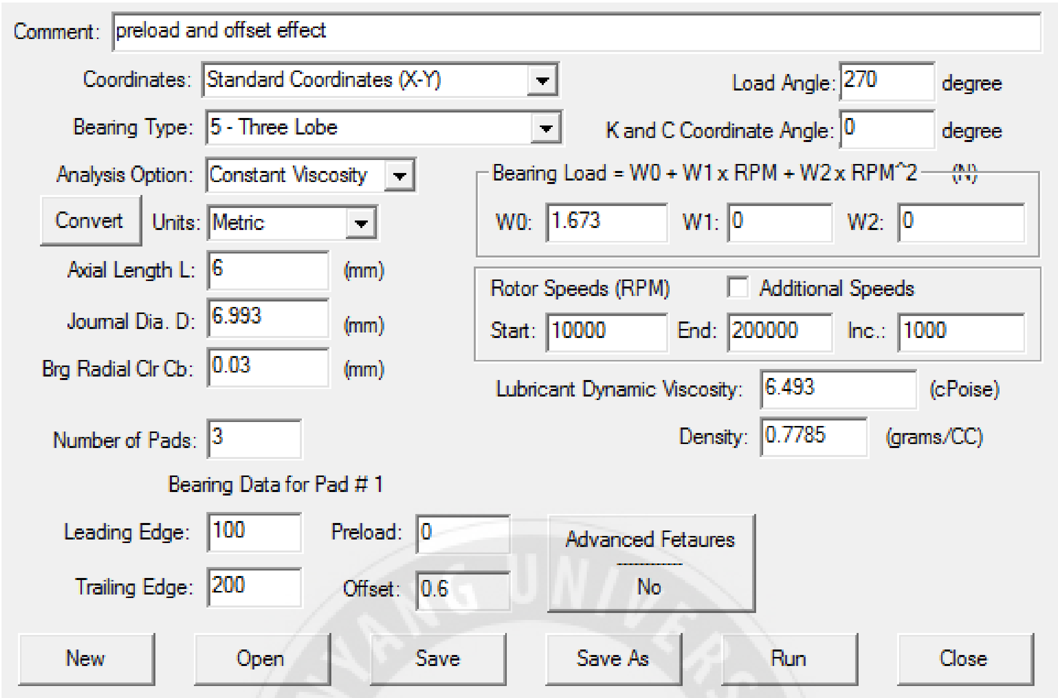

Fig. A. 2 Input data of preload and offset effect (3 lobe bearing turbine side; preload=0; offset=0.6)

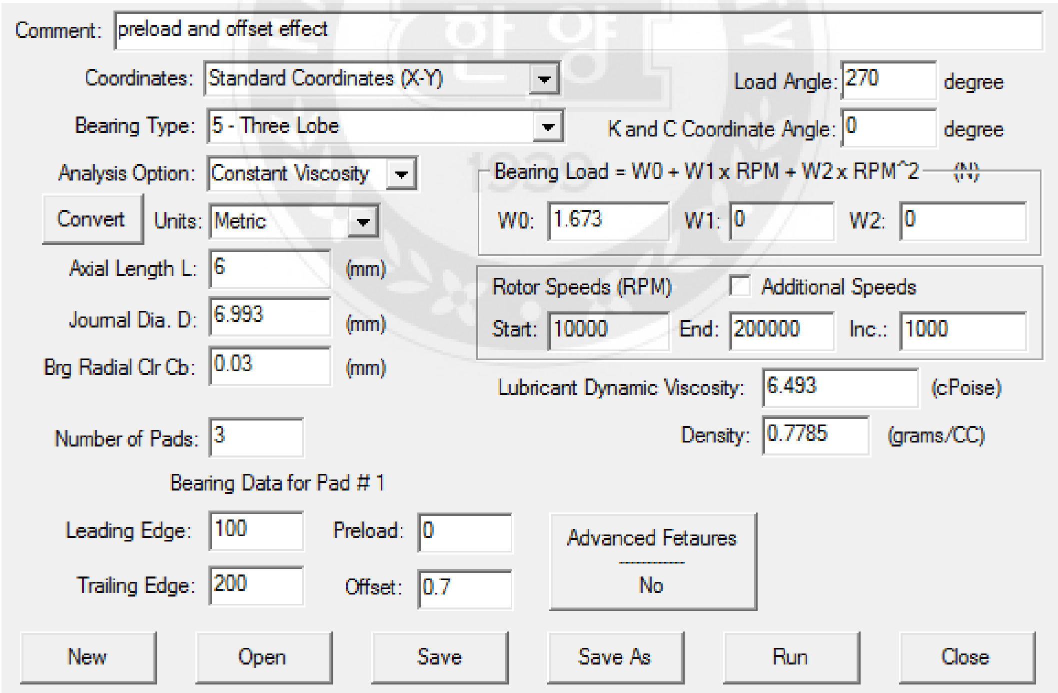

Fig. A. 3 Input data of preload and offset effect (3 lobe bearing turbine side; preload=0; offset=0.7)

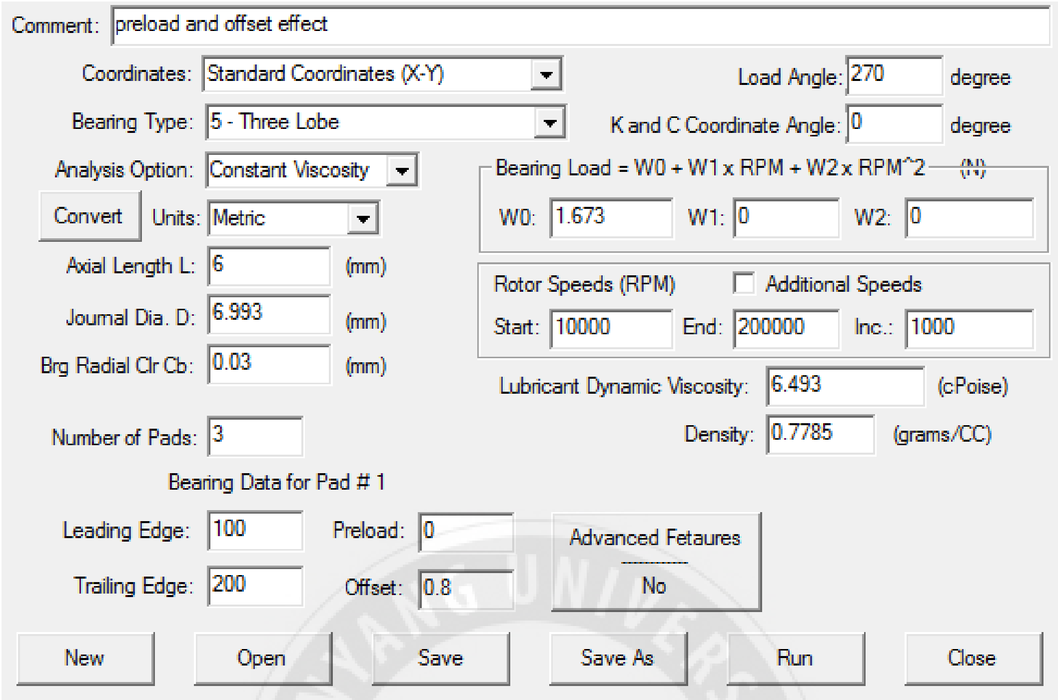

Fig. A. 4 Input data of preload and offset effect (3 lobe bearing turbine side; preload=0; offset=0.8)

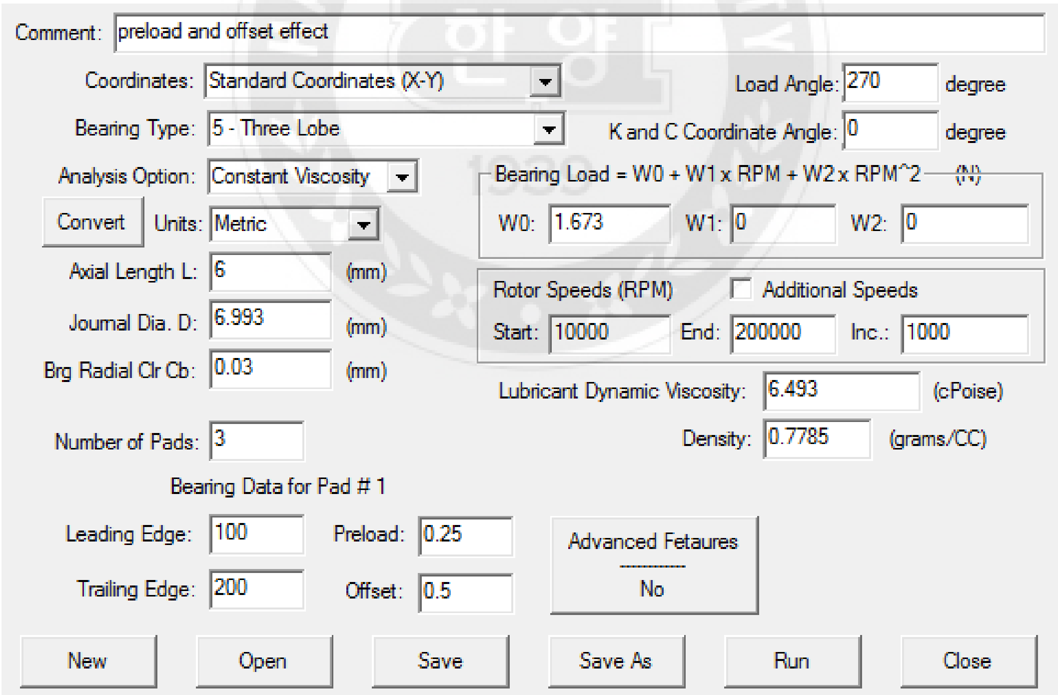

Fig. A. 5 Input data of preload and offset effect (3 lobe bearing turbine side; preload=0.25; offset=0.5)

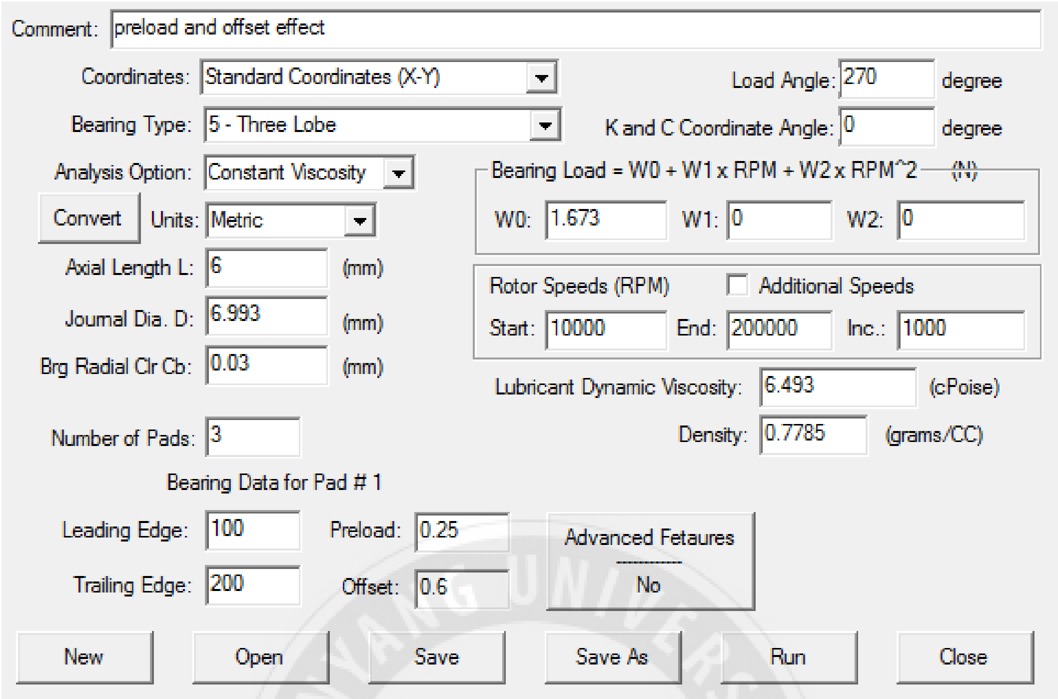

Fig. A. 6 Input data of preload and offset effect (3 lobe bearing turbine side; preload=0.25; offset=0.6)

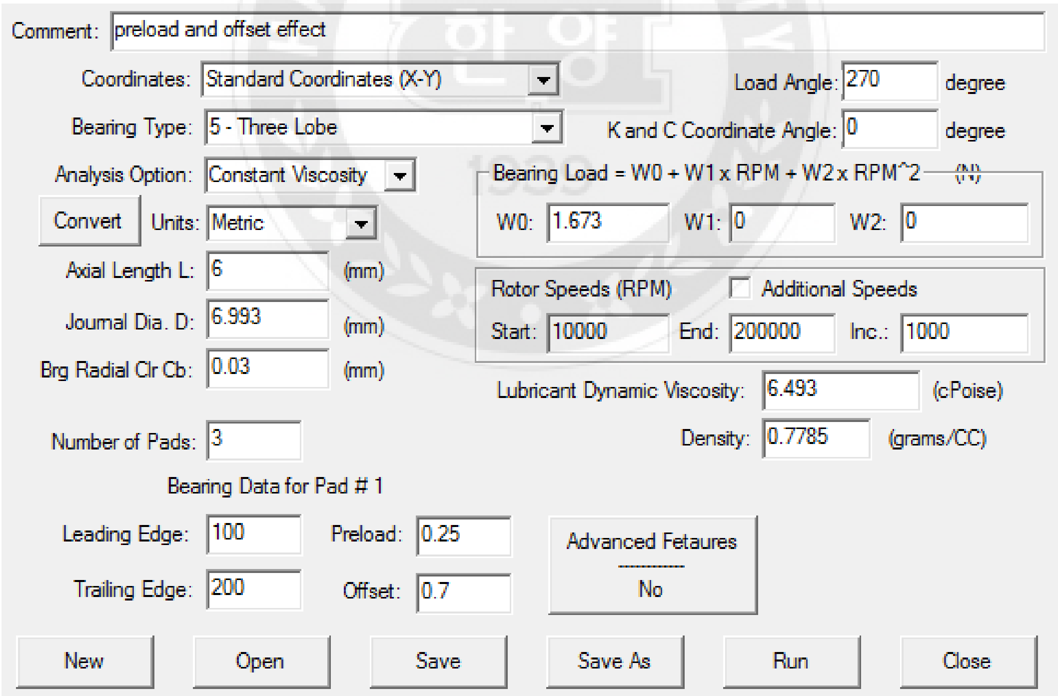

Fig. A. 7 Input data of preload and offset effect (3 lobe bearing turbine side; preload=0.25; offset=0.7)

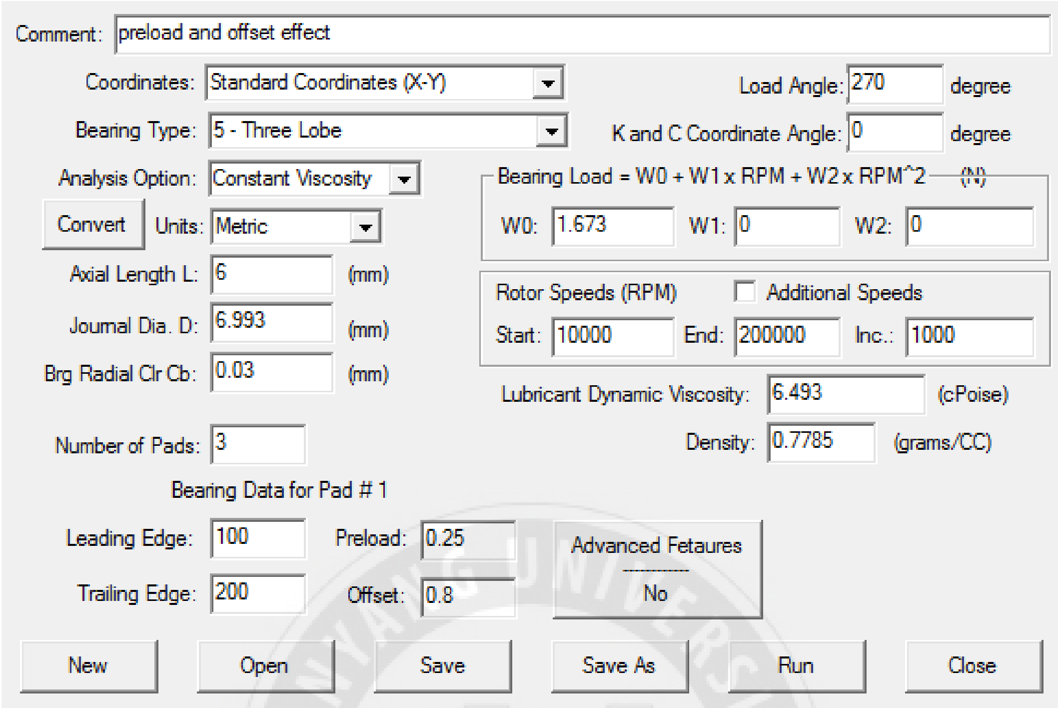

Fig. A. 8 Input data of preload and offset effect (3 lobe bearing turbine side; preload=0.25; offset=0.8)

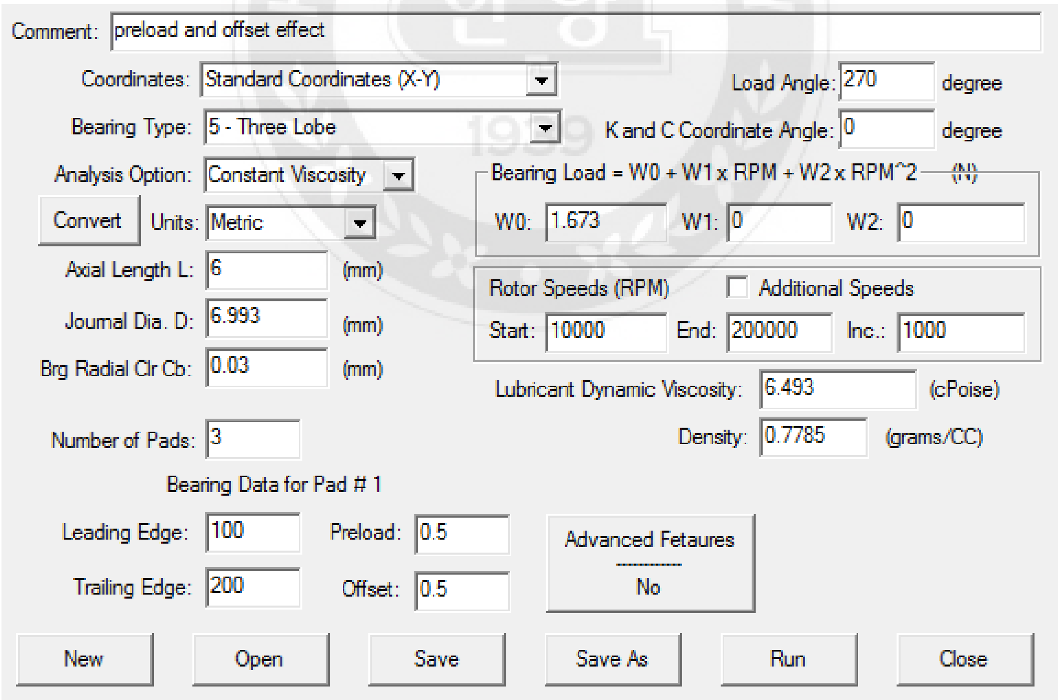

Fig. A. 9 Input data of preload and offset effect (3 lobe bearing turbine side; preload=0.5; offset=0.5)

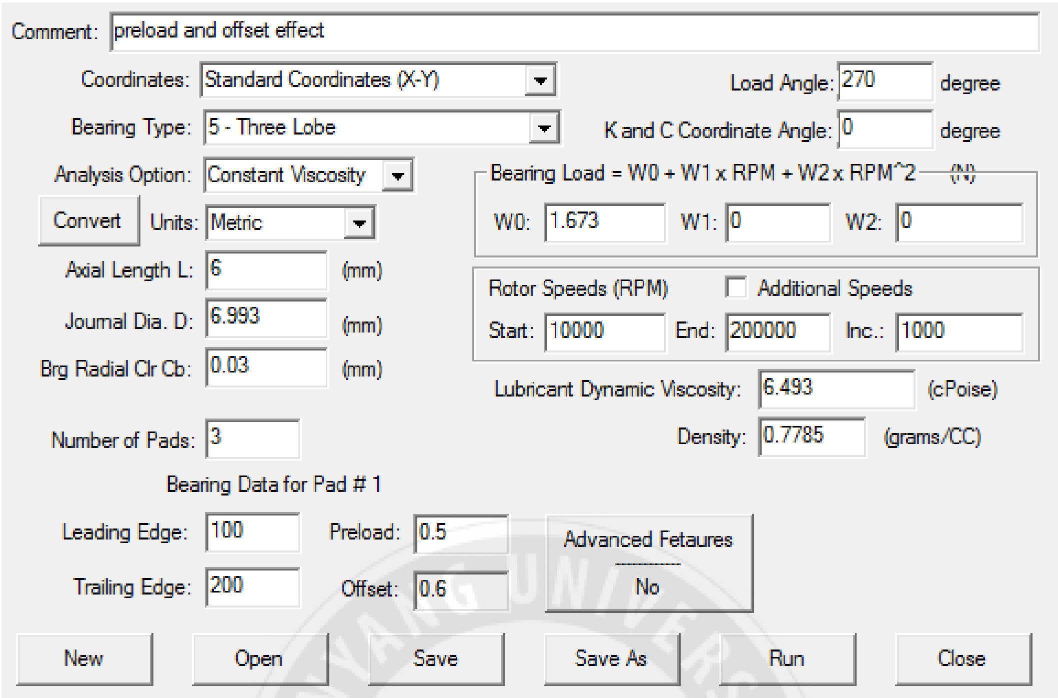

Fig. A. 10 Input data of preload and offset effect (3 lobe bearing turbine side; preload=0.5; offset=0.6)

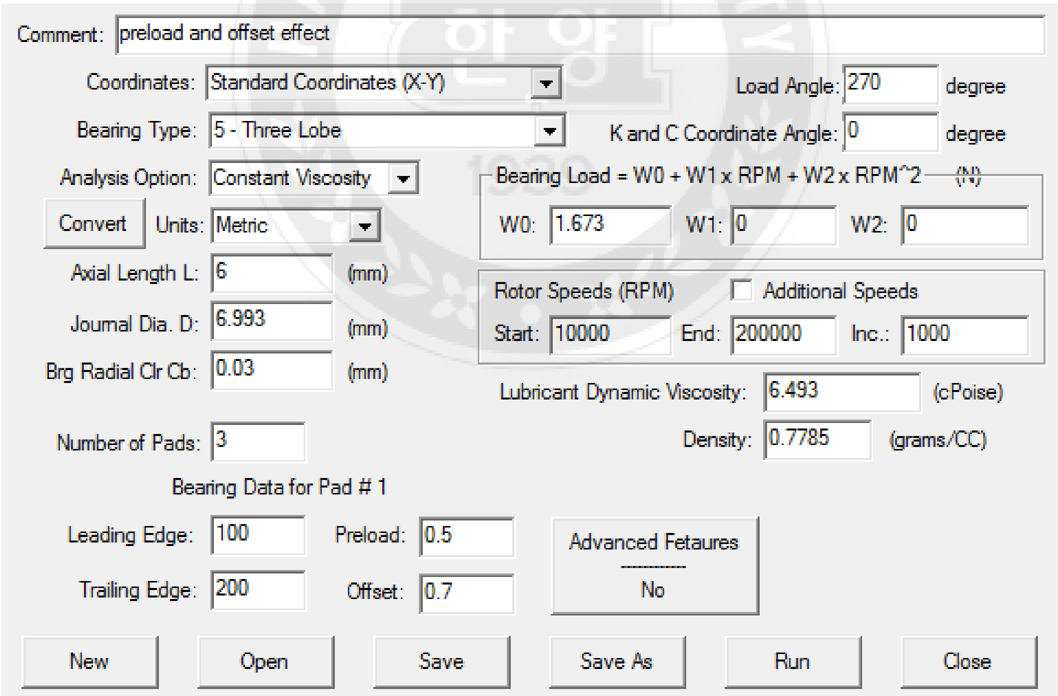

Fig. A. 11 Input data of preload and offset effect (3 lobe bearing turbine side; preload=0.5; offset=0.7)

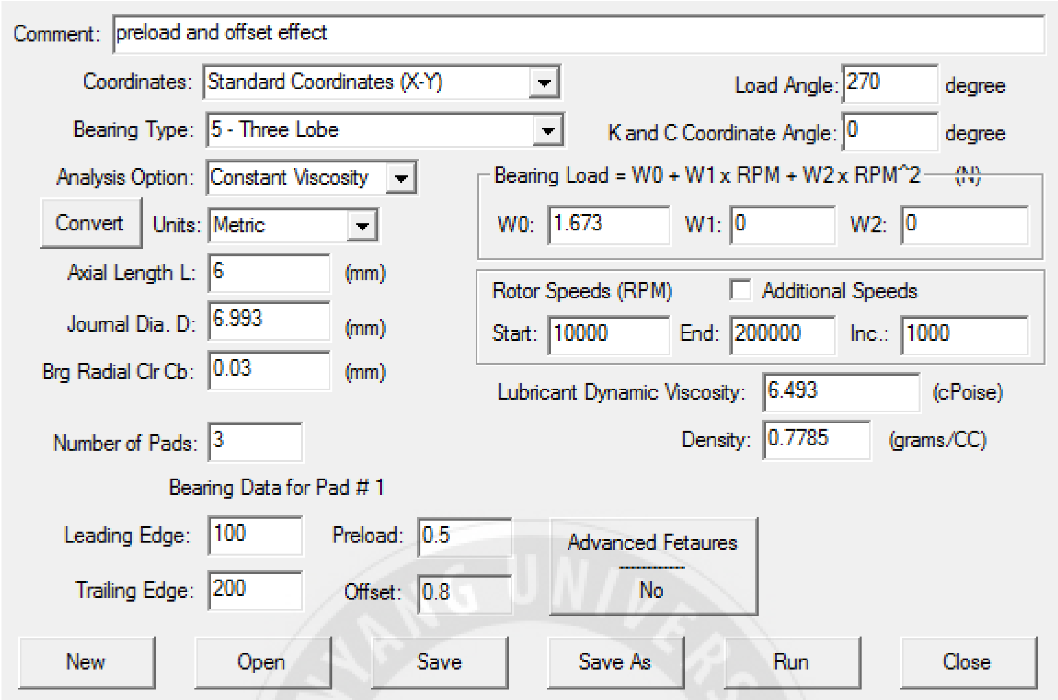

Fig. A. 12 Input data of preload and offset effect (3 lobe bearing turbine side; preload=0.5; offset=0.8)

Figure A.13 through A.15 depict the input data of pad angle effect of 3 lobe bearing analysis. The preload=0.5 and offset=0.5 of 3 lobe bearings are set for each analysis condition.

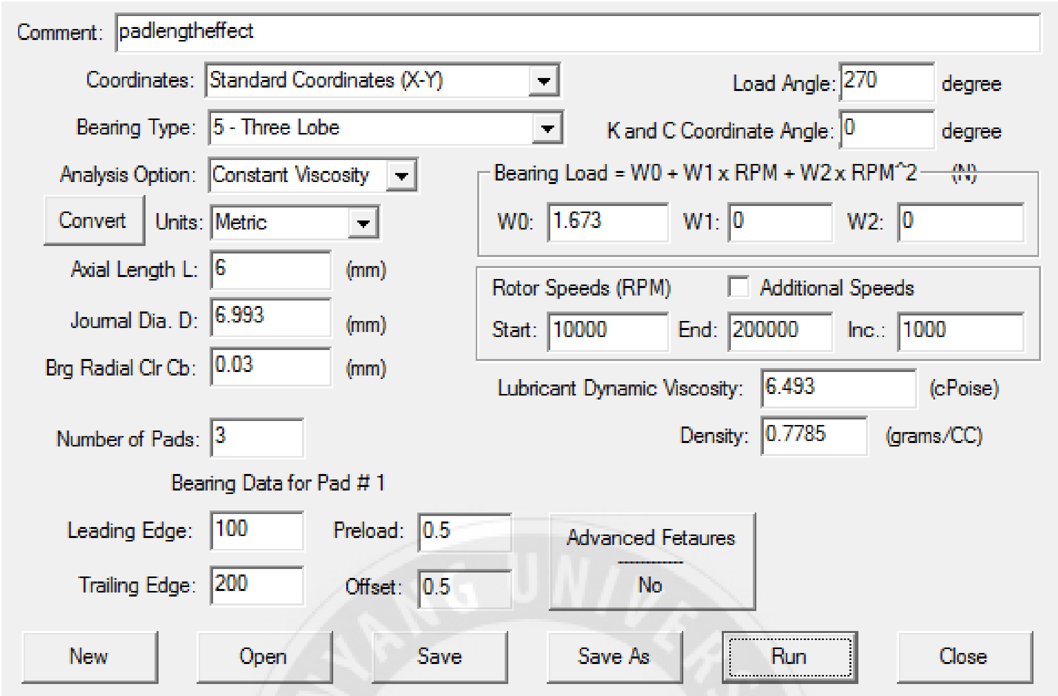

Fig. A. 13 Input data of pad angle effect (3 lobe bearing turbine side; preload=0.5; offset=0.5; 100 degree)

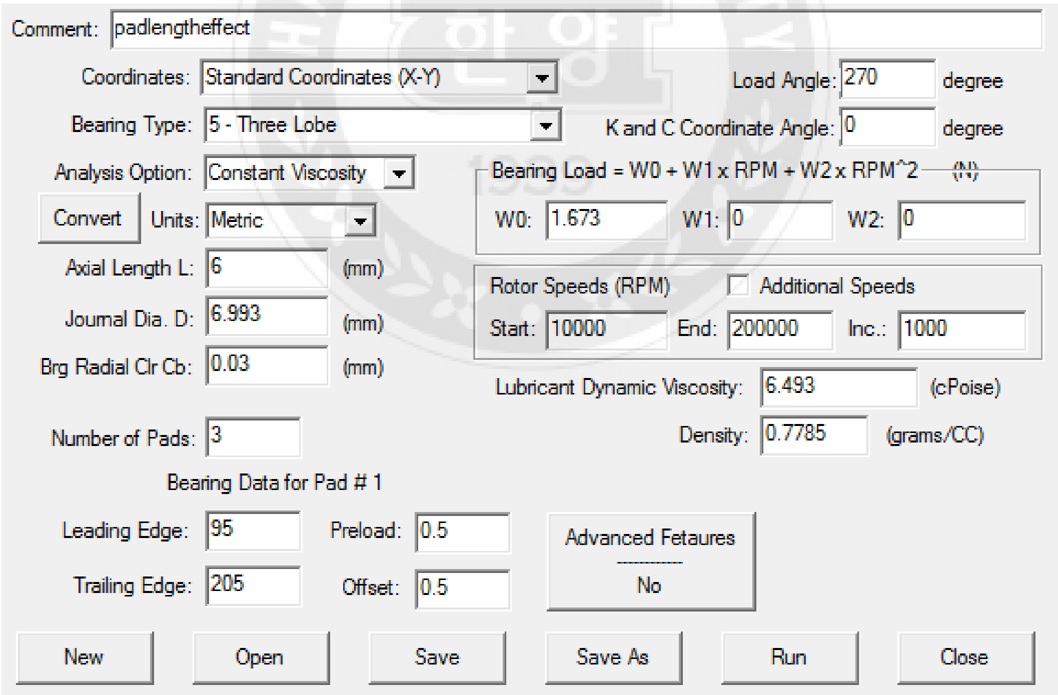

Fig. A. 14 Input data of pad angle effect (3 lobe bearing turbine side; preload=0.5; offset=0.5; 110 degree)

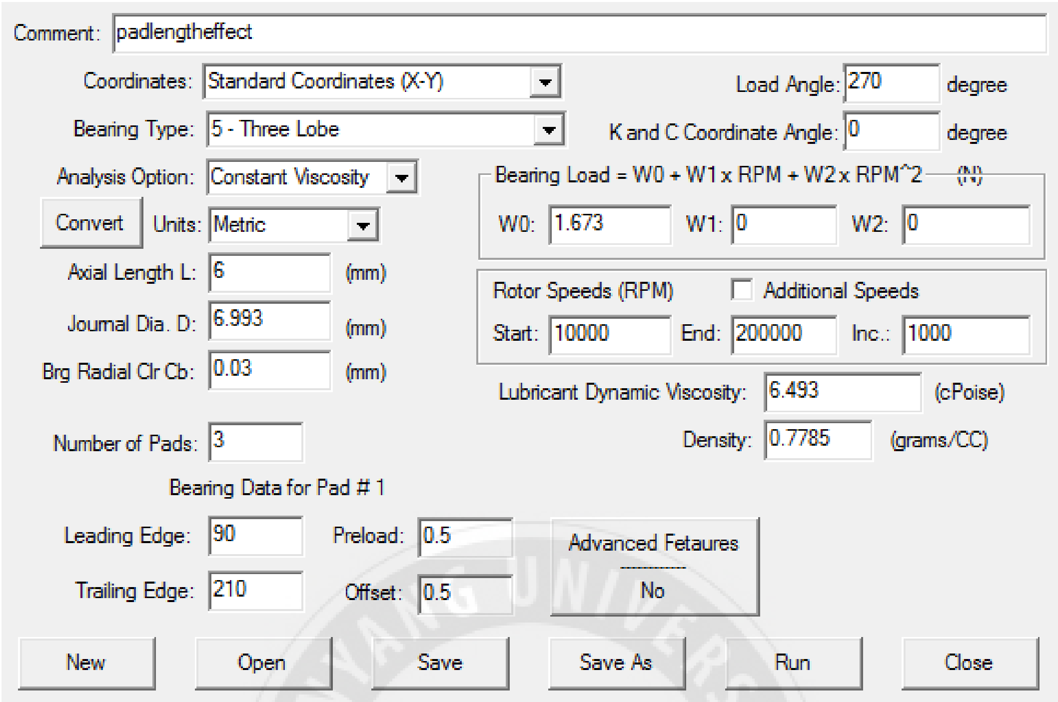

Fig. A. 15 Input data of pad angle effect (3 lobe bearing turbine side; preload=0.5; offset=0.5; 120 degree)

Figure A.16 through A.23 depict the input data of bearing type effect analysis. Each TCs supported on two bearings, compressor side bearings, and turbine side bearings. 2-axial groove bearings have 160 degree angle of each pad. The preload and offset of 2-axial groove bearings are all 0. Offset-halves bearings, 3 lobe bearings, and 4 lobe bearings have 0.5 preload and 0.8 offset.

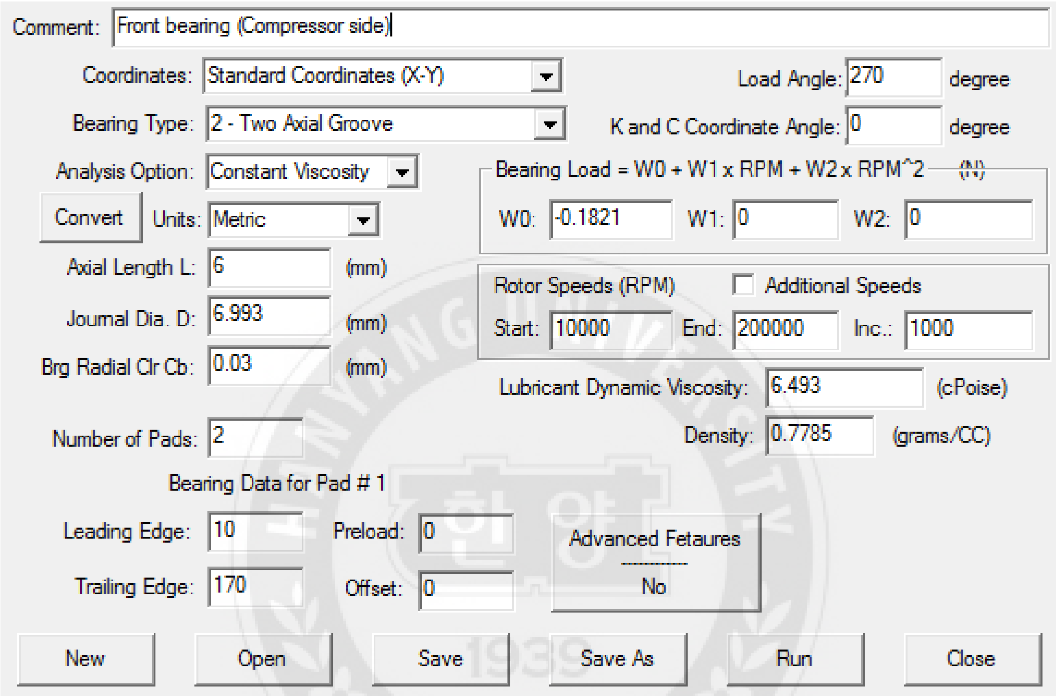

Fig. A. 16 Input data of bearing type effect (2-axial groove bearing compressor side; preload=0; offset=0)

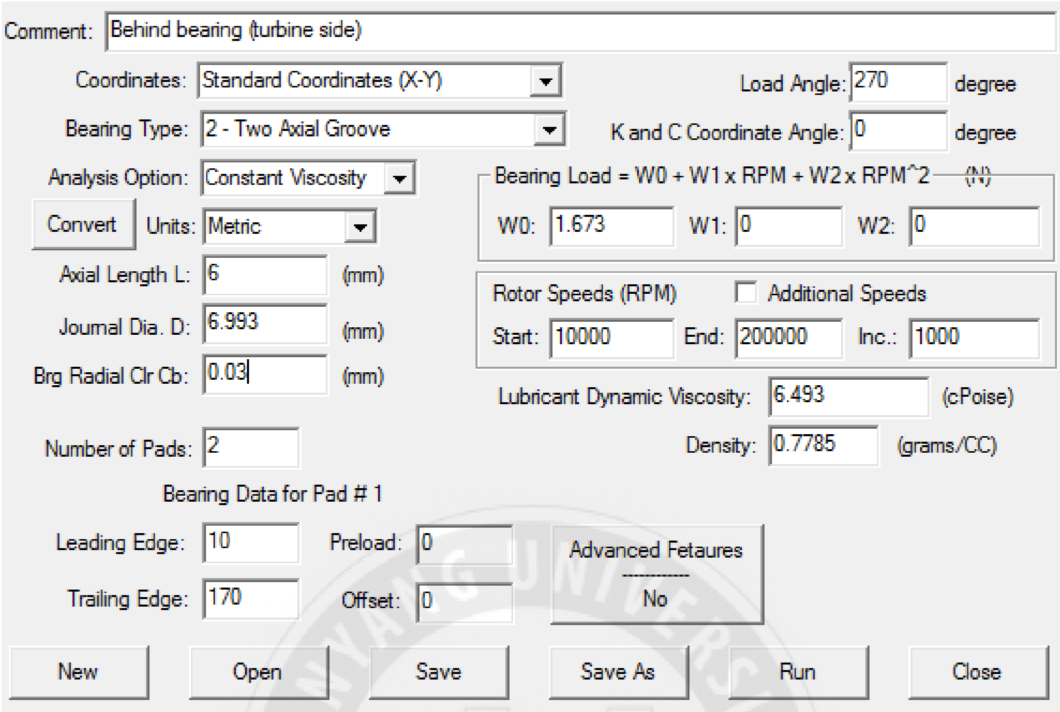

Fig. A. 17 Input data of bearing type effect (2-axial groove bearing turbine side; preload=0; offset=0)

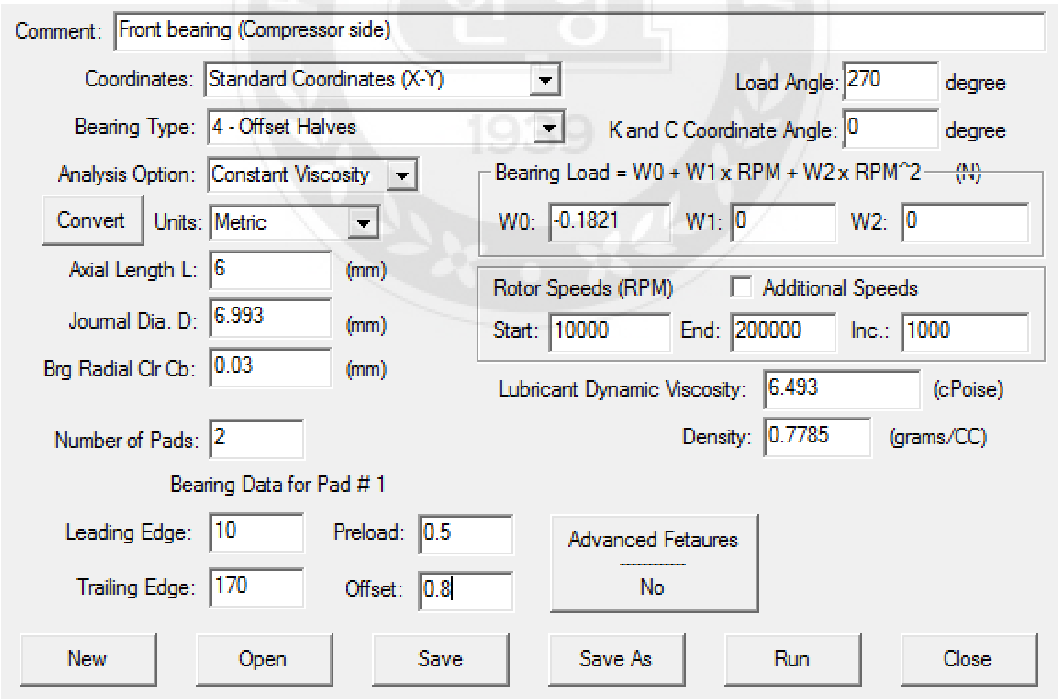

Fig. A. 18 Input data of bearing type effect (offset-halves bearing compressor side; preload=0.5; offset=0.8)

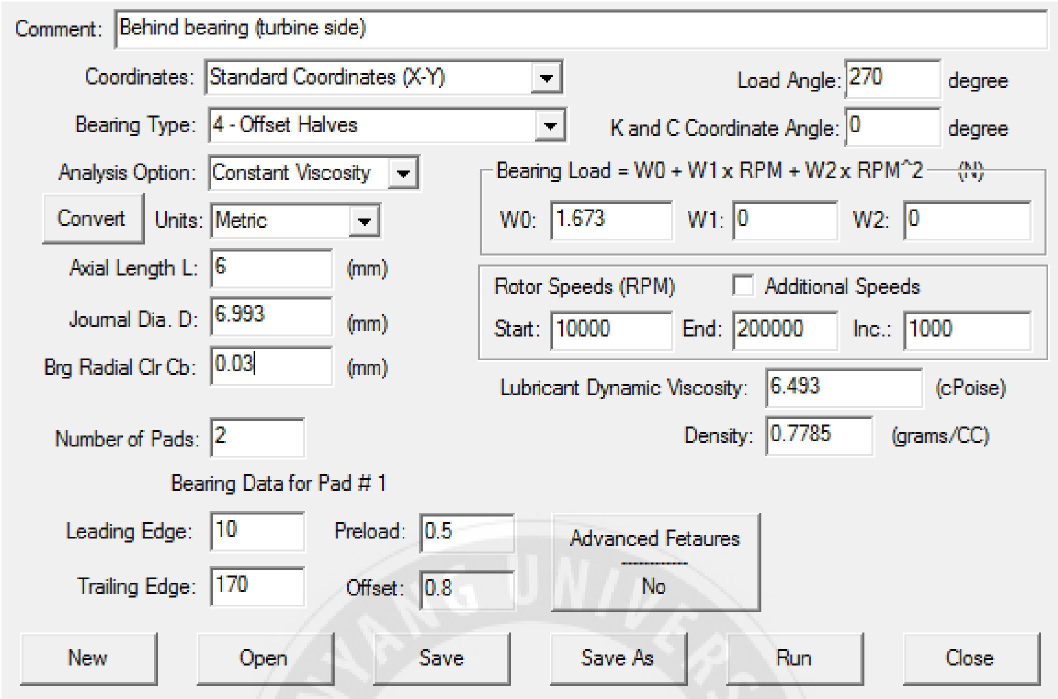

Fig. A. 19 Input data of bearing type effect (offset-halves bearing turbine side; preload=0.5; offset=0.8)

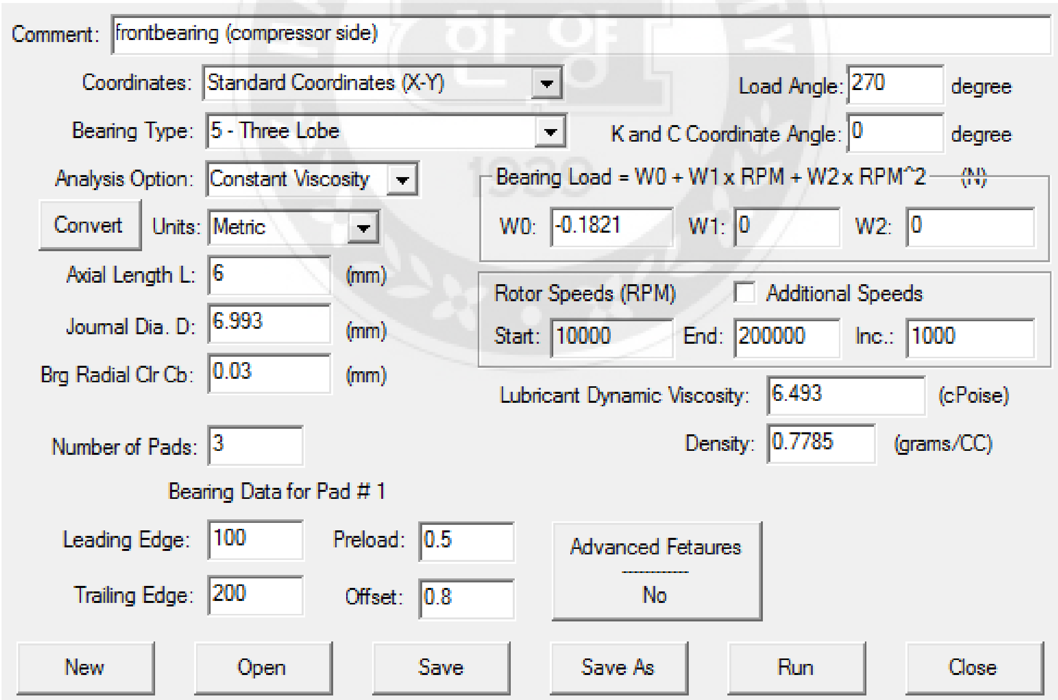

Fig. A. 20 Input data of bearing type effect (3 lobe bearing compressor side; preload=0.5; offset=0.8)

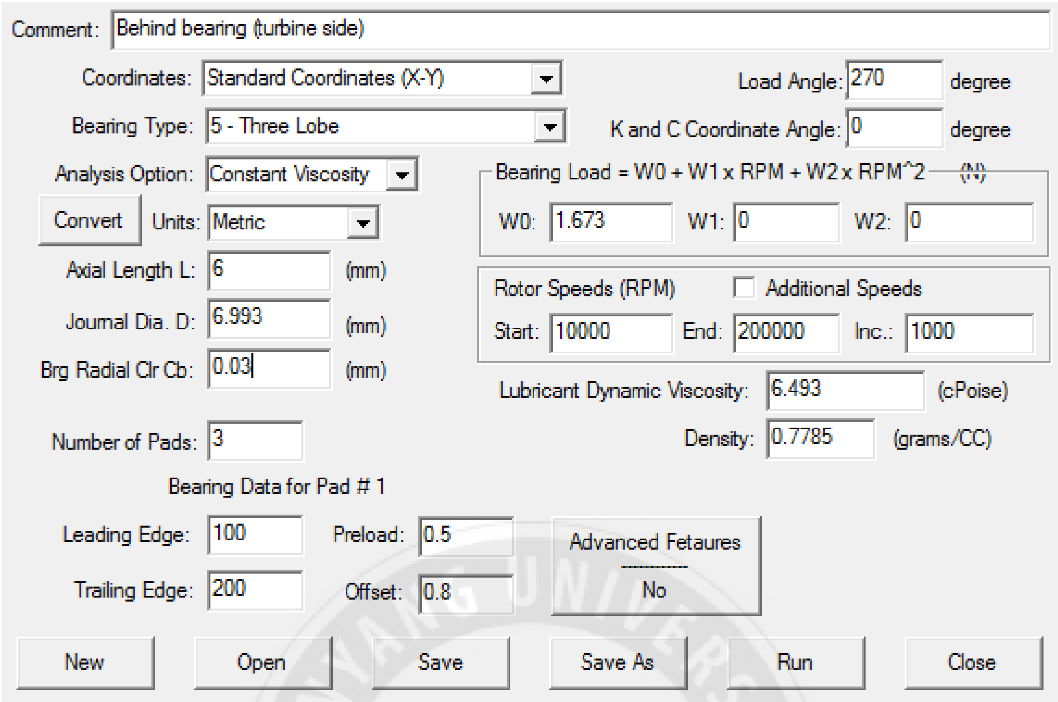

Fig. A. 21 Input data of bearing type effect (3 lobe bearing turbine side; preload=0.5; offset=0.8)

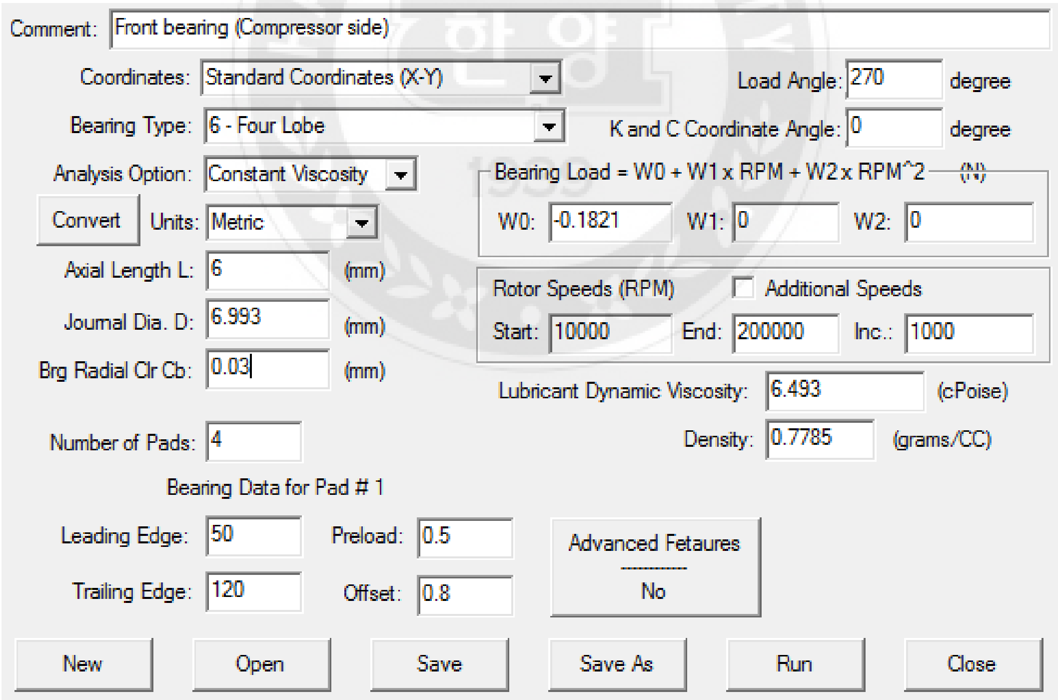

Fig. A. 22 Input data of bearing type effect (4 lobe bearing compressor side; preload=0.5; offset=0.8)

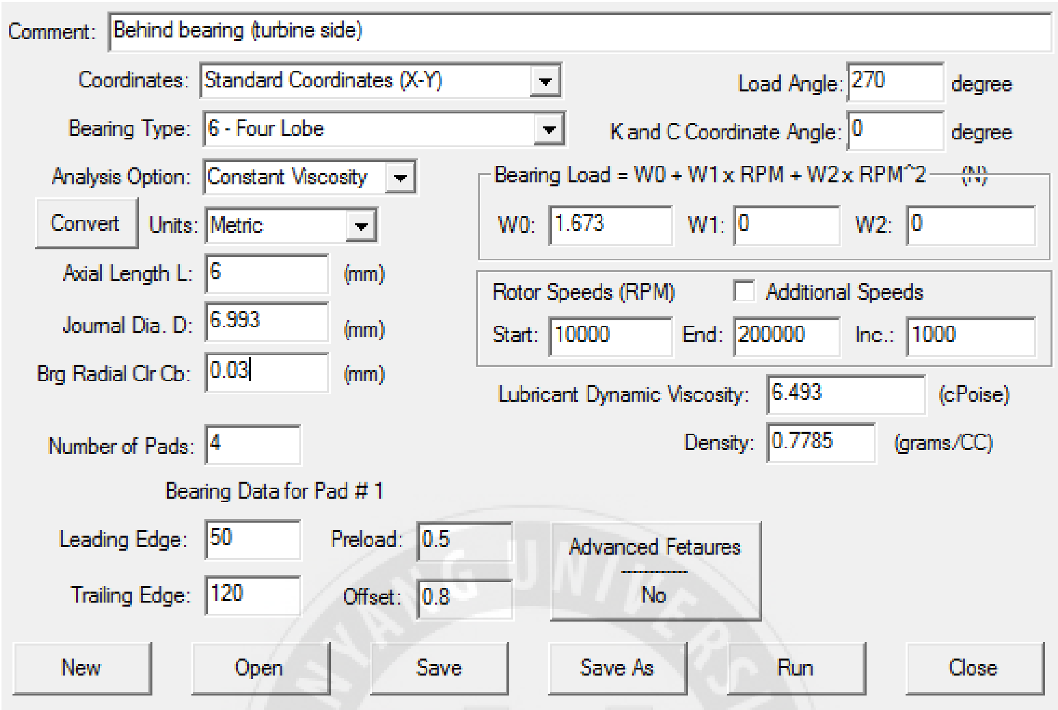

Fig. A. 23 Input data of bearing type effect (4 lobe bearing turbine side; preload=0.5; offset=0.8)

Appendix B

Figure B.1 through B.4 depict the shaft elements input of rotor-bearing system analysis.

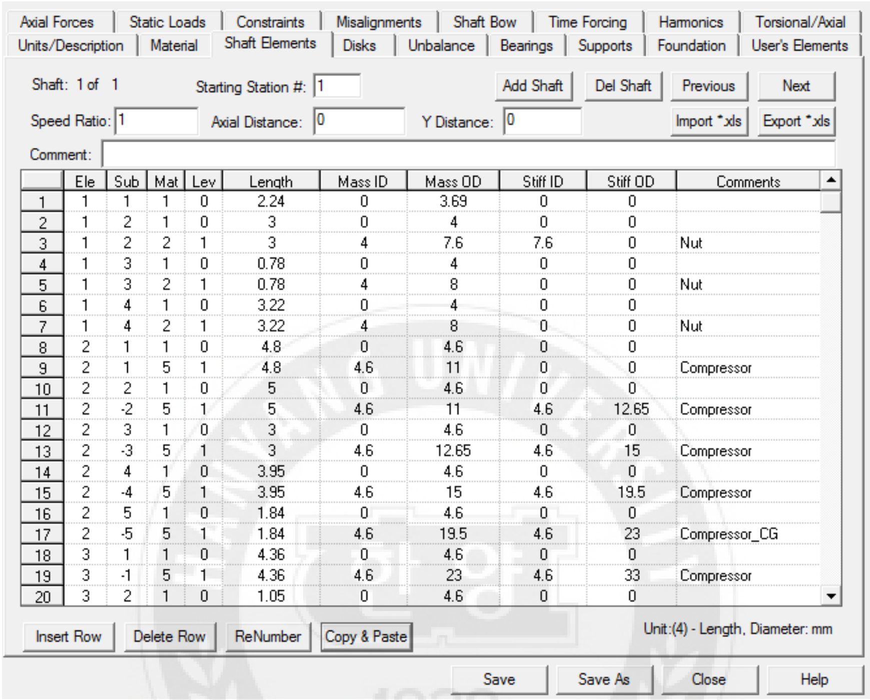

	Ele	Sub	Mat	Lev	Length	Mass ID	Mass OD	Stiff ID	Stiff OD	Comments
1	1	1	1	0	2.24	0	3.69	0	0	
2	1	2	1	0	3	0	4	0	0	
3	1	2	2	1	3	4	7.6	7.6	0	Nut
4	1	3	1	0	0.78	0	4	0	0	
5	1	3	2	1	0.78	4	8	0	0	Nut
6	1	4	1	0	3.22	0	4	0	0	
7	1	4	2	1	3.22	4	8	0	0	Nut
8	2	1	1	0	4.8	0	4.6	0	0	
9	2	1	5	1	4.8	4.6	11	0	0	Compressor
10	2	2	1	0	5	0	4.6	0	0	
11	2	-2	5	1	5	4.6	11	4.6	12.65	Compressor
12	2	3	1	0	3	0	4.6	0	0	
13	2	-3	5	1	3	4.6	12.65	4.6	15	Compressor
14	2	4	1	0	3.95	0	4.6	0	0	
15	2	-4	5	1	3.95	4.6	15	4.6	19.5	Compressor
16	2	5	1	0	1.84	0	4.6	0	0	
17	2	-5	5	1	1.84	4.6	19.5	4.6	23	Compressor_CG
18	3	1	1	0	4.36	0	4.6	0	0	
19	3	-1	5	1	4.36	4.6	23	4.6	33	Compressor
20	3	2	1	0	1.05	0	4.6	0	0	

Fig. B. 1 Input data of rotor-bearing analysis model (shaft elements 1-20)

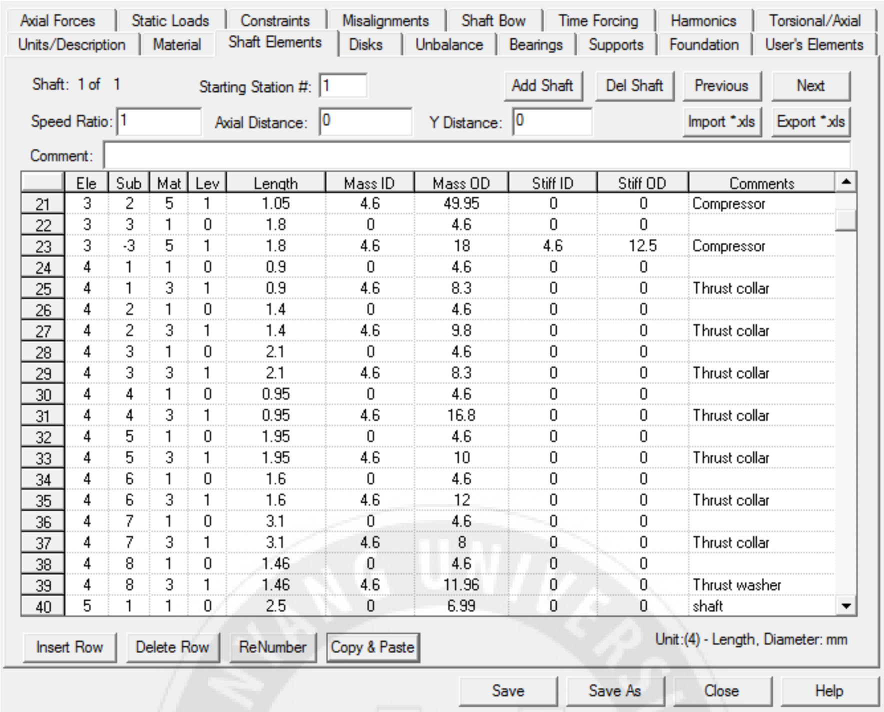

	Ele	Sub	Mat	Lev	Length	Mass ID	Mass OD	Stiff ID	Stiff OD	Comments
21	3	2	5	1	1.05	4.6	49.95	0	0	Compressor
22	3	3	1	0	1.8	0	4.6	0	0	
23	3	-3	5	1	1.8	4.6	18	4.6	12.5	Compressor
24	4	1	1	0	0.9	0	4.6	0	0	
25	4	1	3	1	0.9	4.6	8.3	0	0	Thrust collar
26	4	2	1	0	1.4	0	4.6	0	0	
27	4	2	3	1	1.4	4.6	9.8	0	0	Thrust collar
28	4	3	1	0	2.1	0	4.6	0	0	
29	4	3	3	1	2.1	4.6	8.3	0	0	Thrust collar
30	4	4	1	0	0.95	0	4.6	0	0	
31	4	4	3	1	0.95	4.6	16.8	0	0	Thrust collar
32	4	5	1	0	1.95	0	4.6	0	0	
33	4	5	3	1	1.95	4.6	10	0	0	Thrust collar
34	4	6	1	0	1.6	0	4.6	0	0	
35	4	6	3	1	1.6	4.6	12	0	0	Thrust collar
36	4	7	1	0	3.1	0	4.6	0	0	
37	4	7	3	1	3.1	4.6	8	0	0	Thrust collar
38	4	8	1	0	1.46	0	4.6	0	0	
39	4	8	3	1	1.46	4.6	11.96	0	0	Thrust washer
40	5	1	1	0	2.5	0	6.99	0	0	shaft

Fig. B. 2 Input data of rotor-bearing analysis model (shaft elements 21-40)

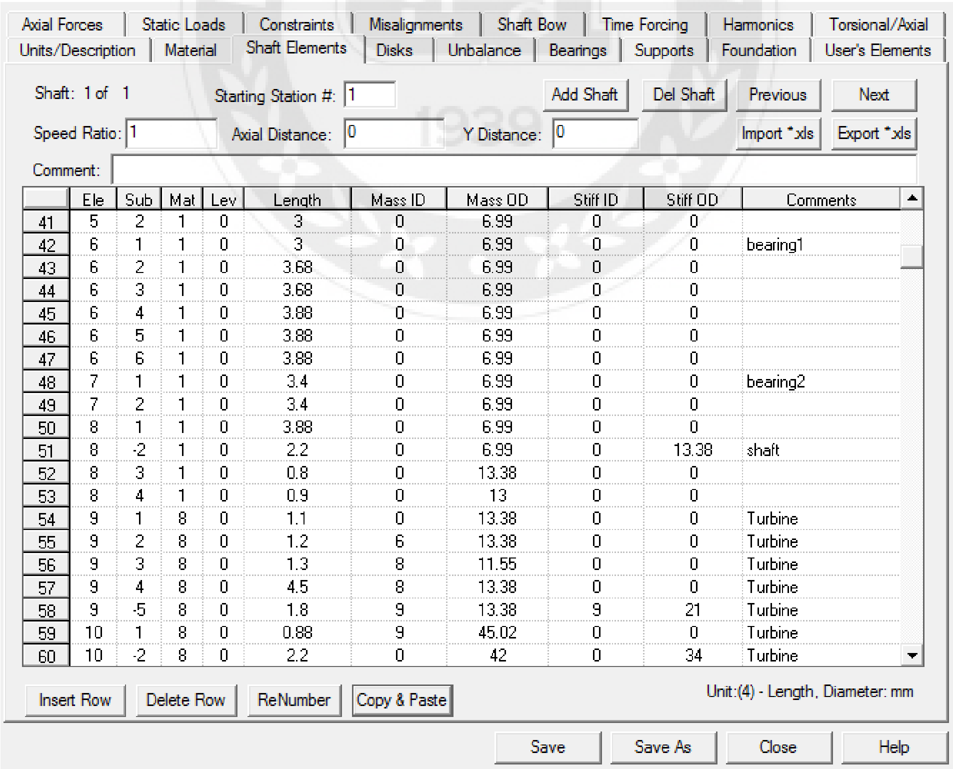

	Ele	Sub	Mat	Lev	Length	Mass ID	Mass OD	Stiff ID	Stiff OD	Comments
41	5	2	1	0	3	0	6.99	0	0	
42	6	1	1	0	3	0	6.99	0	0	bearing1
43	6	2	1	0	3.68	0	6.99	0	0	
44	6	3	1	0	3.68	0	6.99	0	0	
45	6	4	1	0	3.88	0	6.99	0	0	
46	6	5	1	0	3.88	0	6.99	0	0	
47	6	6	1	0	3.88	0	6.99	0	0	
48	7	1	1	0	3.4	0	6.99	0	0	bearing2
49	7	2	1	0	3.4	0	6.99	0	0	
50	8	1	1	0	3.88	0	6.99	0	0	
51	8	-2	1	0	2.2	0	6.99	0	13.38	shaft
52	8	3	1	0	0.8	0	13.38	0	0	
53	8	4	1	0	0.9	0	13	0	0	
54	9	1	8	0	1.1	0	13.38	0	0	Turbine
55	9	2	8	0	1.2	6	13.38	0	0	Turbine
56	9	3	8	0	1.3	8	11.55	0	0	Turbine
57	9	4	8	0	4.5	8	13.38	0	0	Turbine
58	9	-5	8	0	1.8	9	13.38	9	21	Turbine
59	10	1	8	0	0.88	9	45.02	0	0	Turbine
60	10	-2	8	0	2.2	0	42	0	34	Turbine

Fig. B. 3 Input data of rotor-bearing analysis model (shaft elements 41-60)

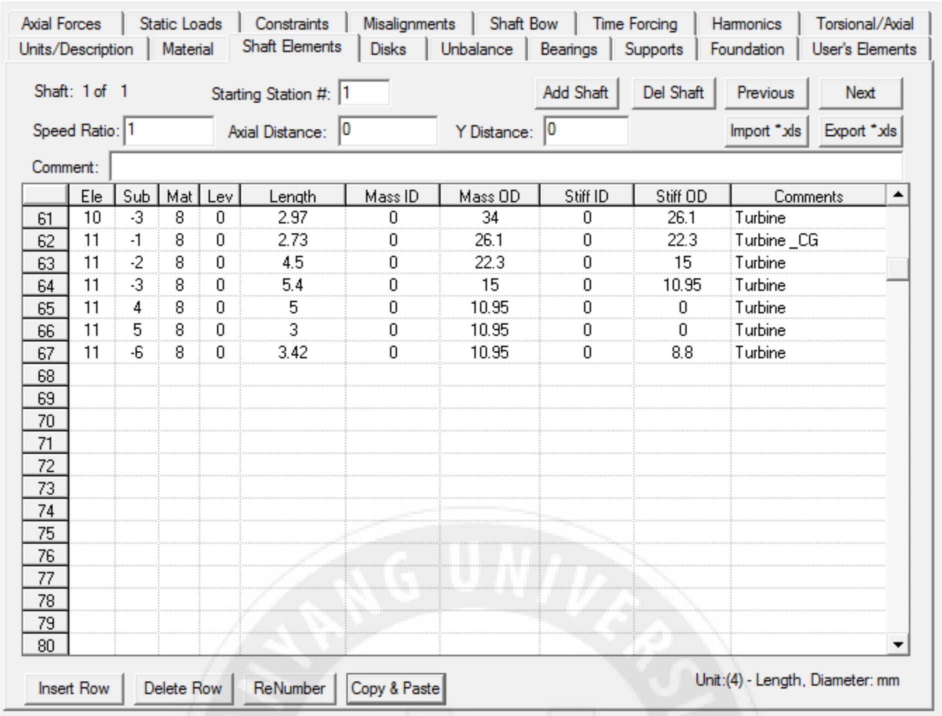

	Ele	Sub	Mat	Lev	Length	Mass ID	Mass OD	Stiff ID	Stiff OD	Comments
61	10	-3	8	0	2.97	0	34	0	26.1	Turbine
62	11	-1	8	0	2.73	0	26.1	0	22.3	Turbine _CG
63	11	-2	8	0	4.5	0	22.3	0	15	Turbine
64	11	-3	8	0	5.4	0	15	0	10.95	Turbine
65	11	4	8	0	5	0	10.95	0	0	Turbine
66	11	5	8	0	3	0	10.95	0	0	Turbine
67	11	-6	8	0	3.42	0	10.95	0	8.8	Turbine
68										
69										
70										
71										
72										
73										
74										
75										
76										
77										
78										
79										
80										

Fig. B. 4 Input data of rotor-bearing analysis model (shaft elements 61-67)

Figure B.5 depict the unbalance input of rotor-bearing system analysis. Figure B.6 depict the eigenvalue analysis input of rotor-bearing system analysis.

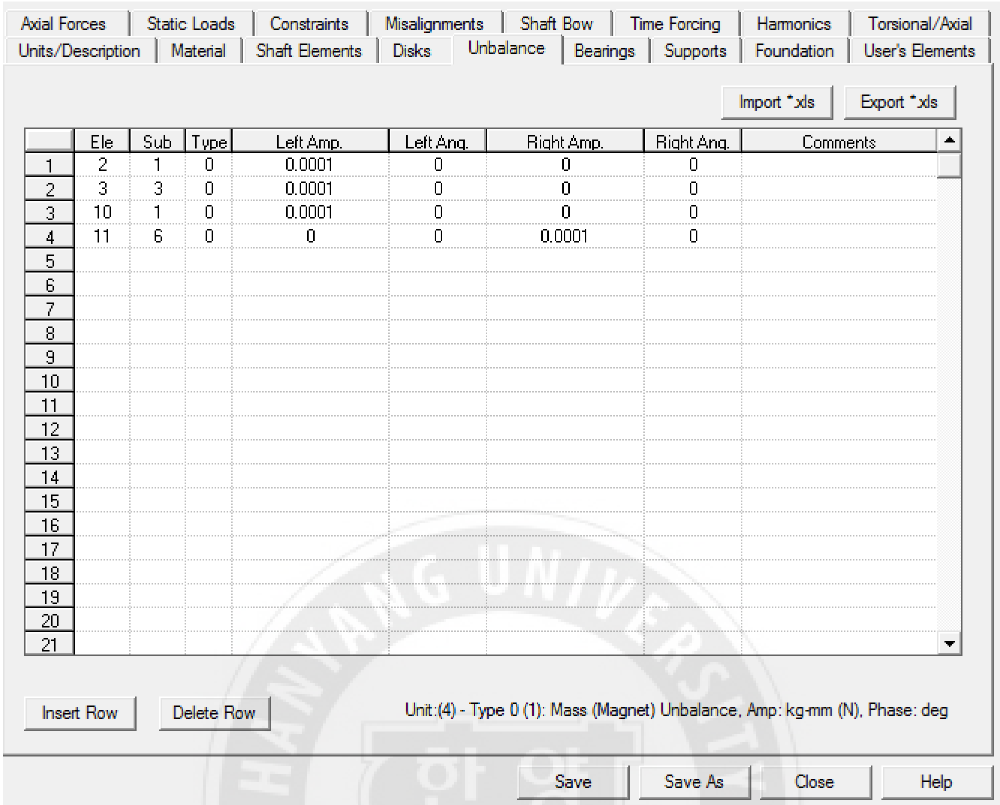

Fig. B. 5 Input data of rotor-bearing analysis model (unbalance)

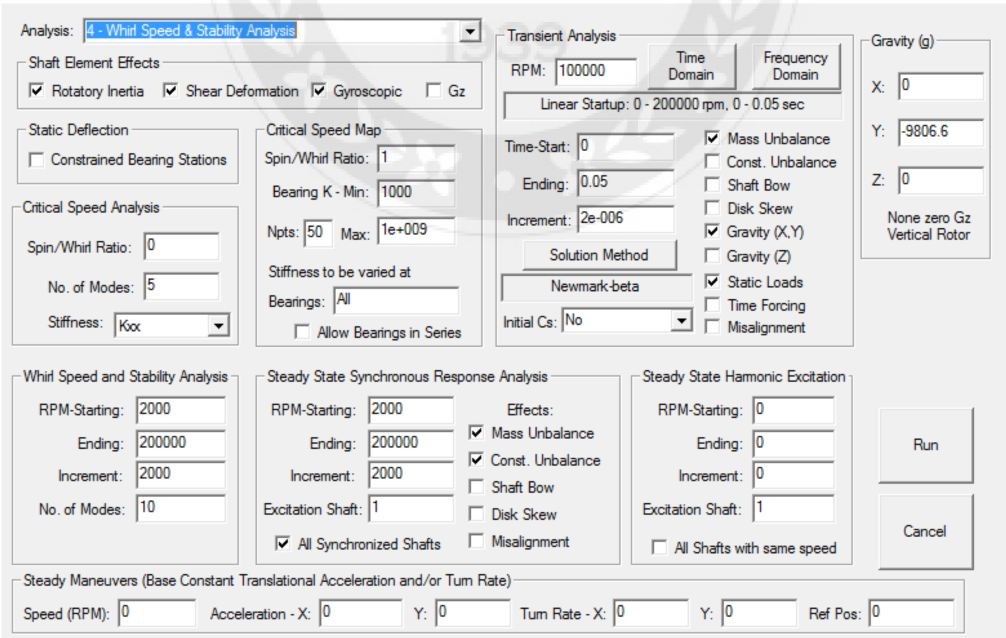

Fig. B. 6 Input data of rotor-bearing analysis

Declaration of Ethical Conduct in Research

I, as a graduate student of Hanyang University, hereby declare that I have abided by the following Code of Research Ethics while writing this dissertation thesis, during my degree program.

"First, I have strived to be honest in my conduct, to produce valid and reliable research conforming with the guidance of my thesis supervisor, and I affirm that my thesis contains honest, fair and reasonable conclusions based on my own careful research under the guidance of my thesis supervisor.

Second, I have not committed any acts that may discredit or damage the credibility of my research. These include, but are not limited to : falsification, distortion of research findings or plagiarism.

Third, I need to go through with Copykiller Program(Internet-based Plagiarism-prevention service) before submitting a thesis."

DECEMBER 19, 2017

Degree : Master

Department : DEPARTMENT OF MECHANICAL DESIGN ENGINEERING

Thesis Supervisor : Keun Ryu

Name : Fang Xiao (Signature)

연구 윤리 서약서

본인은 한양대학교 대학원생으로서 이 학위논문 작성 과정에서 다음과 같이 연구 윤리의 기본 원칙을 준수하였음을 서약합니다.

첫째, 지도교수의 지도를 받아 정직하고 엄정한 연구를 수행하여 학위논문을 작성한다.

둘째, 논문 작성시 위조, 변조, 표절 등 학문적 진실성을 훼손하는 어떤 연구 부정행위도 하지 않는다.

셋째, 논문 작성시 논문유사도 검증시스템 "카피킬러"등을 거쳐야 한다.

2017년12월19일

학위명 : 석사

학과 : 기계설계공학과

지도교수 : 류근

성명 : 방효 (서명)

한 양 대 학 교 대 학 원 장 귀 하